[redacted]

NASA TECHNICAL MEMORANDUM

NASA TM X-2284

NASA TM X-2284

DOWNGRADED TO Unclassified
BY AUTHORITY OF NASA CLASSIFICATION CHANGE NOTICES NO. 242 DATED 30 Sept 76
ITEM NO. 23

CASE FILE COPY

STABILITY AND CONTROL CHARACTERISTICS AT MACH NUMBERS 1.60 TO 2.86 OF A VARIABLE-SWEEP FIGHTER CONFIGURATION WITH SUPERCRITICAL AIRFOIL SECTIONS

by Samuel M. Dollyhigh

Langley Research Center
Hampton, Va. 23365

NATIONAL AERONAUTICS AND SPACE ADMINISTRATION • WASHINGTON, D. C. • JUNE 1971

[redacted]

[redacted] 71-976

1. Report No. NASA TM X-2284	2. Government Accession No.	3. Recipient's Catalog No.
4. Title and Subtitle STABILITY AND CONTROL CHARACTERISTICS AT MACH NUMBERS 1.60 TO 2.86 OF A VARIABLE-SWEEP FIGHTER CONFIGURATION WITH SUPERCRITICAL AIRFOIL SECTIONS (U)		5. Report Date June 1971 6. Performing Organization Code
7. Author(s) Samuel M. Dollyhigh		8. Performing Organization Report No. L-7583 10. Work Unit No. 720-01-11-02
9. Performing Organization Name and Address NASA Langley Research Center Hampton, Va. 23365		11. Contract or Grant No. 13. Type of Report and Period Covered Technical Memorandum
12. Sponsoring Agency Name and Address National Aeronautics and Space Administration Washington, D.C. 20546		14. Sponsoring Agency Code

15. Supplementary Notes

16. Abstract

An experimental investigation has been made in the Mach number range from 1.60 to 2.86 to determine the longitudinal and lateral aerodynamic characteristics of a variable-sweep fighter configuration with supercritical airfoil sections, twin rectangular inlets, twin vertical tails, and boom-mounted aft horizontal tails. The results of the investigation indicated that the configuration had good longitudinal stability characteristics and a relatively high horizontal-tail control effectiveness. This horizontal-tail effectiveness, coupled with relatively high levels of zero-lift pitching moment, results in a high instantaneous normal-acceleration capability for the configuration at a Mach number of 1.60 and an altitude of 10 668 m (35 000 ft). Indications were that the normal-acceleration capability could be increased somewhat by reducing the longitudinal stability of the configuration. The lateral-stability results, however, indicated rather poor directional characteristics for an angle of attack greater than 10°. For the Mach number range of the tests, static directional stability was maintained only to angles of attack of 10° to 12°, which were well below the angles of attack at which the configuration had longitudinal trim capability.

CLASSIFICATION CHANGE
To UNCLASSIFIED
By authority of NASA HDQ. T.D. 77-163
Changed by J. Shirley Date 6-15-76
Classified Document Master Control Station, NASA
Scientific and Technical Information Facility

CLASSIFIED BY FT/DD254(10/3/72) NASw-2431
SUBJECT TO GENERAL DECLASSIFICATION
SCHEDULE OF EXECUTIVE ORDER 11652.
AUTOMATICALLY DOWNGRADED AT

17. Key Words (Suggested by Author(s))
Fighter configuration
Supercritical airfoil

19. Security Classif. (of this report) [redacted]	20. Security Classif. (of this page)
[redacted]	This page with mis

STABILITY AND CONTROL CHARACTERISTICS AT MACH NUMBERS 1.60 TO 2.86 OF A VARIABLE-SWEEP FIGHTER CONFIGURATION WITH SUPERCRITICAL AIRFOIL SECTIONS*

By Samuel M. Dollyhigh
Langley Research Center

SUMMARY

An experimental investigation has been made in the Mach number range from 1.60 to 2.86 to determine the longitudinal and lateral aerodynamic characteristics of a variable-sweep fighter configuration with supercritical airfoil sections, twin rectangular inlets, twin vertical tails, and boom-mounted aft horizontal tails. The results of the investigation indicated that the configuration had good longitudinal stability characteristics and a relatively high horizontal-tail control effectiveness. This horizontal-tail effectiveness, coupled with relatively high levels of zero-lift pitching moment, results in an instantaneous normal-acceleration capability of approximately 10g for the configuration at a Mach number of 1.60 and an altitude of 10 668 m (35 000 ft). Indications were that the normal-acceleration capability could be increased somewhat by reducing the longitudinal stability of the configuration. The lateral-stability results, however, indicated rather poor directional characteristics for an angle of attack greater than 10°. For the Mach number range of the tests, static directional stability was maintained only to angles of attack of 10° to 12°, which were well below the angles of attack at which the configuration had longitudinal trim capability.

INTRODUCTION

The National Aeronautics and Space Administration has recently completed a study of advanced configuration concepts applicable to fighter aircraft to assess attainable performance levels and to provide a focal point for current and future research programs. One of the configurations studied was a variable-sweep fighter, designated LFAX 4, which incorporated a supercritical-wing airfoil section in an effort to provide the good subsonic and supersonic aerodynamic characteristics required for multimission capability. In order to minimize the shift in aerodynamic center with wing sweep and thus avoid large static margins at supersonic speeds, an outboard wing-pivot location was selected. The

*Title, Unclassified.

twin horizontal tails were mounted low and outboard on booms to provide a uniform variation of pitching moment with lift and to provide good control effectiveness and high instantaneous normal-acceleration capability.

The LFAX 4 was designed to have minimum wave drag at a Mach number of 1.60 by a computer program that evolved from the method discussed in reference 1 and good drag due to lift and pitching-moment characteristics at a Mach number of 1.60 by modifying the wing-twist distribution by the method of reference 2. Because of the importance of good subsonic performance in a fighter with multimission capability, the wing-camber distribution was designed from subsonic considerations.

The purpose of the present investigation was to determine the experimental longitudinal and lateral aerodynamic characteristics of the LFAX 4 configuration at supersonic speeds. Wind-tunnel tests of a scaled model of the LFAX 4 were conducted in the Langley Unitary Plan wind tunnel at Mach numbers from 1.60 to 2.86. The results of the wind-tunnel investigation are reported herein.

SYMBOLS

The longitudinal results ($\beta = 0^{o}$) are referred to the wind-axis system, and the lateral results are referred to the body-axis system. All coefficients are based on the geometric characteristics of the wing in the 30^{o} leading-edge-sweep position (with leading and trailing edges projected into plane of symmetry). The moment reference point was located at fuselage station 54.935 cm (21.628 in.).

Measurements and calculations were made in U.S. Customary Units. They are presented herein in the International System of Units (SI) with the equivalent values given parenthetically in the U.S. Customary Units.

A	aspect ratio
b	wing span
c	aerodynamic chord
$\bar{c}$	mean aerodynamic chord
C_D	drag coefficient, $\frac{\text{Drag}}{qS}$
$C_{D,b}$	base-drag coefficient, $\frac{\text{Base drag}}{qS}$

$C_{D,c}$ chamber-drag coefficient, $\frac{\text{Chamber drag}}{qS}$

$C_{D,i}$ internal-drag coefficient, $\frac{\text{Internal drag}}{qS}$

$C_{D,o}$ drag coefficient at zero lift

$\frac{\Delta C_D}{C_L^2}$ drag-due-to-lift parameter

C_L lift coefficient, $\frac{\text{Lift}}{qS}$

C_{L_α} slope of lift curve, per deg

C_l rolling-moment coefficient, $\frac{\text{Rolling moment}}{qSb}$

C_{l_β} effective-dihedral parameter, $\frac{\Delta C_l}{\Delta \beta}$, per deg (where $\beta = 0^o$ and 3^o)

C_m pitching-moment coefficient, $\frac{\text{Pitching moment}}{qS\bar{c}}$

$\frac{\partial C_m}{\partial C_L}$ longitudinal stability parameter

$\frac{\partial C_m}{\partial \delta_h}$ pitching effectiveness of horizontal tail

C_n yawing-moment coefficient, $\frac{\text{Yawing moment}}{qSb}$

C_{n_β} directional-stability parameter, $\frac{\Delta C_n}{\Delta \beta}$, per deg (where $\beta = 0^o$ and 3^o)

C_Y side-force coefficient, $\frac{\text{Side force}}{qS}$

C_{Y_β} side-force parameter, $\frac{\Delta C_Y}{\Delta \beta}$, per deg (where $\beta = 0^o$ and 3^o)

L/D lift-drag ratio

M free-stream Mach number

q	free-stream dynamic pressure
S	reference area of wing including fuselage intercept
x	longitudinal direction
y	lateral direction
z	vertical direction
α	angle of attack, deg
β	angle of sideslip, deg
Γ	dihedral angle, deg
δ_h	horizontal-tail deflection angle, positive when trailing edge is down, deg
Λ	leading-edge sweep angle, deg

Model components:

B	body
H	horizontal tail
U	ventral fin
V	vertical tail
W	wing

Subscript:

max	maximum

DESCRIPTION OF MODEL

A three-view drawing of the complete model configuration is shown in figure 1, and some geometric characteristics are given in table I. A photograph of the model is

presented in figure 2. The configuration incorporates a fuselage; a variable-sweep wing with horizontal ramp-type inlets located ahead of the wings; twin horizontal tails, twin vertical tails, and twin ventral fins mounted on booms; and lateral strakes on the forebody.

The wing on this configuration utilized the variable-sweep concept with an outboard pivot and had a supercritical airfoil section. The streamwise airfoil ordinates are defined with the wing in the 30° sweep position. The airfoil ordinates are presented in table II for three spanwise stations. The wing had a thickness ratio of 11.0 percent at the wing pivot station and 10.0 percent at the wing tip. The range of wing leading-edge sweep angle was from 23° (forward position) to 71° (aft position). There was an intermediate sweep angle of 30° for subsonic cruise and maneuver that was used as the reference sweep angle. The model was tested with the wing fixed in the swept mode. The wing in the aft sweep position ($\Lambda = 71^{\circ}$) had optimum twist for a Mach number of 1.6.

The configuration employed low twin horizontal tails with an airfoil section that was 4 percent biconvex. The horizontal tails had a negative dihedral of 9.3°. The twin vertical tails were toed-in at an angle of 12° and had an airfoil section that was of a 3.5 percent half-biconvex. The ventral fins were made from a 0.318-cm-thick (0.125-in.) flat plate with a beveled-edge angle of 30°. The tail surfaces and ventral fins could be removed from the model, and the horizontal tail could be deflected over a range from 5° to -20°.

TESTS AND CORRECTIONS

The tests were conducted in the Langley Unitary Plan wind tunnel at Mach numbers of 1.60, 2.00, 2.50, and 2.86. The Reynolds number was 9.8×10^6 per meter (3.0×10^6 per foot) for all tests except those at the higher angles of attack at Mach numbers of 1.60, 2.00, and 2.50. For these tests, the Reynolds number was reduced to 8.2×10^6 per meter (2.5×10^6 per foot) and 6.6×10^6 per meter (2.0×10^6 per foot) in order to stay within balance load limits. The dewpoint was maintained sufficiently low to prevent measurable condensation effects in the test section. The angle-of-attack range was from approximately 6° to 23°, and the angle of sideslip was from approximately -4° to 6°. In order to assure boundary-layer transition to turbulent flow, 0.16-cm-wide (1/16 in.) transition strips of No. 50 carborundum grit were placed on the body 3.05 cm (1.2 in.) aft of the nose of the model and 1.02 cm (0.40 in.) streamwise on the wings, tails, ventral fins, inlet ramps, and external inlet surfaces.

Aerodynamic forces and moments on the model were measured by means of a six-component strain-gage balance which was housed within the model. The balance was attached to a sting which in turn was rigidly fastened to the tunnel support system. Balance-chamber static pressures were measured with pressure tubes located in the vicinity of the balance. The internal-flow total and static pressures were measured in

each duct with a rake consisting of 13 total-pressure tubes and 5 static-pressure tubes; the rakes were placed 0.25 cm (0.10 in.) inside the exit of the ducts. The base pressure was measured by two pressure tubes which were fastened to the sting and held in proximity to the base of the model. The internal-flow pressure rakes and base-pressure tubes were removed during the force-measurement tests. Corrections to the indicated model angles of attack and sideslip have been made for both tunnel-airflow misalinement and deflection of the balance and sting under load. Figure 3 documents that the aerodynamic characteristics for the model upright and inverted are the same. The drag data presented herein have been corrected for internal drag and also corrected to the condition of free-stream static pressure at the model base and in the balance chamber. Figures 4 to 6 show the values of chamber, base, and internal drag which were used to correct the drag data.

Fluorene sublimation material was used to determine the natural-transition locations on the clean model at zero lift coefficients. An increment in skin friction was analytically calculated between the data for natural transition and the condition of all-turbulent flow behind the transition strips. This correction was added to the natural-transition data. The trip drag was considered to be the difference between the drag data with transition strips on the model and the corrected natural-transition data. The trip drag is presented, but the wind-tunnel data are not corrected for trip drag.

The geometry of the aft end of the LFAX 4 configuration was such that with internal flow there was interference between the sting and model booms. In order to estimate the effects of this interference, the aft end of the model was "extended" to the end of the tail by using a sleeve attached to the sting. The sleeve as pictured in figure 7 was a continuation of the base of the model and was attached to the sting with a gap approximately 0.102 cm (0.040 in.) between the model and sleeve. The gap between model and sleeve was sufficient to insure that no forces on the sleeve were measured by the model balance. The sleeve prevented the internal flow from expanding and resulting in interference between the sting and model booms; thus, the actual flight condition was more nearly represented. The effects on longitudinal characteristics of adding the aft body extension are presented, but no corrections due to removing the estimated sting interference are applied to the remaining data.

PRESENTATION OF RESULTS

The moment reference point is on the body axis 54.935 cm (21.628 in.) from the nose of the model. The results are presented in the following figures:

	Figure
Upright and inverted characteristics, sleeve off	3
Base-drag coefficient	4
Chamber-drag coefficient	5

	Figure
Internal-drag coefficient	6
Longitudinal control characteristics	8
Summary of longitudinal control characteristics	9
Longitudinal trim characteristics	10
Effects of components on longitudinal characteristics	11
Effects of afterbody extension on longitudinal characteristics	12
Trip drag	13
Sublimation photographs	14
Oil-flow photographs	15
Lateral characteristics	16
Effects of vertical components on lateral characteristics at $\alpha \approx -1^{\circ}$	17
Effects of vertical components on lateral characteristics at $\alpha \approx 6^{\circ}$	18
Effects of vertical components on sideslip derivatives	19
Effects of tail deflection on sideslip derivatives	20

DISCUSSION

Longitudinal Characteristics

The longitudinal aerodynamic and control characteristics of the basic LFAX 4 configuration are shown in figure 8 for the test Mach numbers from 1.60 to 2.86. The configuration appears to have good stability characteristics and good horizontal-tail control effectiveness throughout the Mach number range of the tests. The linearity of the pitching-moment variation with lift and the control-surface effectiveness are due principally to the low, outboard location of the twin horizontal tails. As presented, the configuration probably has excessive stability for the supersonic conditions. The center-of-gravity location upon which the data of figure 8 are based is 54.935 cm (21.626 in.) aft of the nose and is the reference center of gravity used in the NASA fighter study mentioned in the Introduction to provide a static stability margin of 1.5 percent at a sweep angle of 23° and low subsonic Mach numbers. However, as the wing is shifted, the center of gravity moves, and a more realistic supersonic center-of-gravity location would be 56.208 cm (22.129 in.) aft of the nose. This condition would be a rearward shift in the center of gravity of 9 percent $\bar{c}$.

A summary plot of the variations of some of the pertinent longitudinal parameters with Mach number is shown in figure 9. The principal points to note in this figure are the relatively high levels of stability $\left(\partial C_m/\partial C_L\right)$ and control-surface effectiveness $\left(\partial C_m/\partial \delta_h\right)$ which are indicated for the LFAX 4 configuration.

Figure 10 presents the trim values of δ_h and C_D as a function of C_L at each Mach number. Again, it should be pointed out that the effect of center-of-gravity shift

with wing-weight shift would change this figure significantly. The aft center-of-gravity location would result in a lower stability level and hence lower drag at trim. At a Mach number of 1.60, a wing loading of 3615 N/m^2 (75.5 lb/ft^2) based on a reference area for $\Lambda = 30^o$, and an altitude of 10 668 m (35 000 ft), the lift coefficient required for level flight would be approximately 0.084. The results of figure 10 indicate that a maximum trimmed C_L of 0.84 is available at $M = 1.60$ and $\delta_h = -20^o$. Thus, the instantaneous normal acceleration (ratio of maximum C_L to C_L required for level flight) is approximately 10g. Since normal acceleration is a function of static margin, the value of instantaneous normal acceleration for the lower static-margin case would be even greater.

Figure 11 presents the effects of the vertical tails and ventral fins on the longitudinal characteristics of the model. The only unusual characteristic to be noted from this data is that the vertical tail provides a noticeable contribution to C_m over most of the C_L range. This is brought about by a slight down load on the vertical tail because of the 12^o toe-in with a region of separated flow around the inboard root chord of the vertical tail.

The effects on the longitudinal characteristics of taking the sting interference out by extending the model aft and past the booms with a sleeve attached to the sting are presented in figure 12. As expected, there is very little effect on the lift curve and pitching moment, but the drag increment due to sting interference is large enough, at least at the lower Mach numbers, to warrant consideration when working with the other longitudinal data.

The trip drag calculated by correcting free-transition data for the difference in skin friction between laminar turbulent flow from the grit location to the natural-transition location is shown in figure 13. At the lower Mach numbers, the grit drag is significant enough to be included in extrapolating the data. Figure 14 presents series of fluorene sublimation photographs used in calculating the trip drag in a time sequence at each Mach number. Also, oil-flow photographs at Mach numbers of 1.60 and 2.86 are presented in figure 15. At each of these Mach numbers an oil-flow photograph was taken at approximately zero lift, maximum lift-drag ratio, and a condition in between.

Sideslip Characteristics

The variations of the lateral coefficients with angle of sideslip for the complete configuration at angles of attack from approximately -2^o to 7^o are shown in figure 16 for $M = 1.60$ to 2.86. These results are intended to show the closeness to linearity of the lateral characteristics with β since all subsequent sideslip derivatives were obtained at sideslip angles of approximately 0^o and 3^o. Within this range, the variations are linear so that the values of sideslip derivative are considered valid.

The effects of the vertical surfaces on the variation of lateral coefficients with angle of sideslip for angles of attack of approximately -1° and 6° are presented in figures 17 and 18, respectively. The variations are linear and indicate no unusual characteristics. The sideslip derivatives for the model with and without the vertical tails and ventral fins are shown in figure 19 as a function of angle of attack. The complete configuration indicates relatively poor directional stability for the reference moment center used, with the static directional stability being maintained only to angles of attack between 10° and 12° for the test Mach number range. The ventral fins were effective in increasing the level of C_{n_β} throughout the angle-of-attack range at each Mach number. Except at $M = 1.60$ and angles of attack less than -4°, the complete configuration indicates positive effective dihedral $\left(-C_{l_\beta}\right)$ throughout the angle-of-attack range at each Mach number.

The effect of a horizontal-tail deflection of -20° on the sideslip derivatives over the Mach number range is shown in figure 20. In general, the effect of negative deflection is slightly favorable in that C_{n_β} is increased and the magnitude of C_{l_β} is reduced, especially at the two highest Mach numbers.

CONCLUDING REMARKS

An investigation has been made in the Mach number range from 1.60 to 2.86 to determine the longitudinal and lateral aerodynamic characteristics of a fighter configuration utilizing a variable-sweep wing with supercritical airfoil sections, twin rectangular inlets, twin vertical tails, and boom-mounted aft horizontal tails.

The results of the investigation indicate good longitudinal stability and a high degree of horizontal-tail control effectiveness. The horizontal-tail effectiveness, coupled with a relatively high value of zero-lift pitching moment, results in a rather high normal-acceleration capability. In addition, the results indicate relatively poor static directional stability, with directional control being maintained only to angles of attack between 10° and 12° over the test Mach number range.

Langley Research Center,
National Aeronautics and Space Administration,
Hampton, Va., April 28, 1971.

REFERENCES

1. Harris, Roy V., Jr.: An Analysis and Correlation of Aircraft Wave Drag. NASA TM X-947, 1964.

2. Middleton, Wilbur D.; and Carlson, Harry W.: Numerical Method of Estimating and Optimizing Supersonic Aerodynamic Characteristics of Arbitrary Planform Wings. J. Aircraft, vol. 2, no. 4, July-Aug. 1965, pp. 261-265.

TABLE I.- GEOMETRIC CHARACTERISTICS

Wing:	
Aspect ratio, A, at –	
$\Lambda = 30^{o}$	7.03
$\Lambda = 71^{o}$	2.36
Leading-edge sweep, Λ:	
Minimum, deg	23
Maximum, deg	71
Reference, deg	30
Mean aerodynamic chord, $\bar{c}$, cm (in.)	14.194 (5.588)
Airfoil section	Supercritical
Area, S, including fuselage intercept, cm^2 (in^2)	1007.346 (156.139)
Maximum thickness at $\Lambda = 30^{o}$:	
Pivot station, percent	11.0
Tip, percent	10.0
Horizontal tail (exposed):	
Area, cm^2 (in^2)	227.980 (35.337)
Aspect ratio	2.113
Span, cm (in.)	21.946 (8.64)
Dihedral angle, Γ, deg	-9.3
Leading-edge sweep, Λ, deg	48
Mean aerodynamic chord, $\bar{c}$, cm (in.)	10.993 (4.328)
Airfoil section	4% biconvex
Vertical tail (each):	
Aspect ratio, A	0.862
Area, cm^2 (in^2)	108.032 (16.745)
Span, cm (in.)	9.652 (3.800)
Chord, c, cm (in.)	12.621 (4.969)
Leading-edge sweep, deg	58
Airfoil section	3.5% half biconvex
Toe-in, deg	12
Inlet area (one duct), cm^2 (in^2)	11.613 (1.800)
Exit area (one duct), cm^2 (in^2)	17.039 (2.641)
Chamber area, cm^2 (in^2)	15.619 (2.421)
Base area (excluding chamber and exit areas), cm^2 (in^2)	9.213 (1.428)

TABLE II.- AIRFOIL COORDINATES AT 30° SWEEP

x/c	Ordinates, z/c, at –					
	$\frac{y}{b/2} = 0.3636$ (pivot station)		$\frac{y}{b/2} = 0.5393$		$\frac{y}{b/2} = 1.000$ (theoretical wing tip)	
	Upper surface	Lower surface	Upper surface	Lower surface	Upper surface	Lower surface
0	0.0000	0.0000	0.0090	0.0090	0.0595	0.0595
.0125	.0217	-.0217	.0305	-.0127	.0800	.0387
.025	.0286	-.0275	.0376	-.0197	.0874	.0341
.050	.0362	-.0366	.0455	-.0291	.0961	.0287
.075	.0406	-.0425	.0502	-.0350	.1022	.0259
.100	.0441	-.0471	.0538	-.0385	.1071	.0238
.150	.0488	-.0526	.0589	-.0430	.1145	.0226
.200	.0521	-.0557	.0625	-.0444	.1207	.0238
.250	.0540	-.0561	.0650	-.0441	.1268	.0263
.300	.0560	-.0549	.0668	-.0426	.1318	.0291
.350	.0562	-.0530	.0679	-.0401	.1367	.0333
.400	.0557	-.0504	.0686	-.0365	.1412	.0382
.450	.0545	-.0463	.0692	-.0323	.1453	.0442
.500	.0528	-.0416	.0692	-.0271	.1490	.0521
.550	.0505	-.0359	.0690	-.0213	.1527	.0612
.600	.0479	-.0288	.0681	-.0139	.1552	.0718
.625	.0463	-.0248	.0677	-.0101	.1564	.0776
.650	.0444	-.0212	.0668	-.0060	.1572	.0833
.675	.0429	-.0168	.0659	-.0011	.1580	.0899
.700	.0410	-.0132	.0645	.0040	.1585	.0960
.725	.0390	-.0093	.0630	.0096	.1585	.1026
.750	.0374	-.0060	.0614	.0142	.1582	.1096
.775	.0349	-.0028	.0592	.0190	.1580	.1162
.800	.0324	.0000	.0569	.0229	.1572	.1219
.825	.0298	.0028	.0542	.0262	.1560	.1264
.850	.0269	.0047	.0513	.0287	.1544	.1305
.875	.0240	.0065	.0482	.0302	.1523	.1338
.900	.0200	.0068	.0439	.0305	.1494	.1351
.925	.0162	.0065	.0388	.0287	.1461	.1351
.950	.0118	.0052	.0329	.0255	.1420	.1326
.975	.0065	.0021	.0258	.0202	.1355	.1283
1.000	.0005	-.0025	.0175	.0135	.1280	.1220

$\frac{y}{b/2}$	L.E. radius
0.3636	0.0246c
.5393	.0242c
1.0000	.0221c

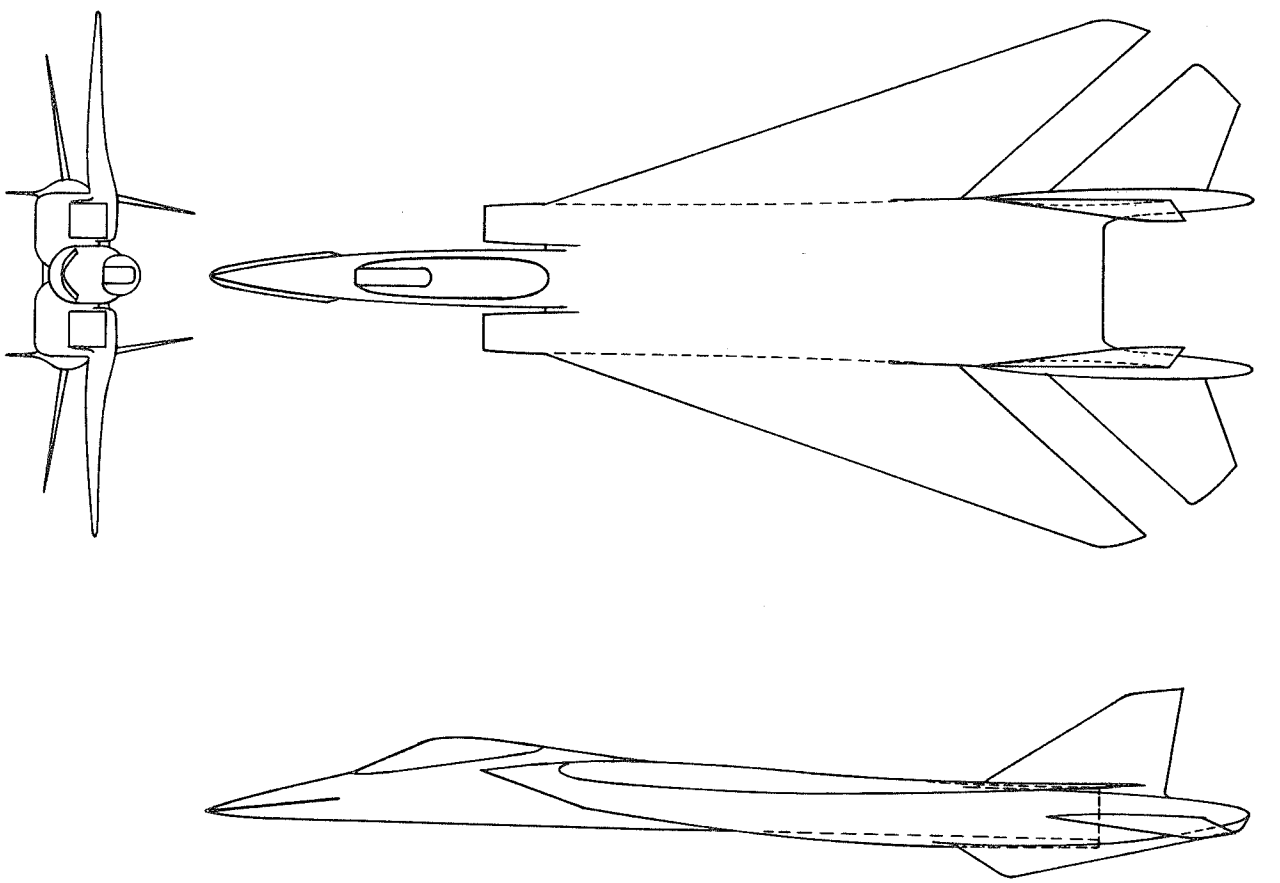

Figure 1.- Three-view drawing of model.

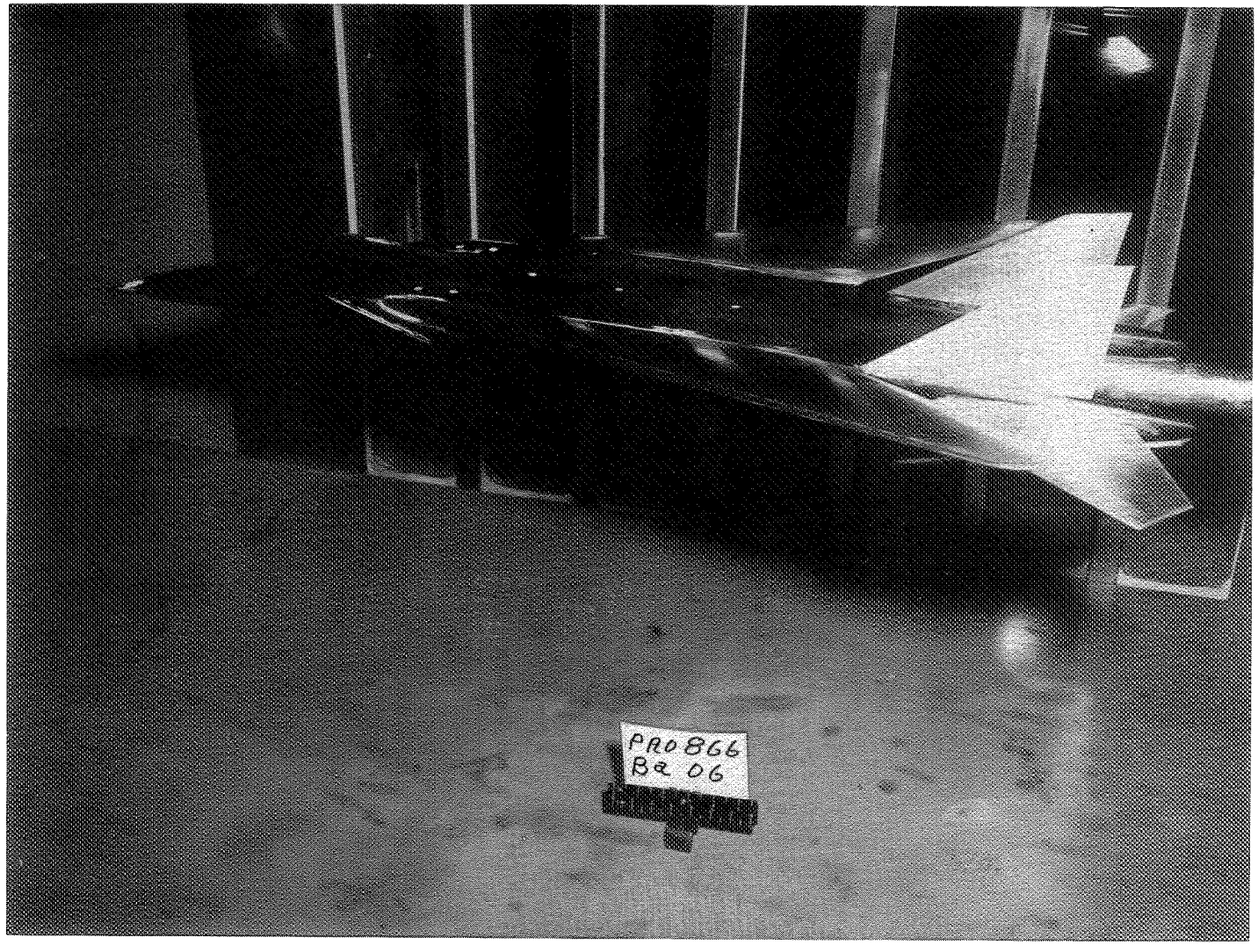

L-70-2620

Figure 2.- Photograph of model.

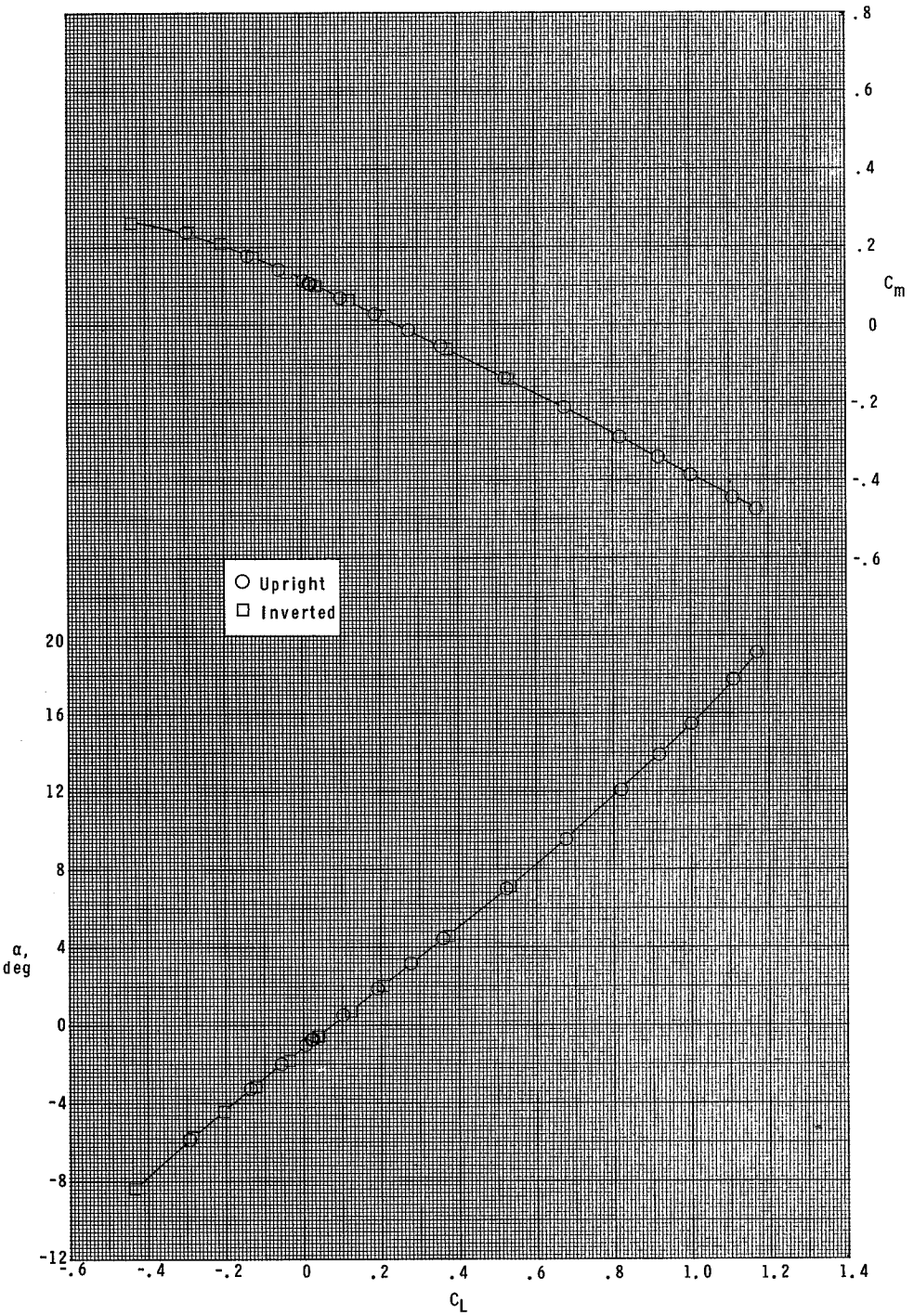

(a) M = 1.60.

Figure 3.- Aerodynamic characteristics for the model upright and inverted (sleeve off).

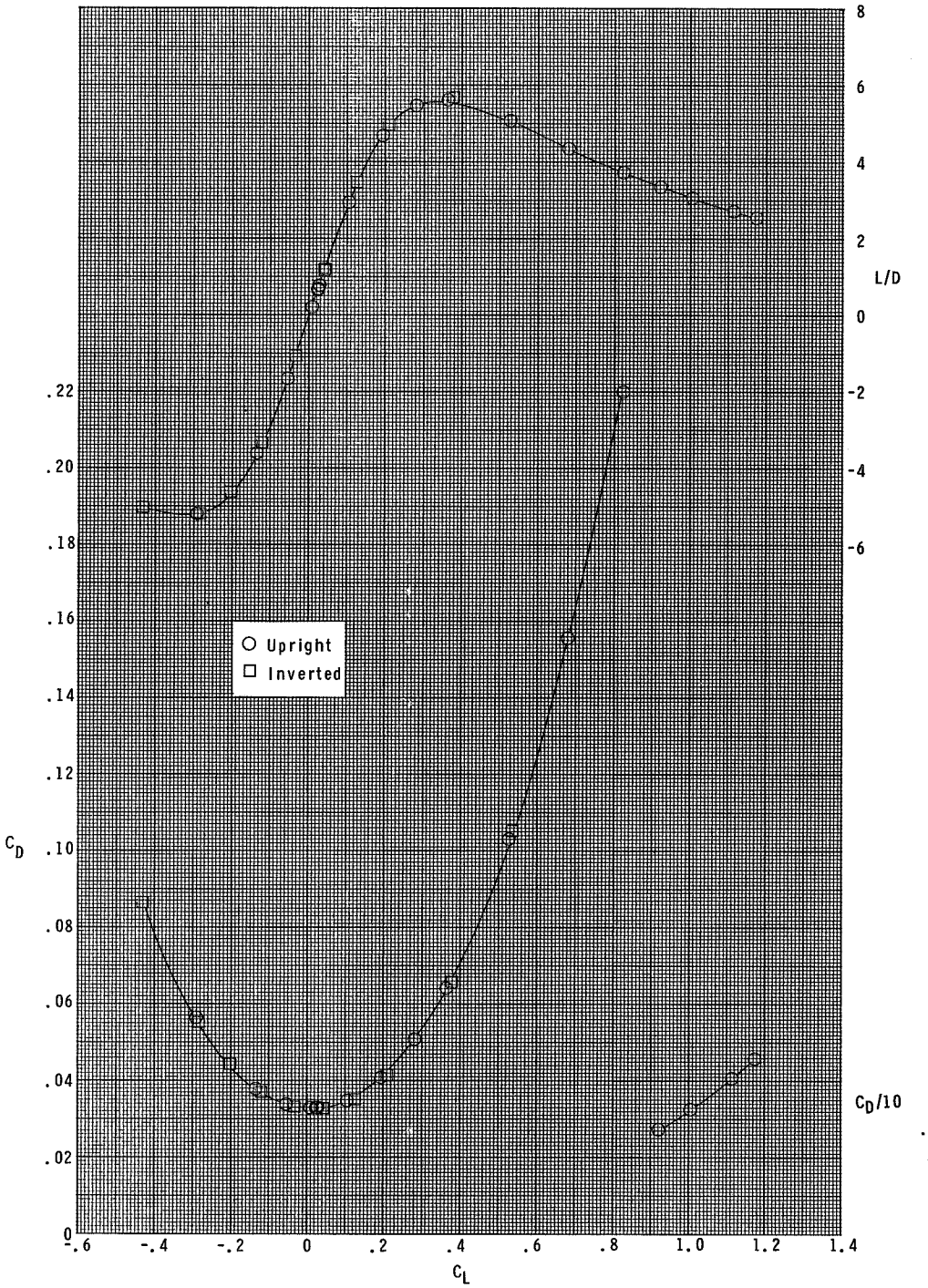

(a) Concluded.

Figure 3.- Continued.

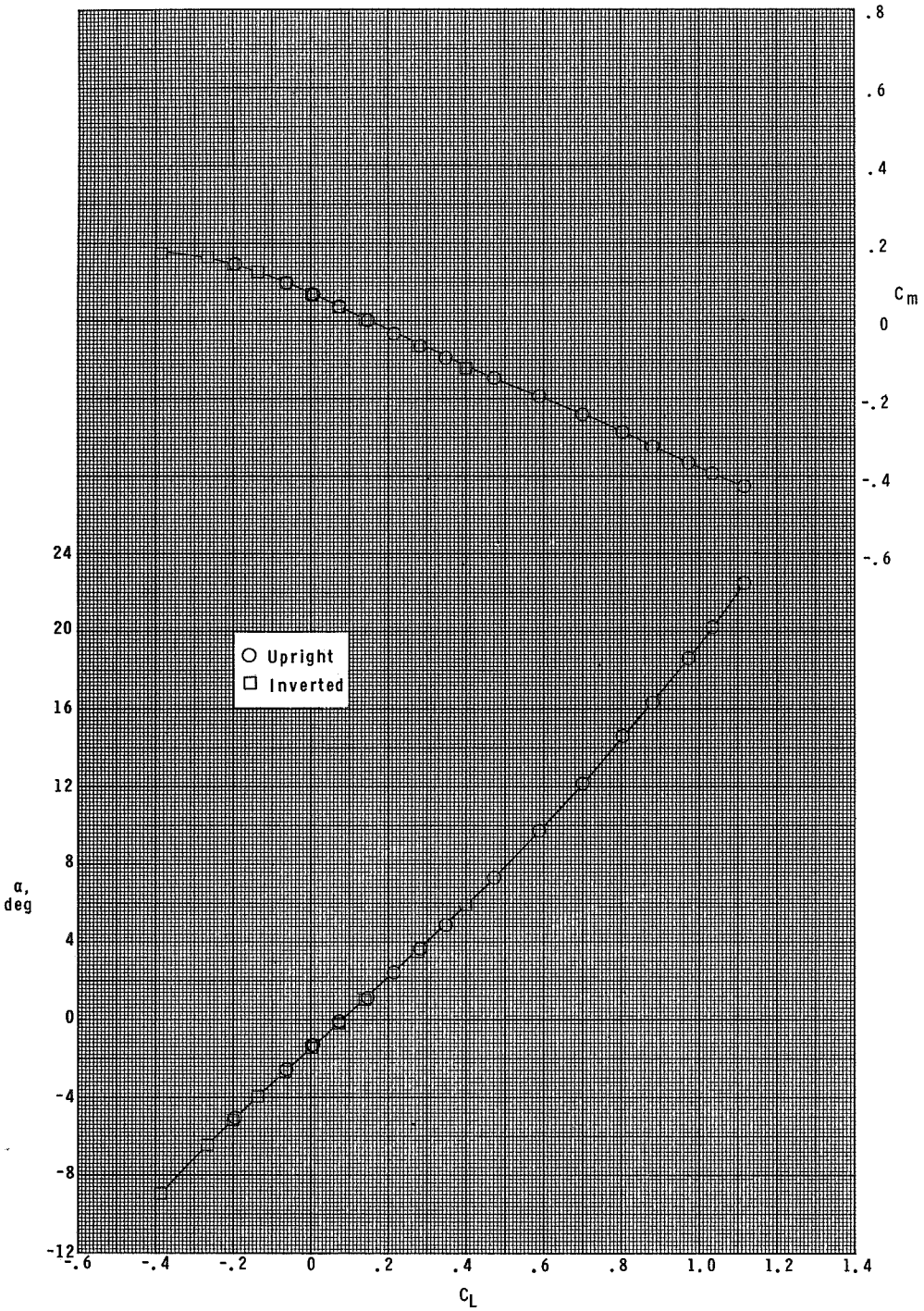

(b) M = 2.00.

Figure 3.- Continued.

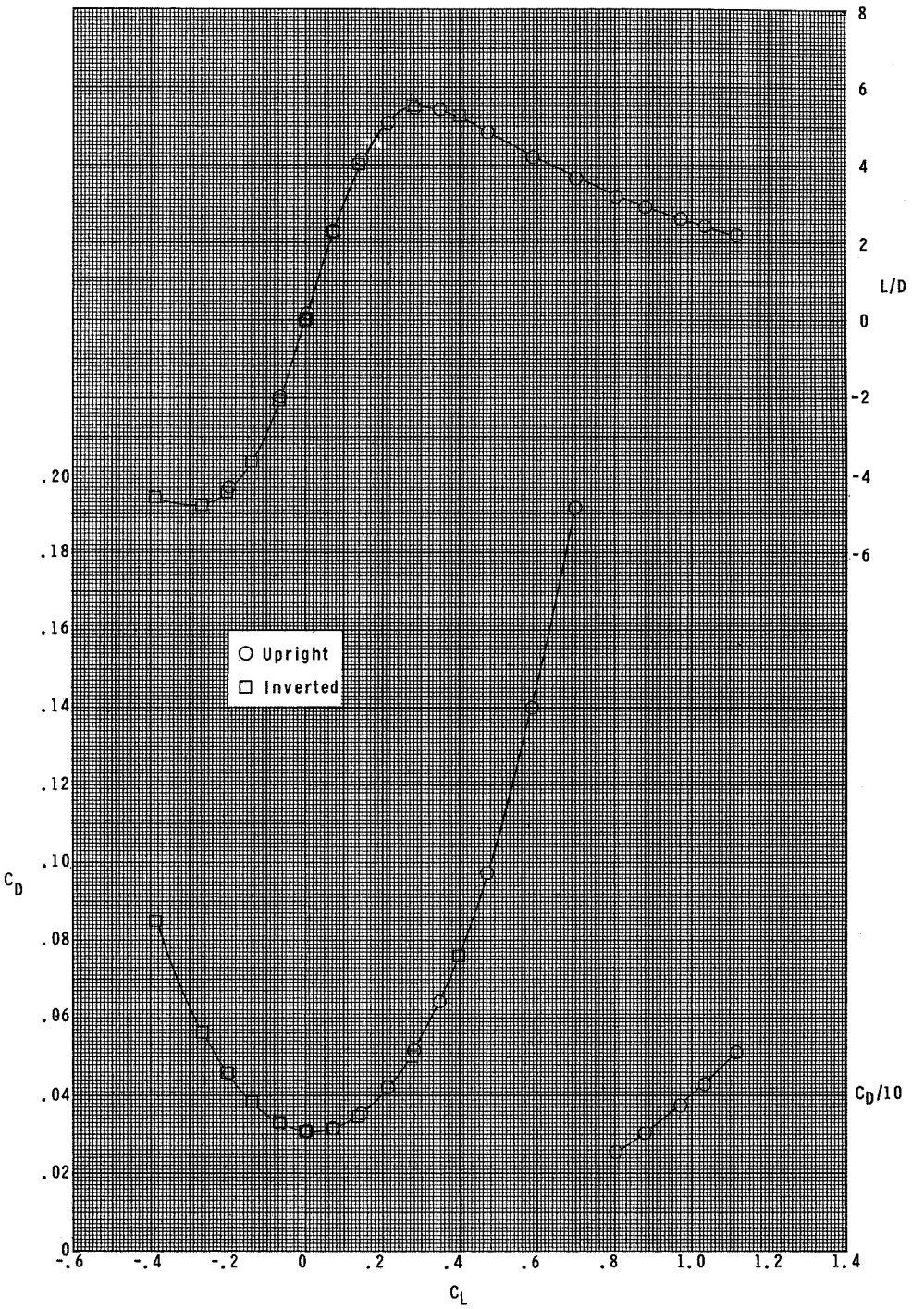

(b) Concluded.

Figure 3.- Continued.

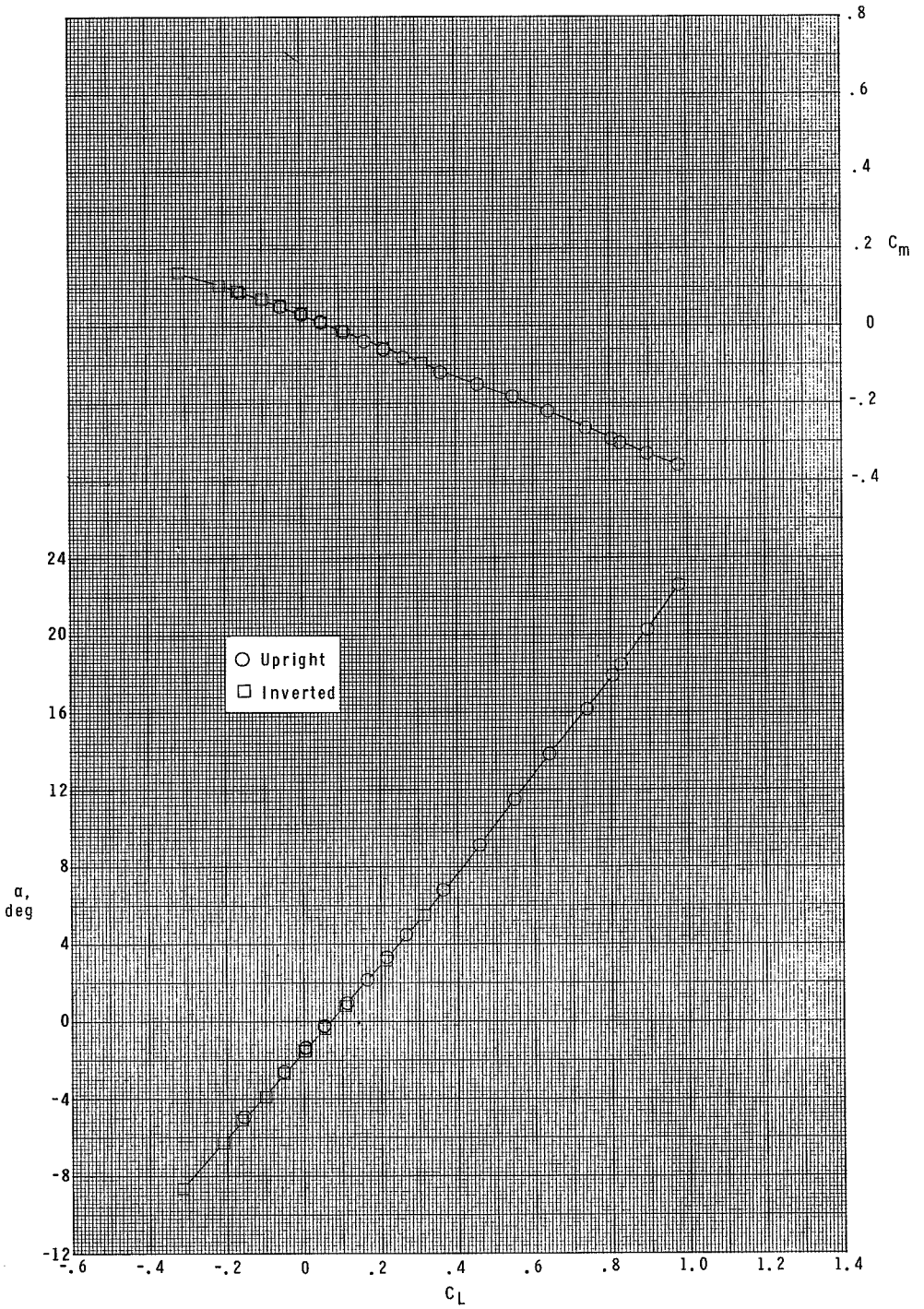

(c) M = 2.50.

Figure 3.- Continued.

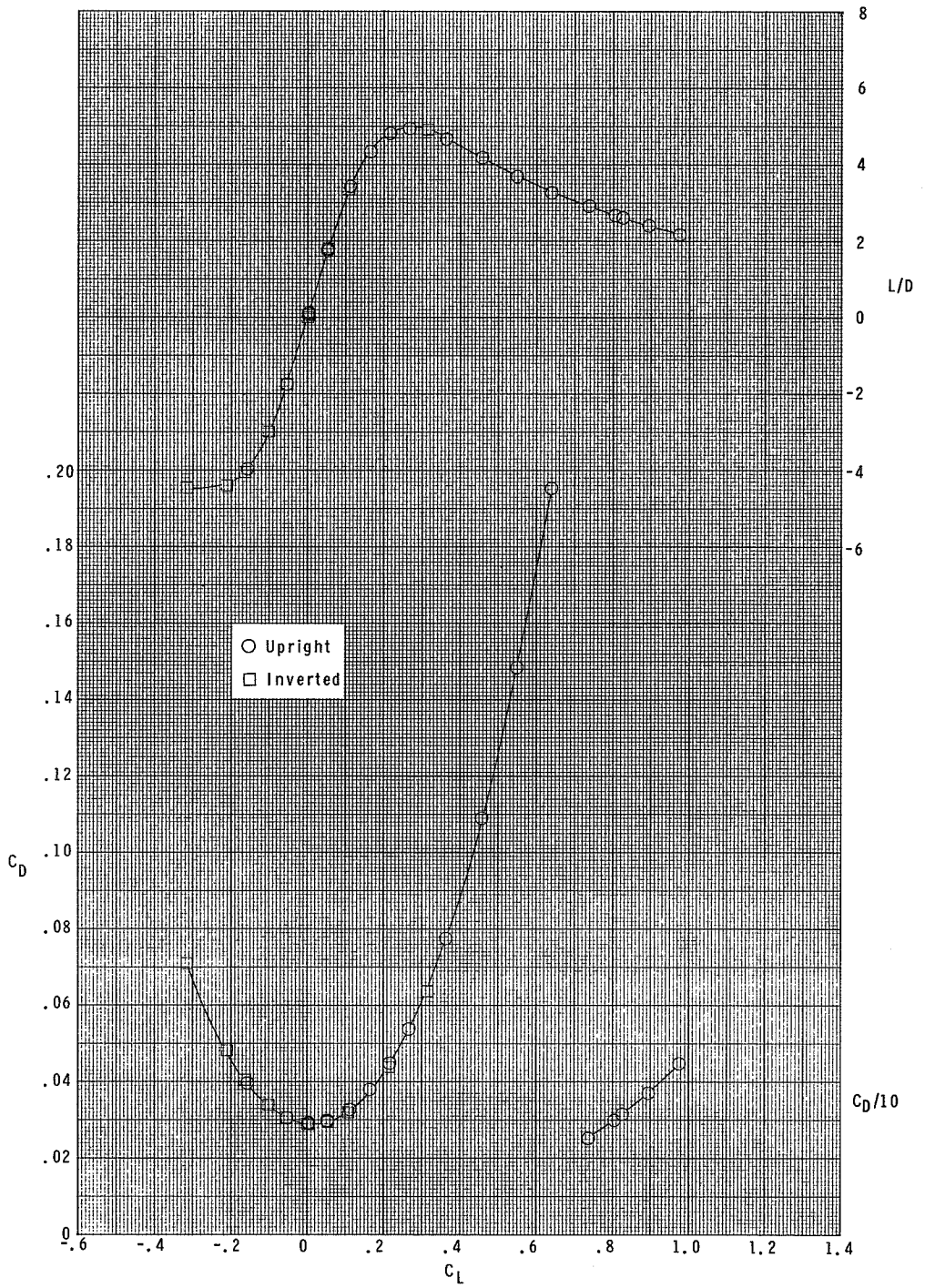

(c) Concluded.

Figure 3.- Continued.

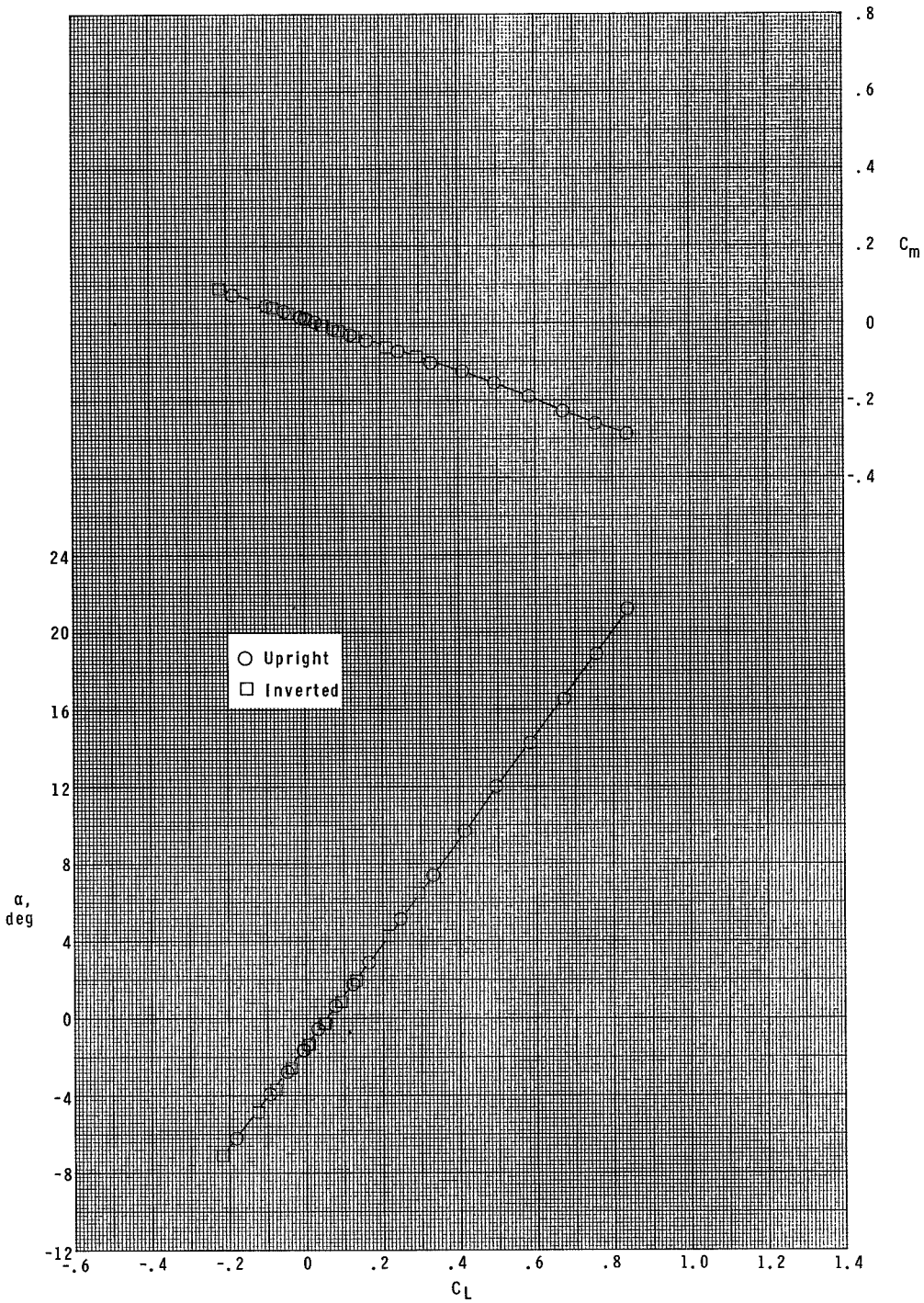

(d) M = 2.86.

Figure 3.- Continued.

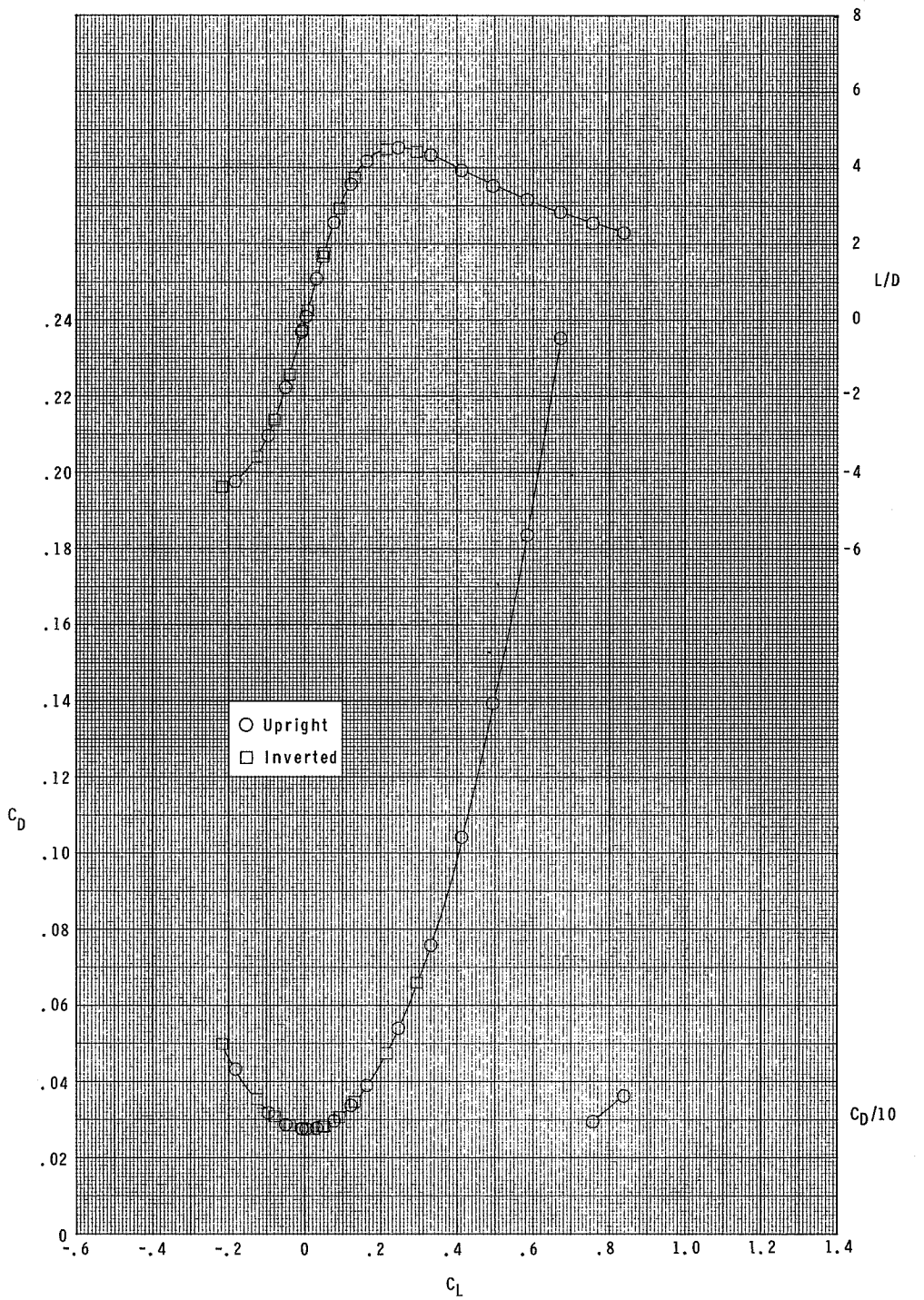

(d) Concluded.

Figure 3.- Concluded.

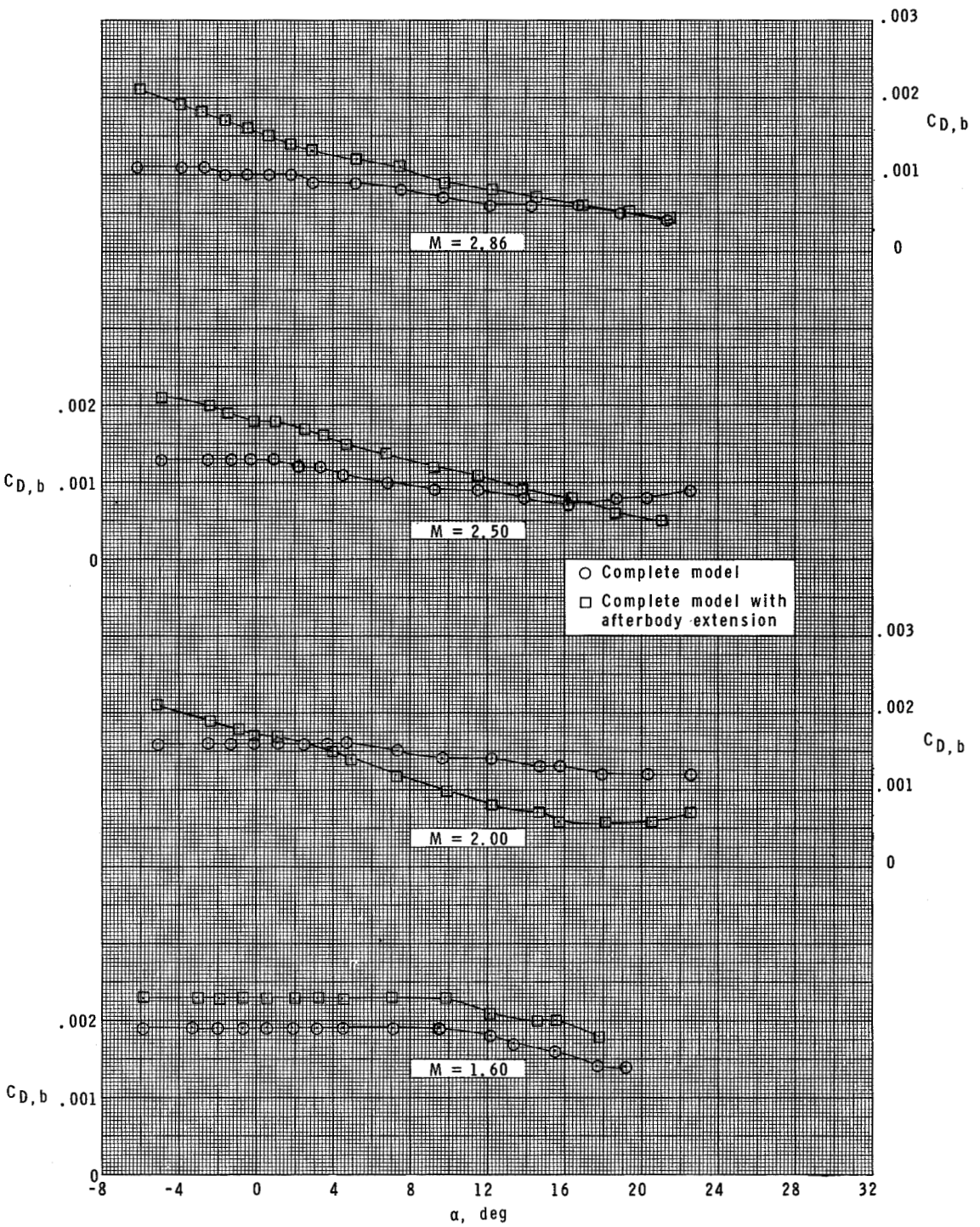

Figure 4.- Base-drag coefficient.

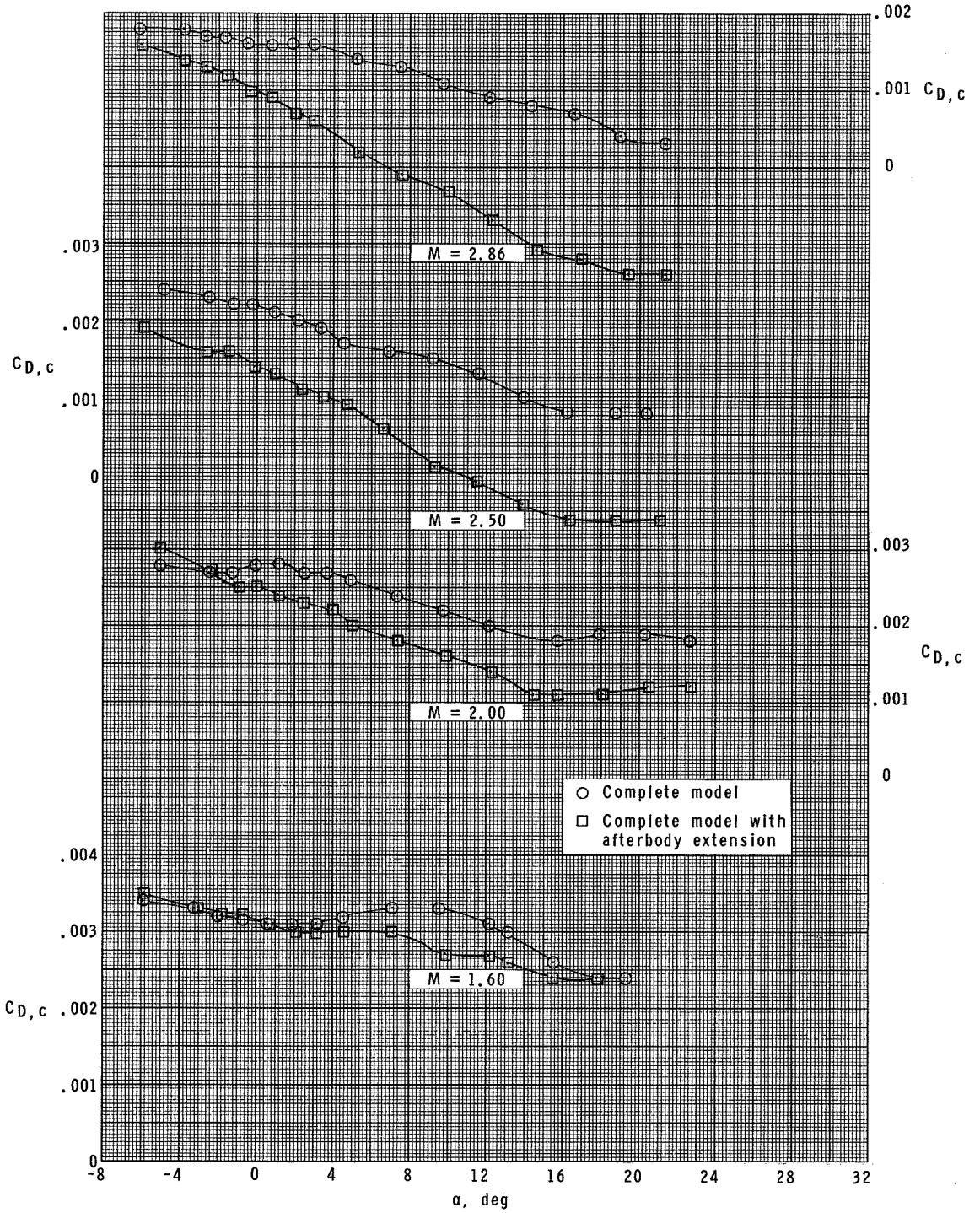

Figure 5.- Chamber-drag coefficient.

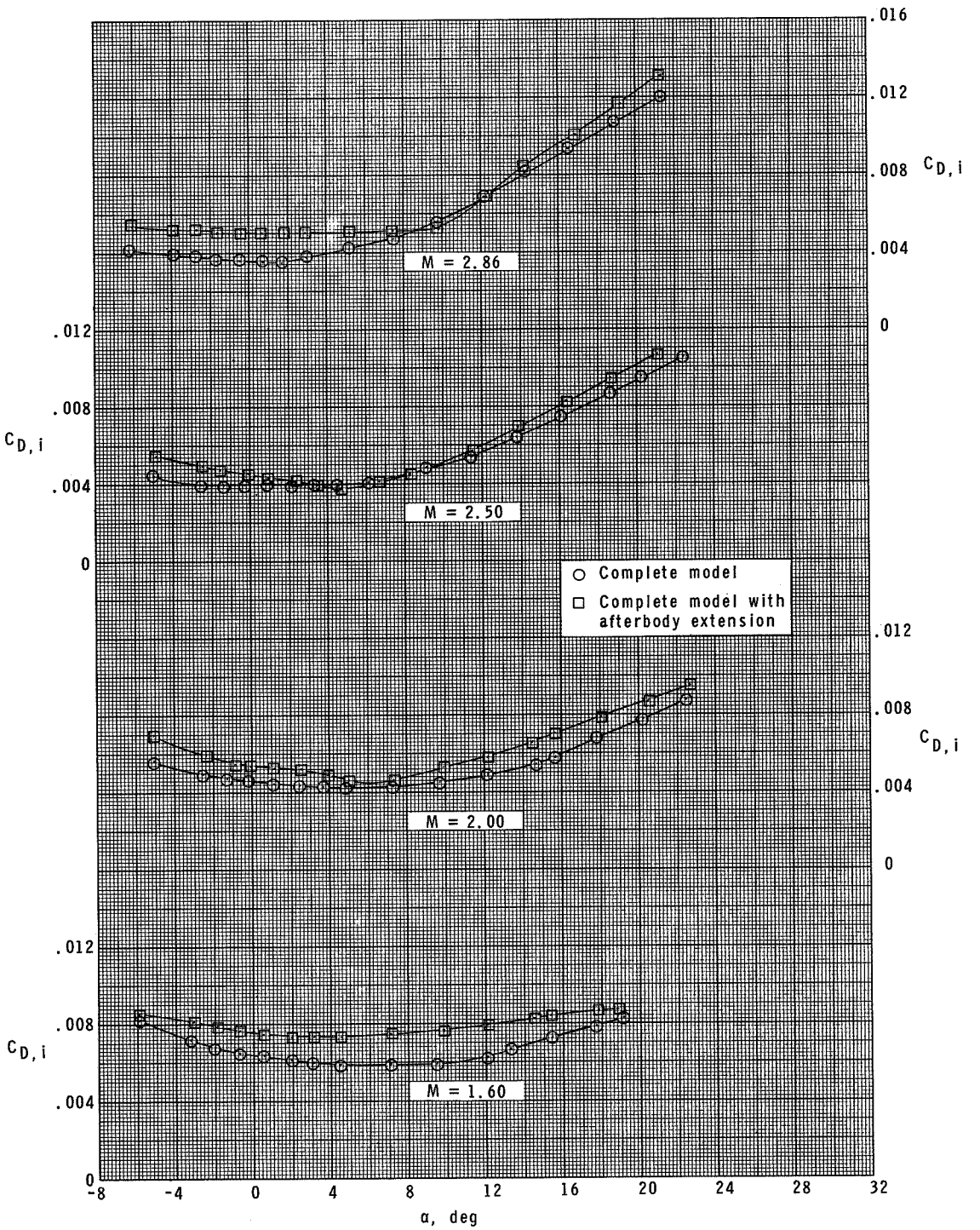

Figure 6.- Internal-drag coefficient.

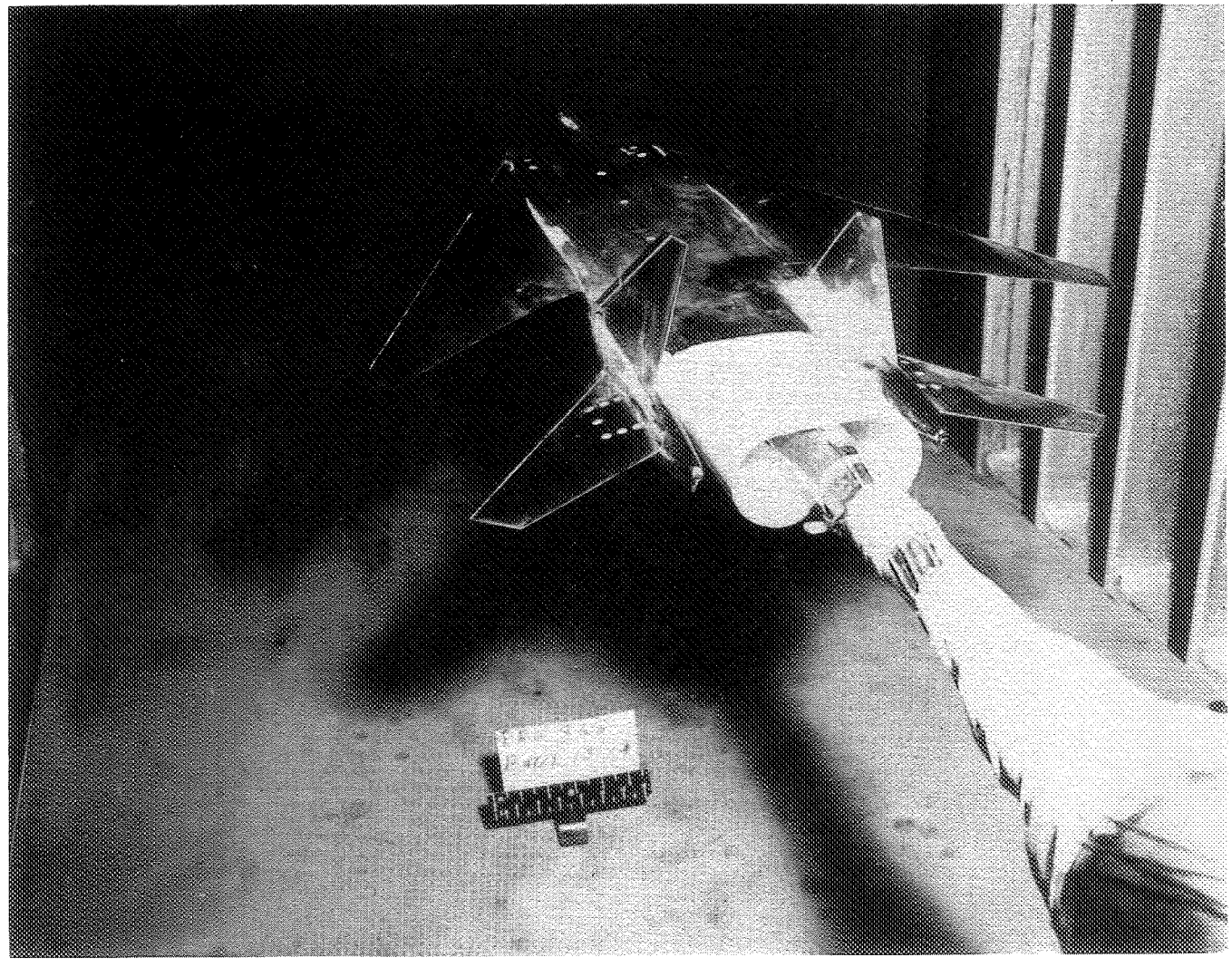

L-71-559

Figure 7.- Photograph of model with afterbody extension.

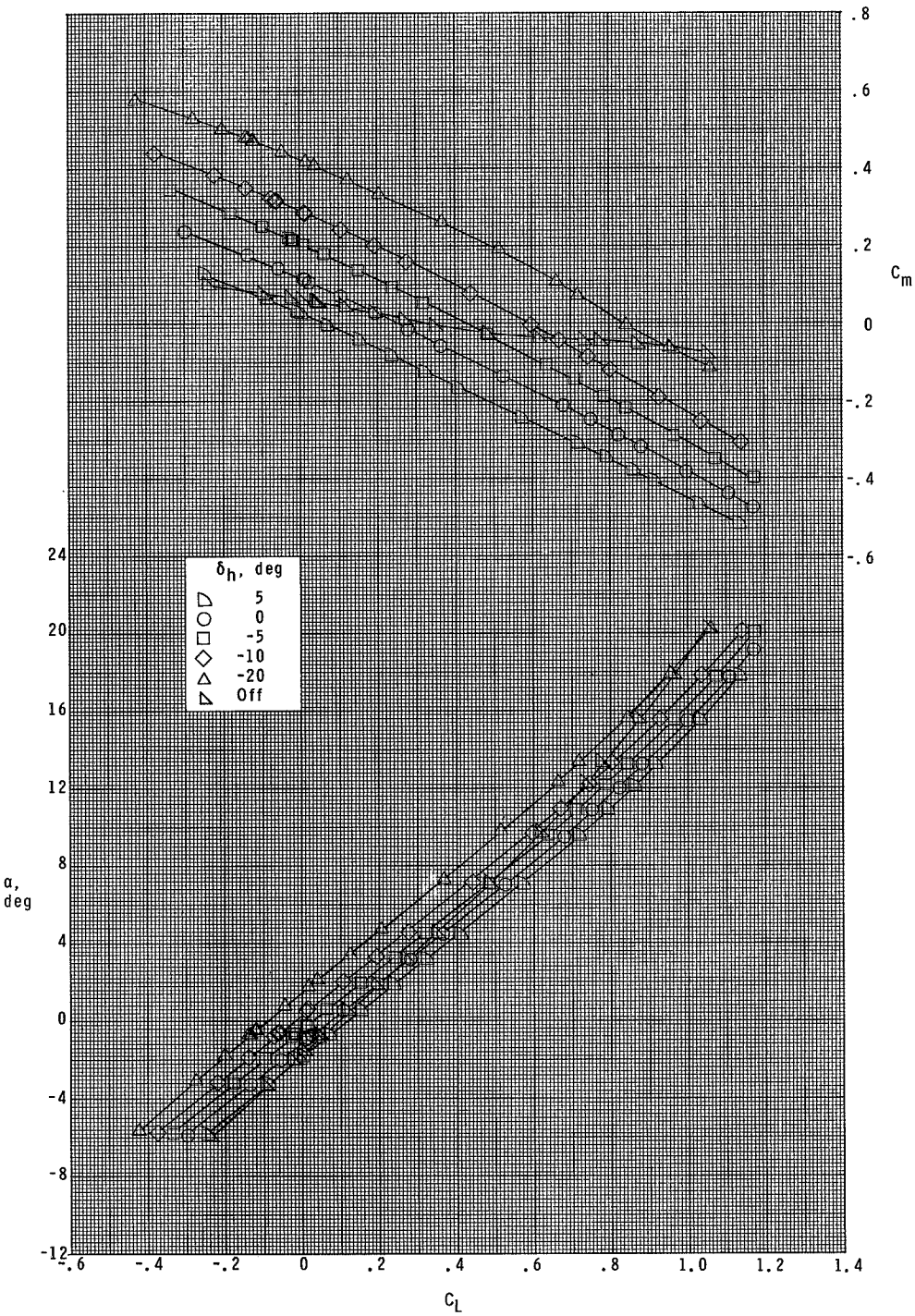

(a) M = 1.60.

Figure 8.- Longitudinal control characteristics.

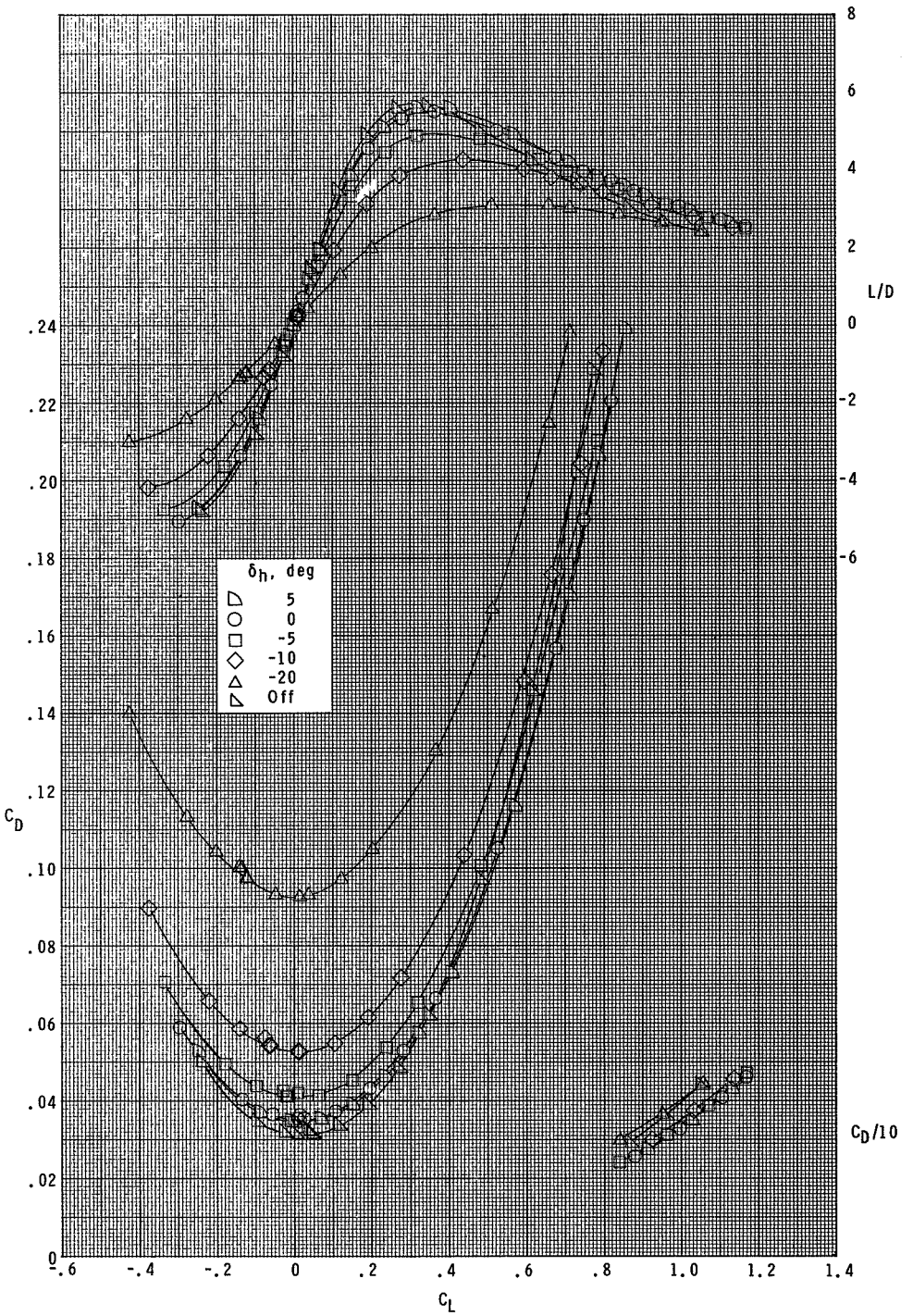

(a) Concluded.

Figure 8.- Continued.

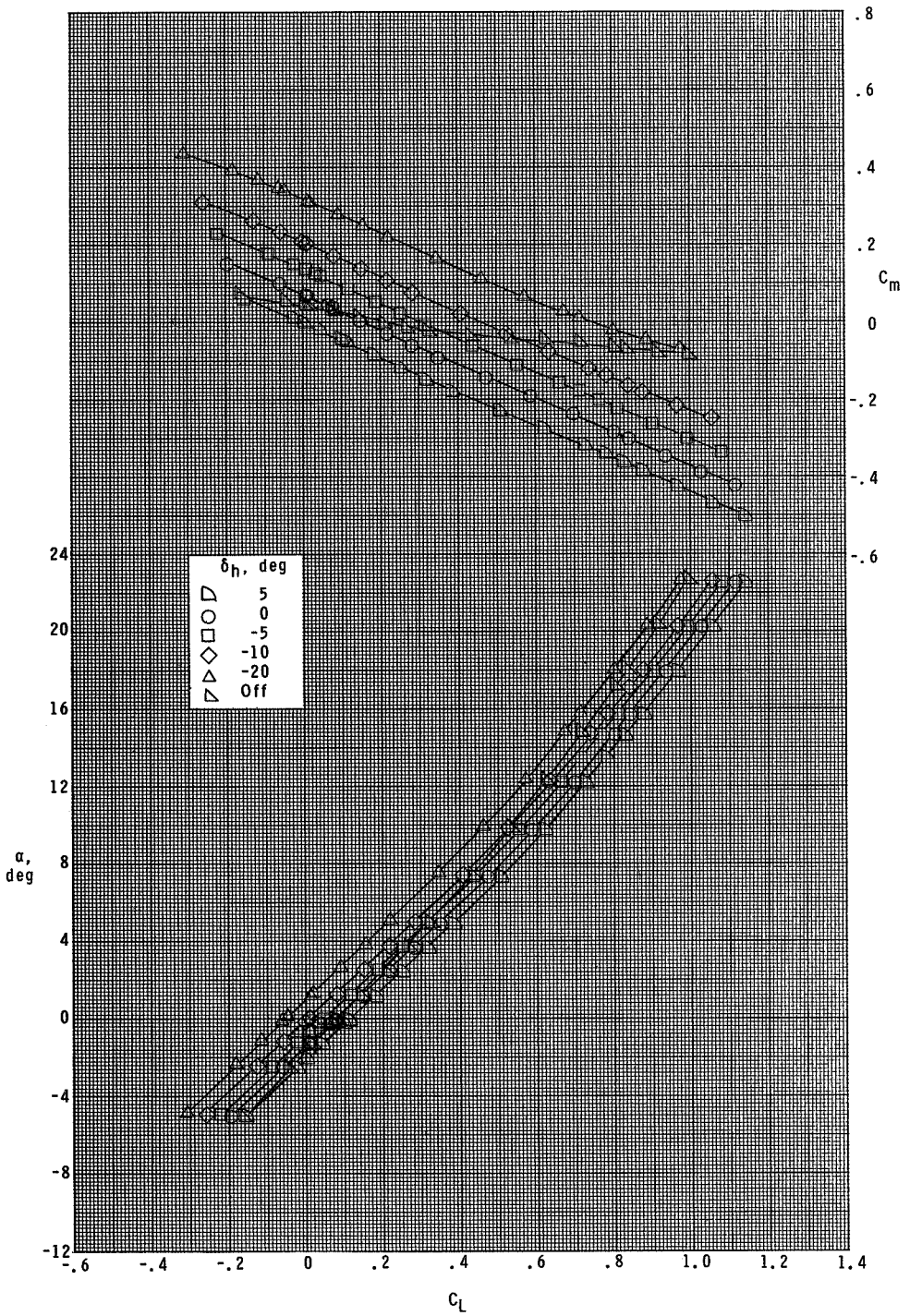

(b) M = 2.00.

Figure 8.- Continued.

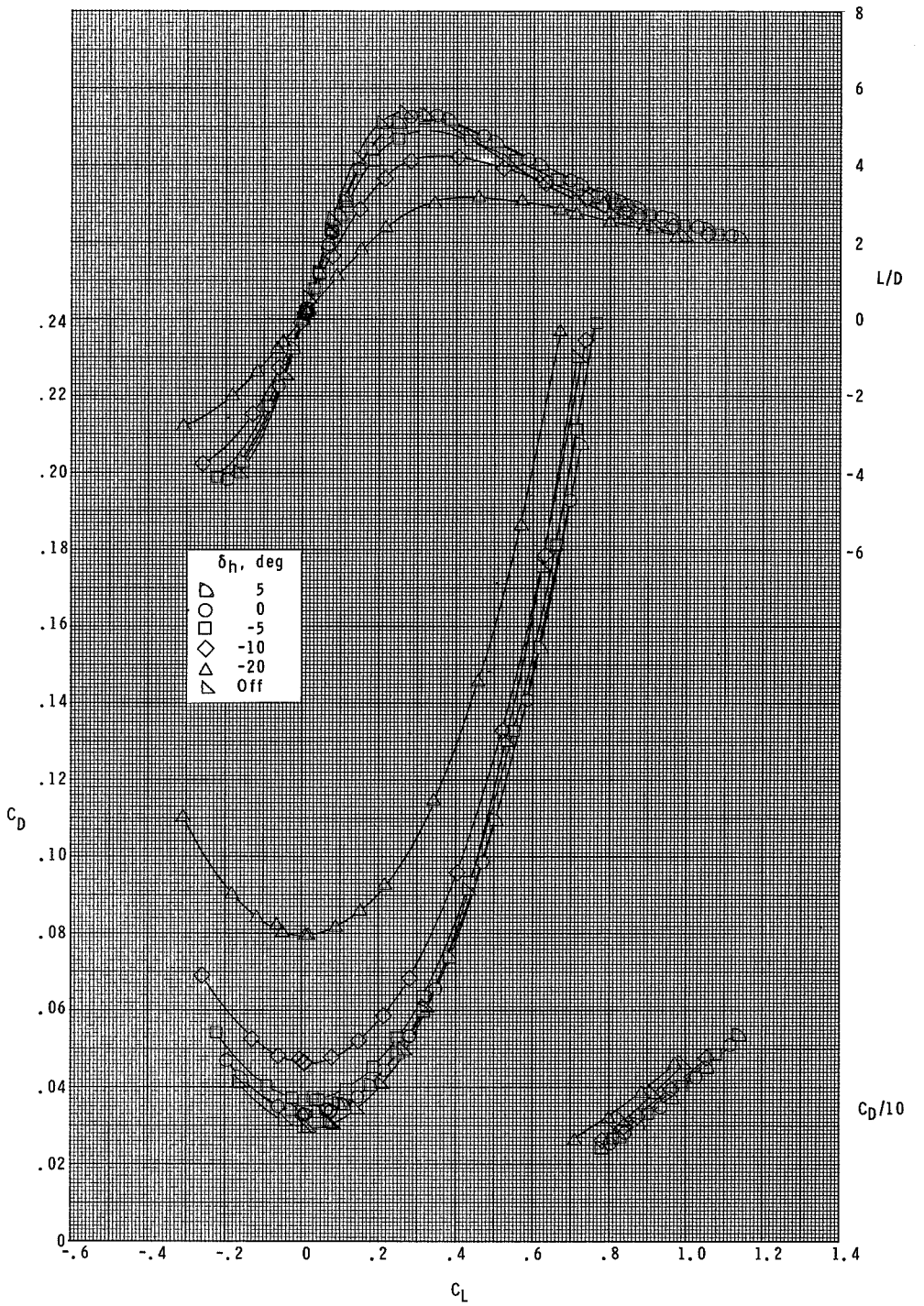

(b) Concluded.

Figure 8.- Continued.

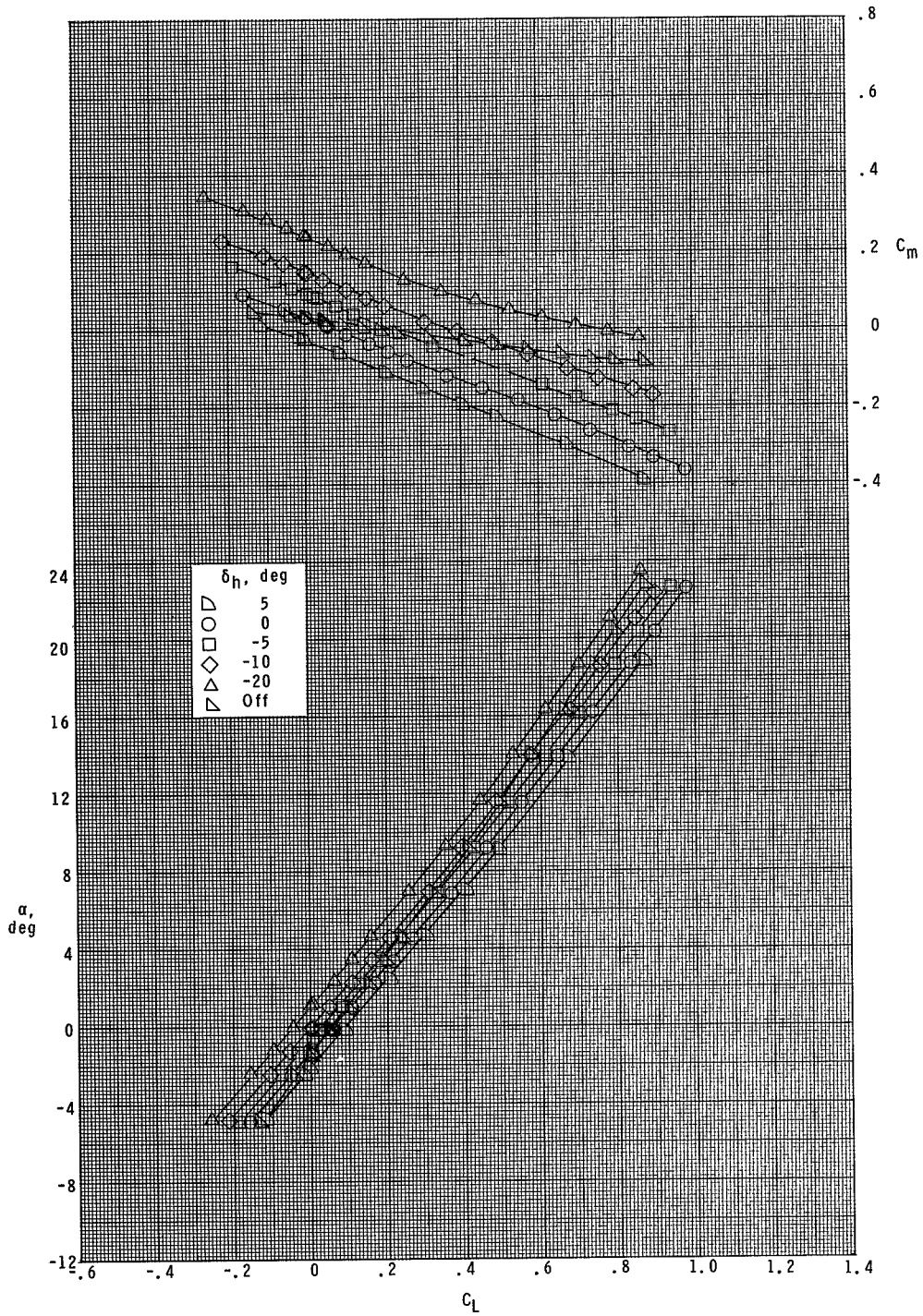

(c) M = 2.50.

Figure 8.- Continued.

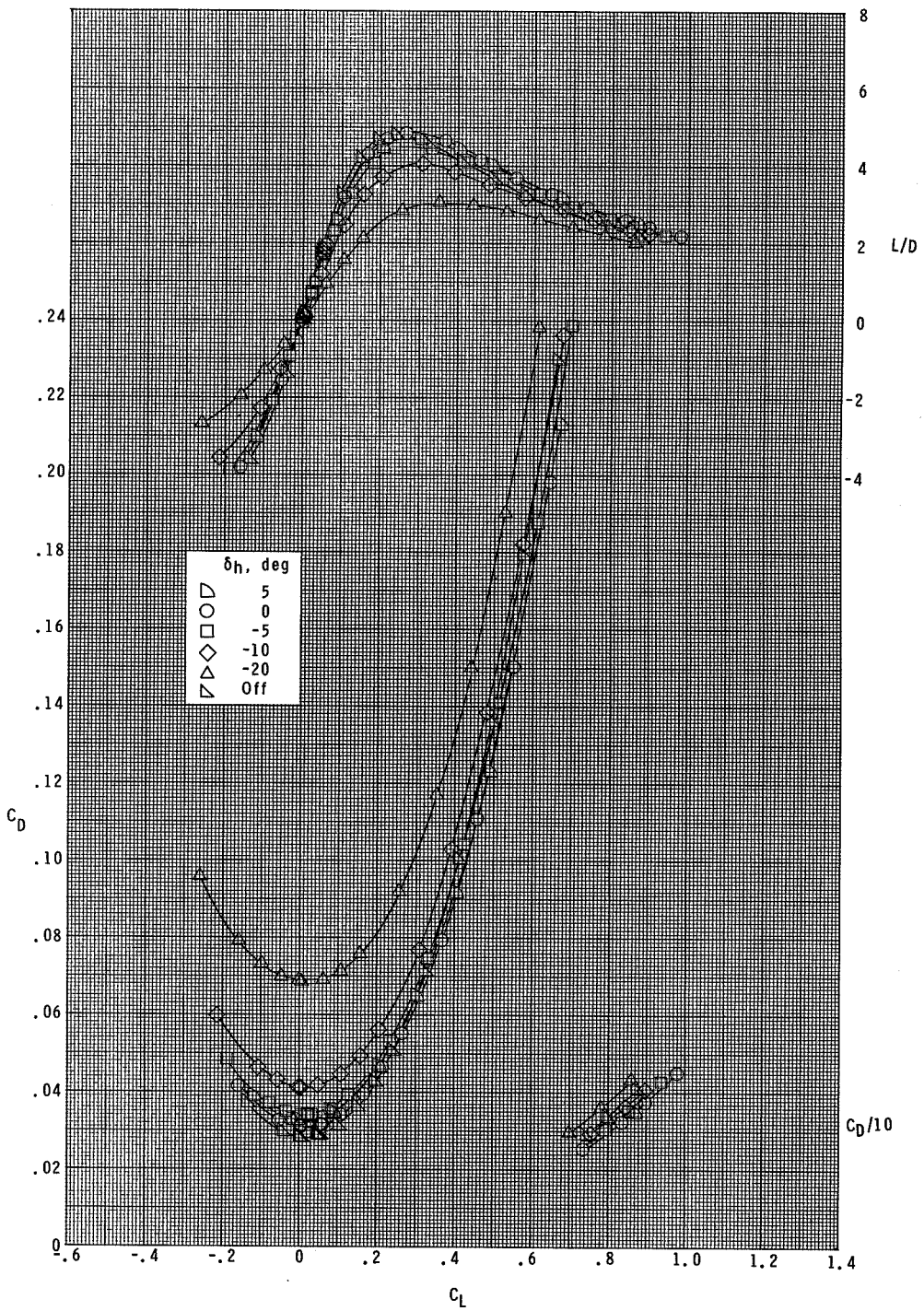

(c) Concluded.

Figure 8.- Continued.

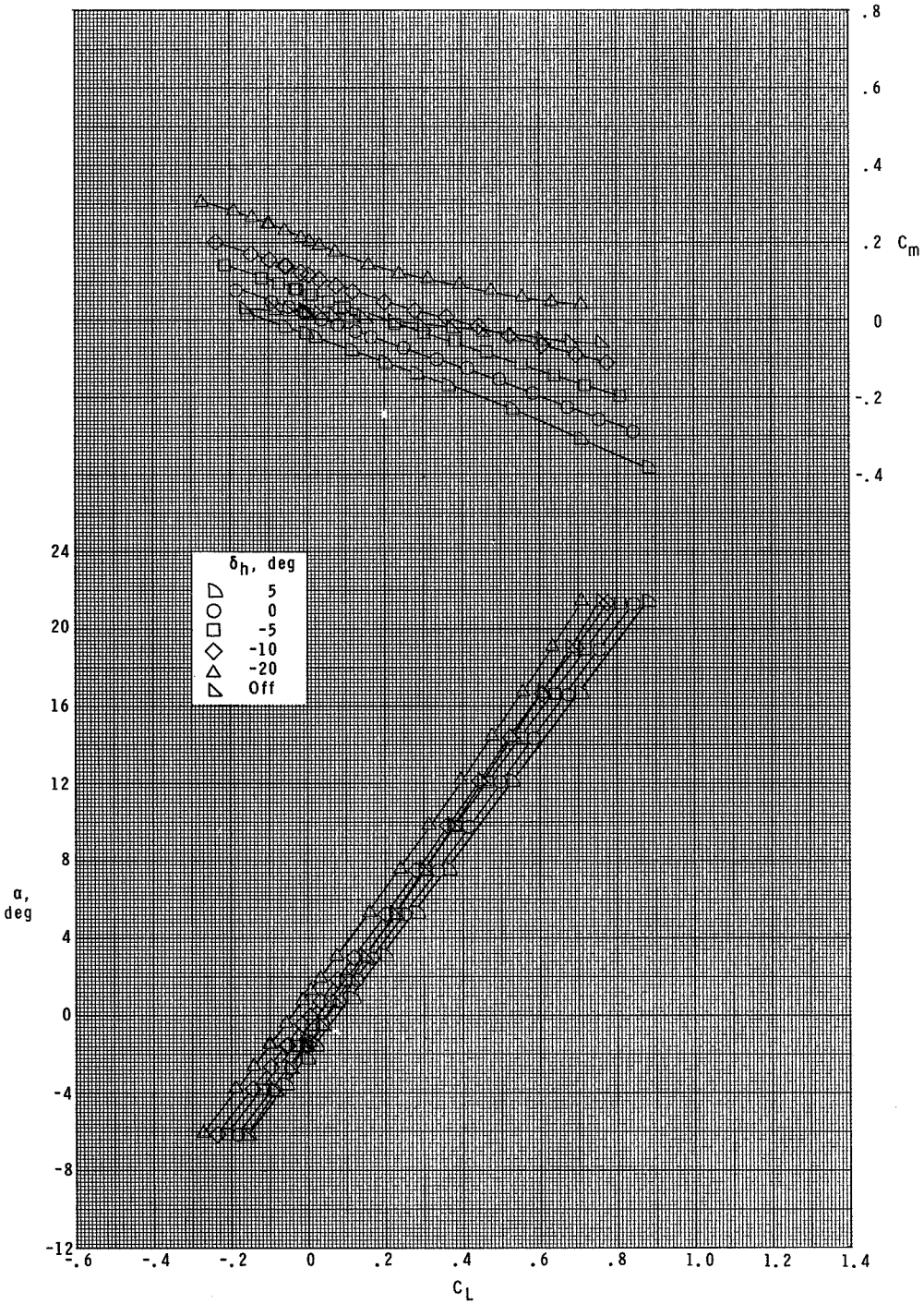

(d) M = 2.86.

Figure 8.- Continued.

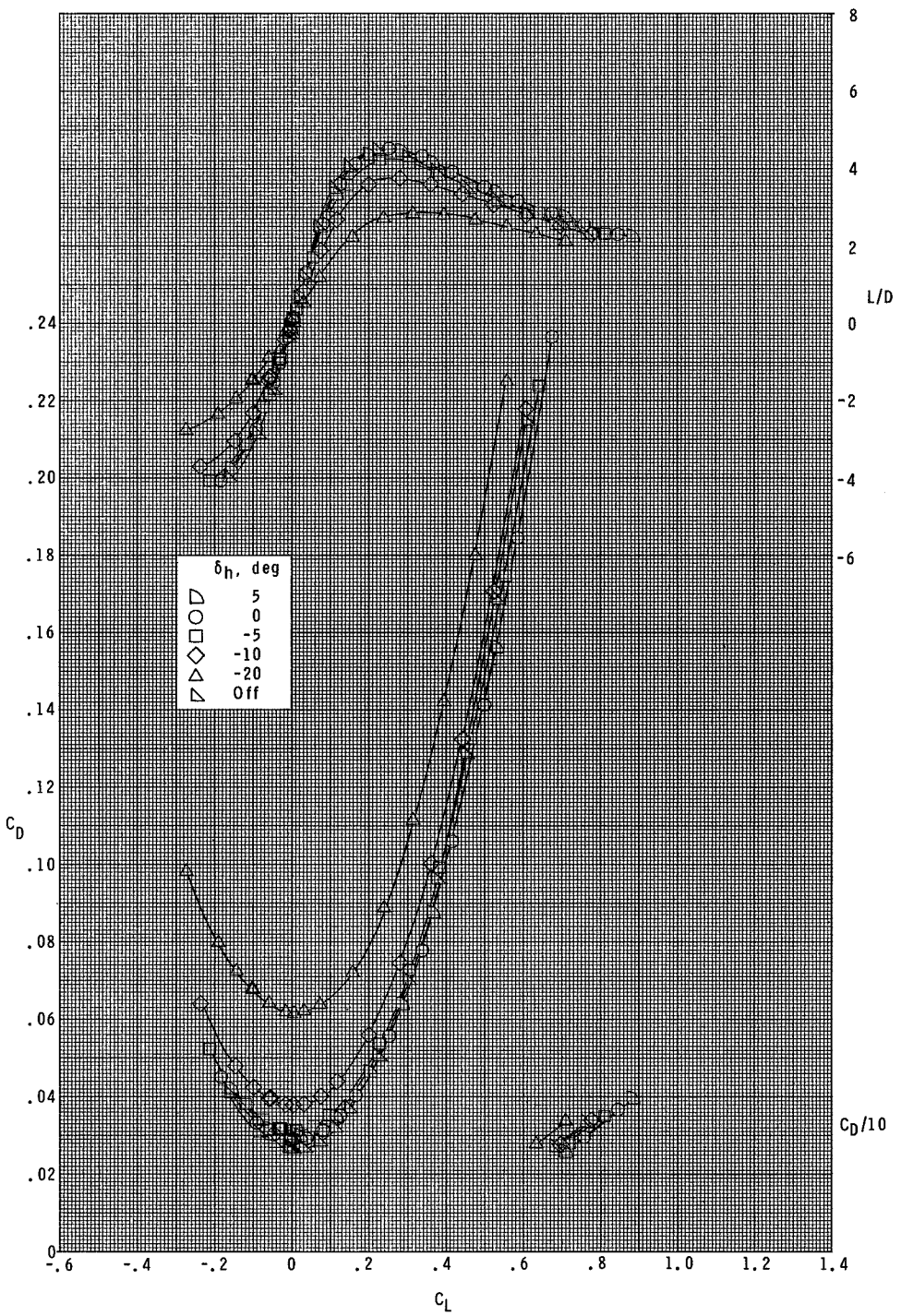

(d) Concluded.

Figure 8.- Concluded.

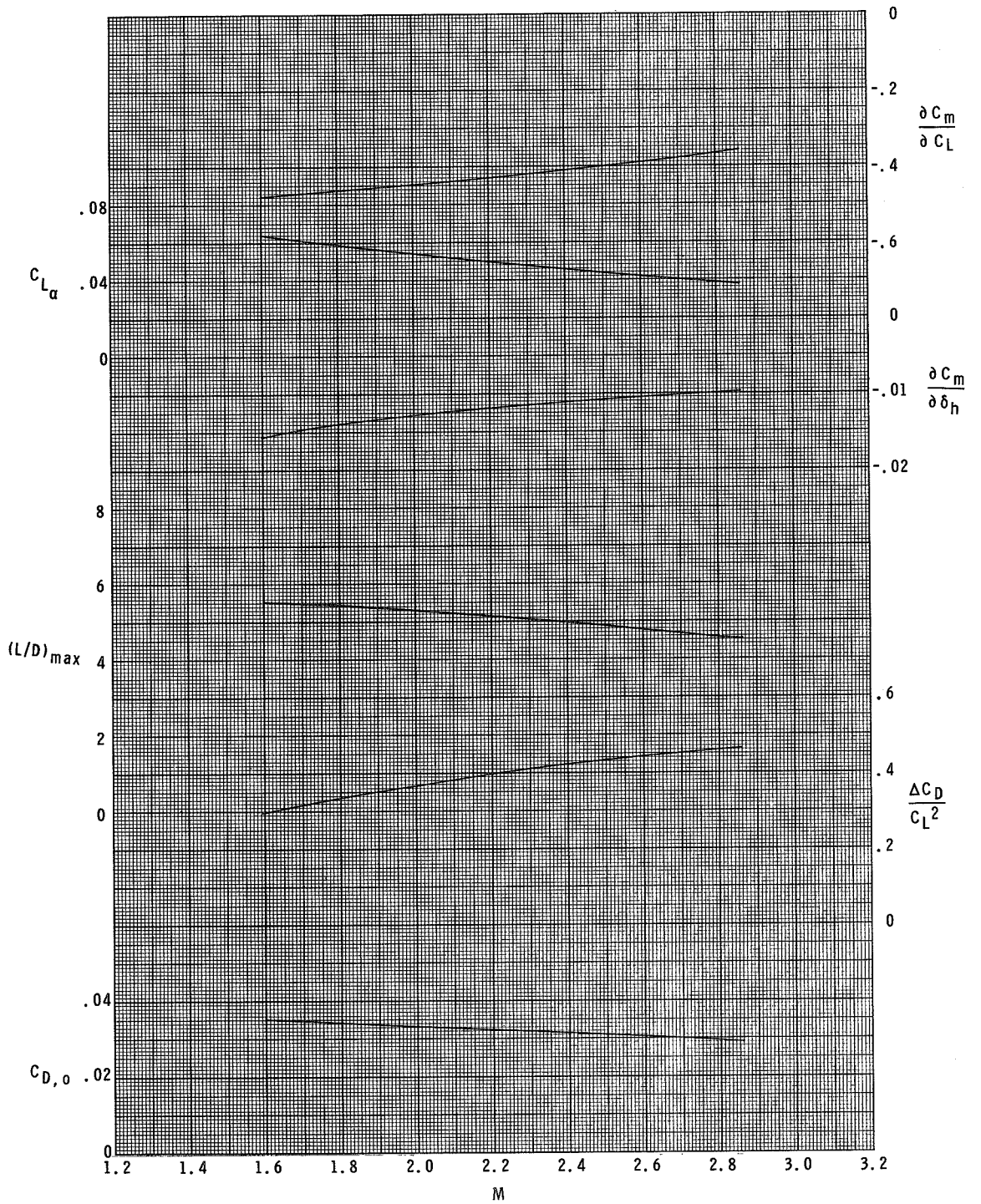

Figure 9.- Summary of longitudinal control characteristics.

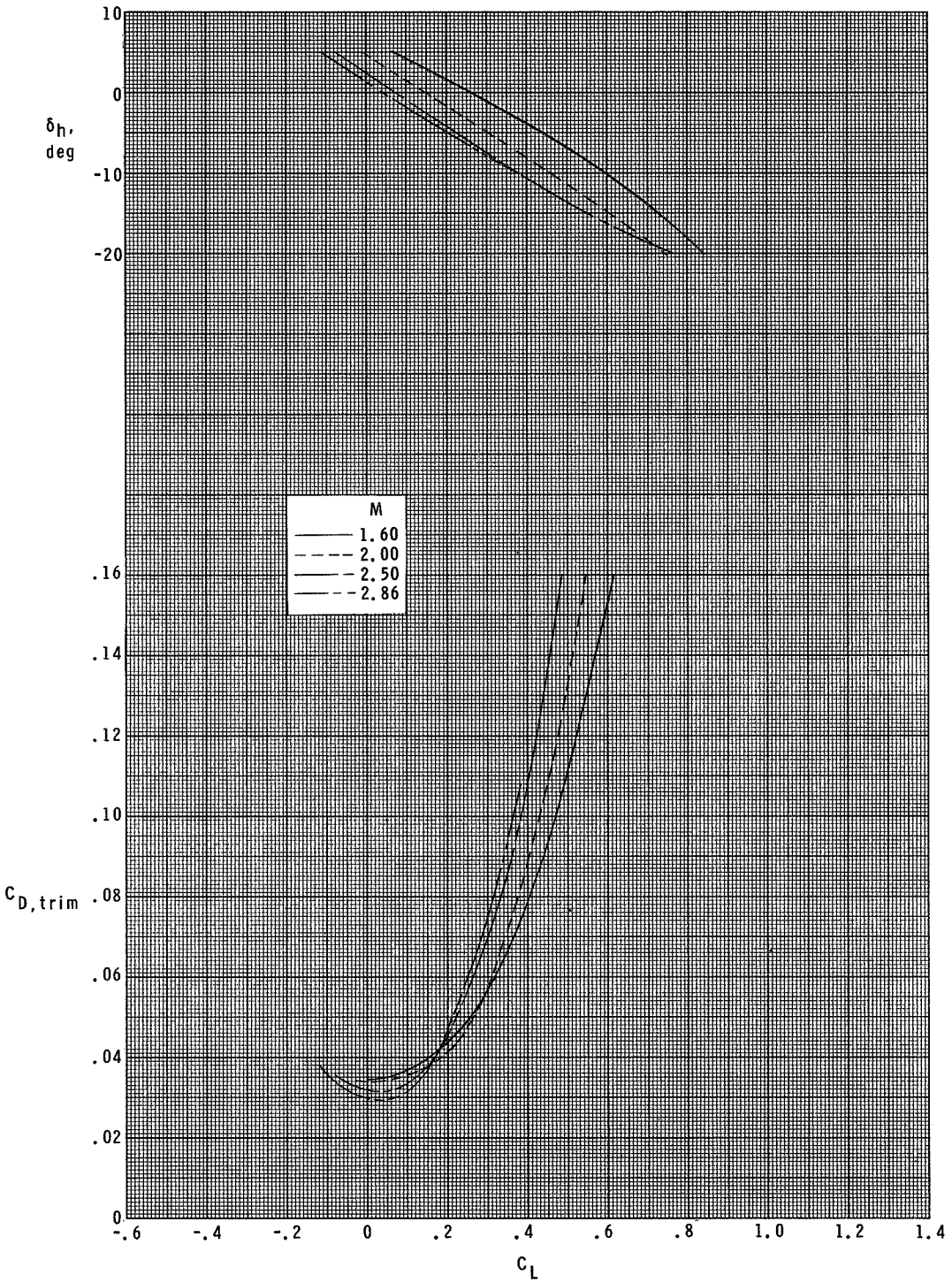

Figure 10.- Longitudinal trim characteristics.

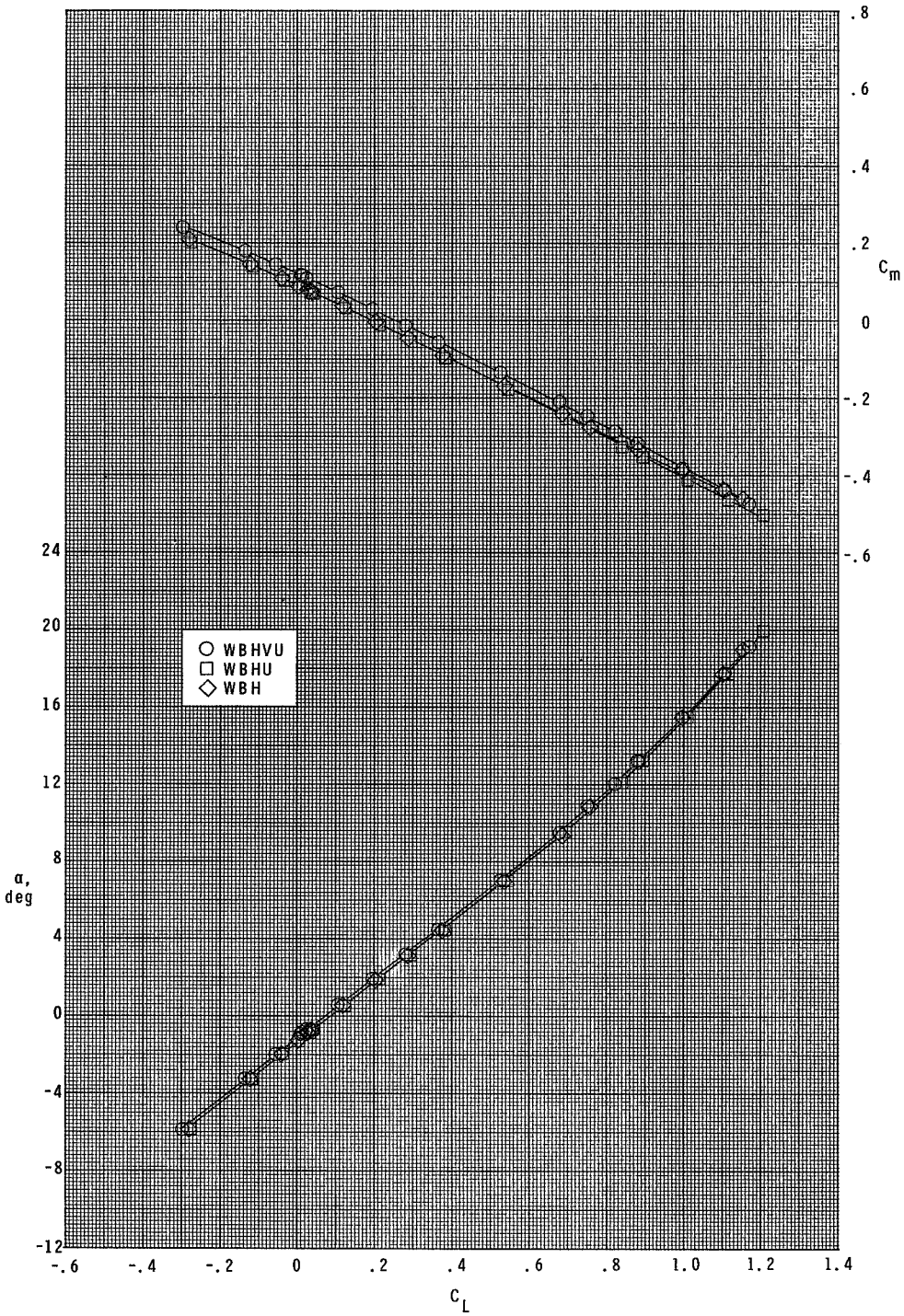

(a) M = 1.60.

Figure 11.- Effects of components on longitudinal characteristics.

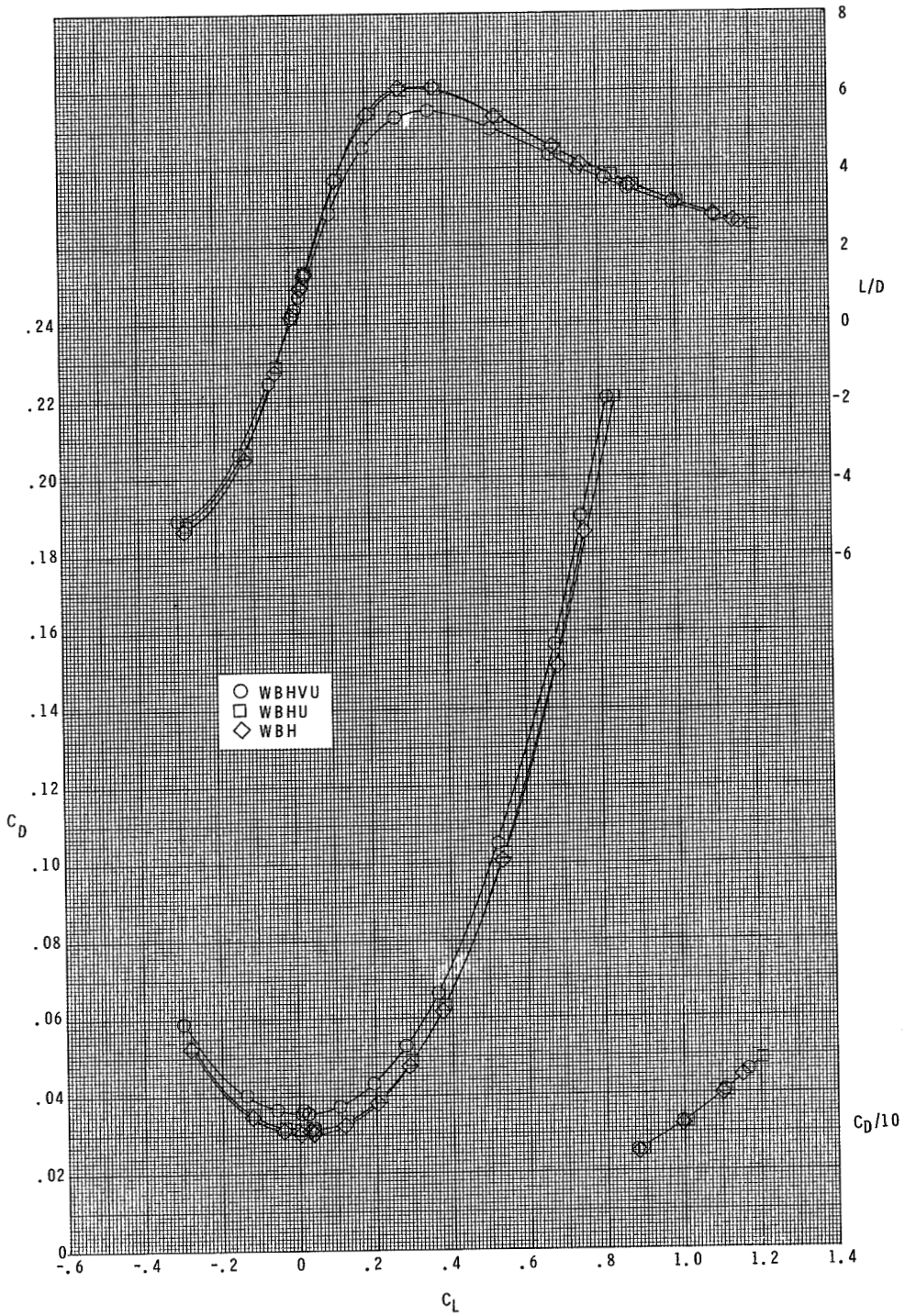

(a) Concluded.

Figure 11.- Continued.

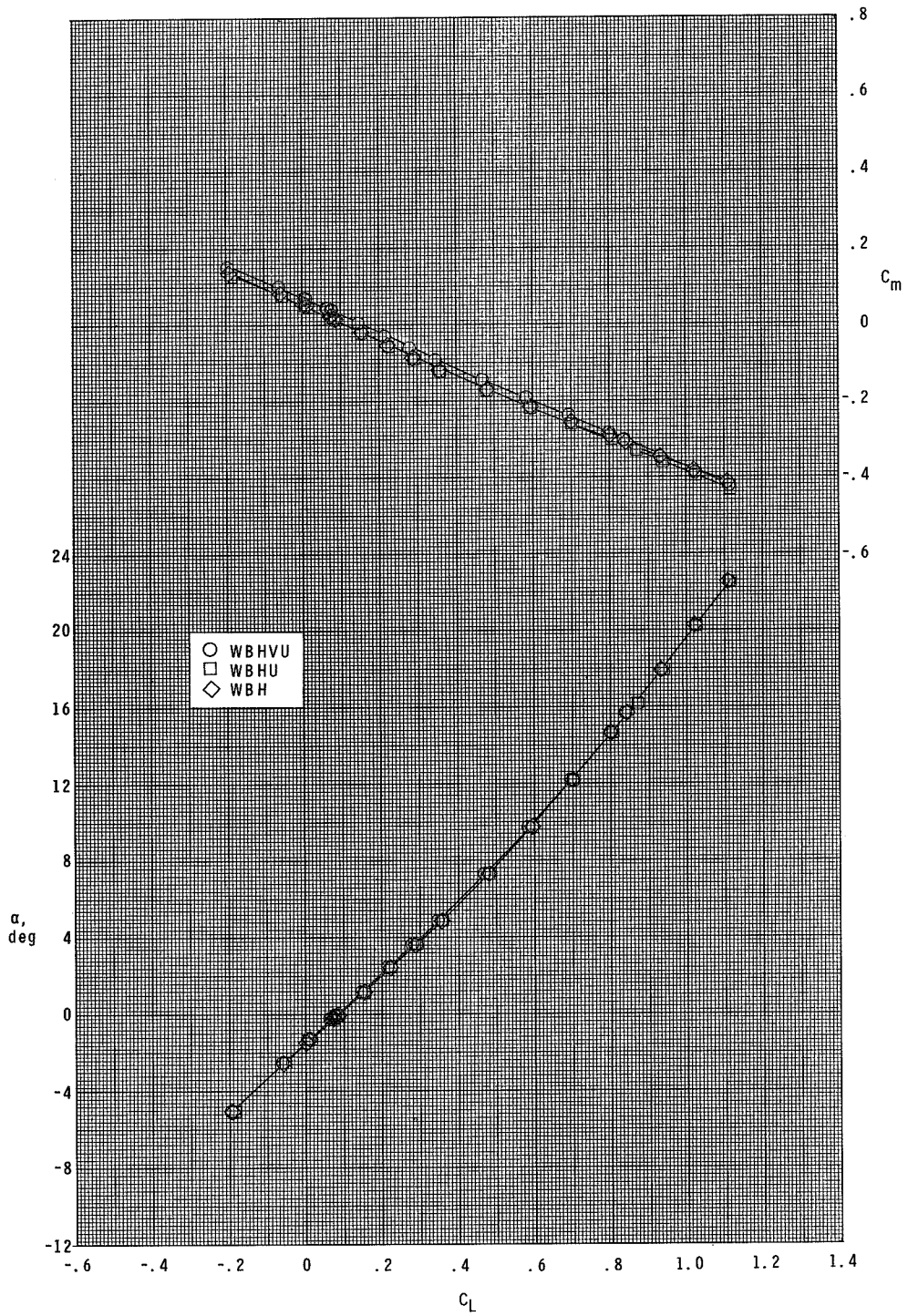

(b) M = 2.00.

Figure 11.- Continued.

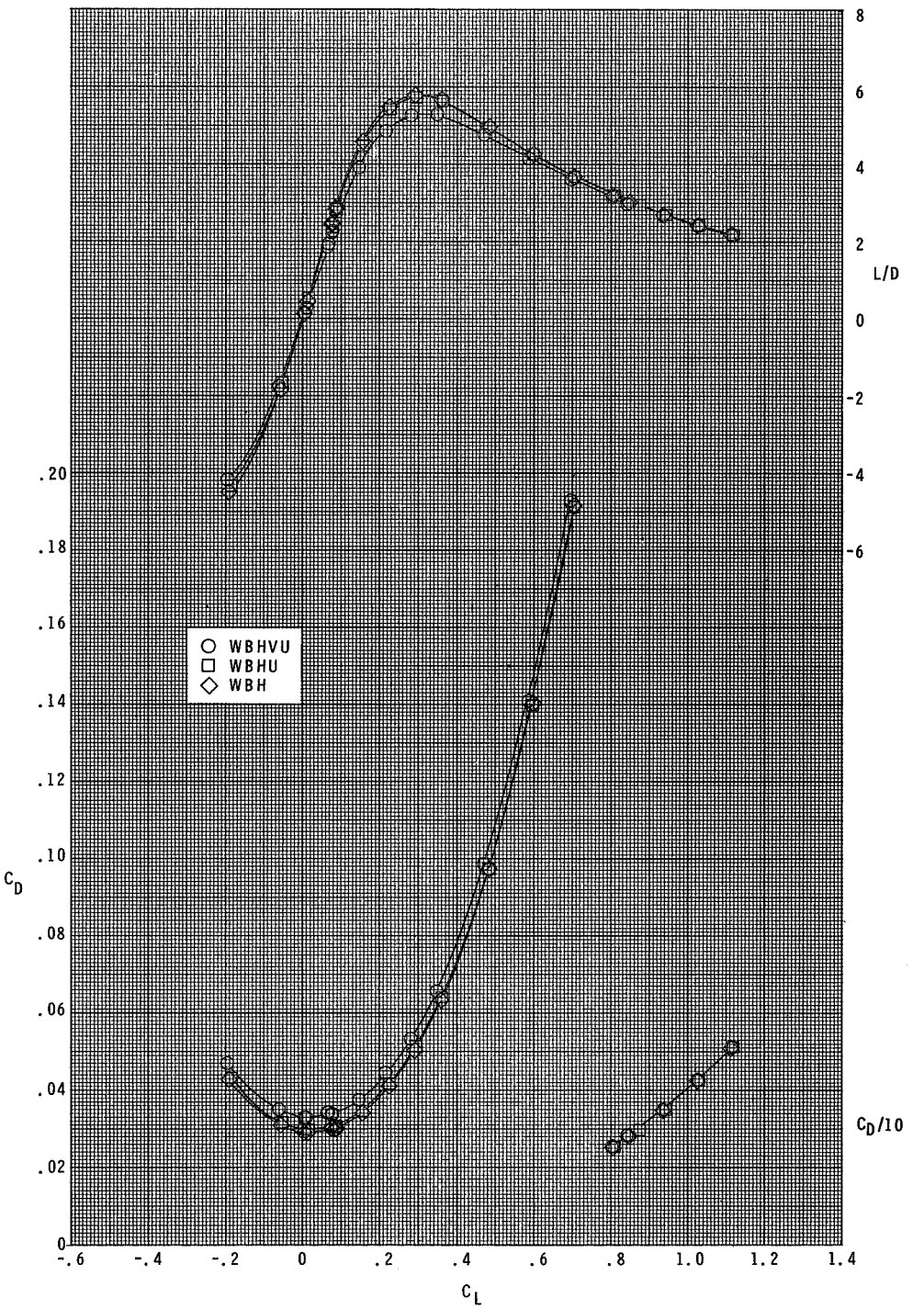

(b) Concluded.

Figure 11.- Continued.

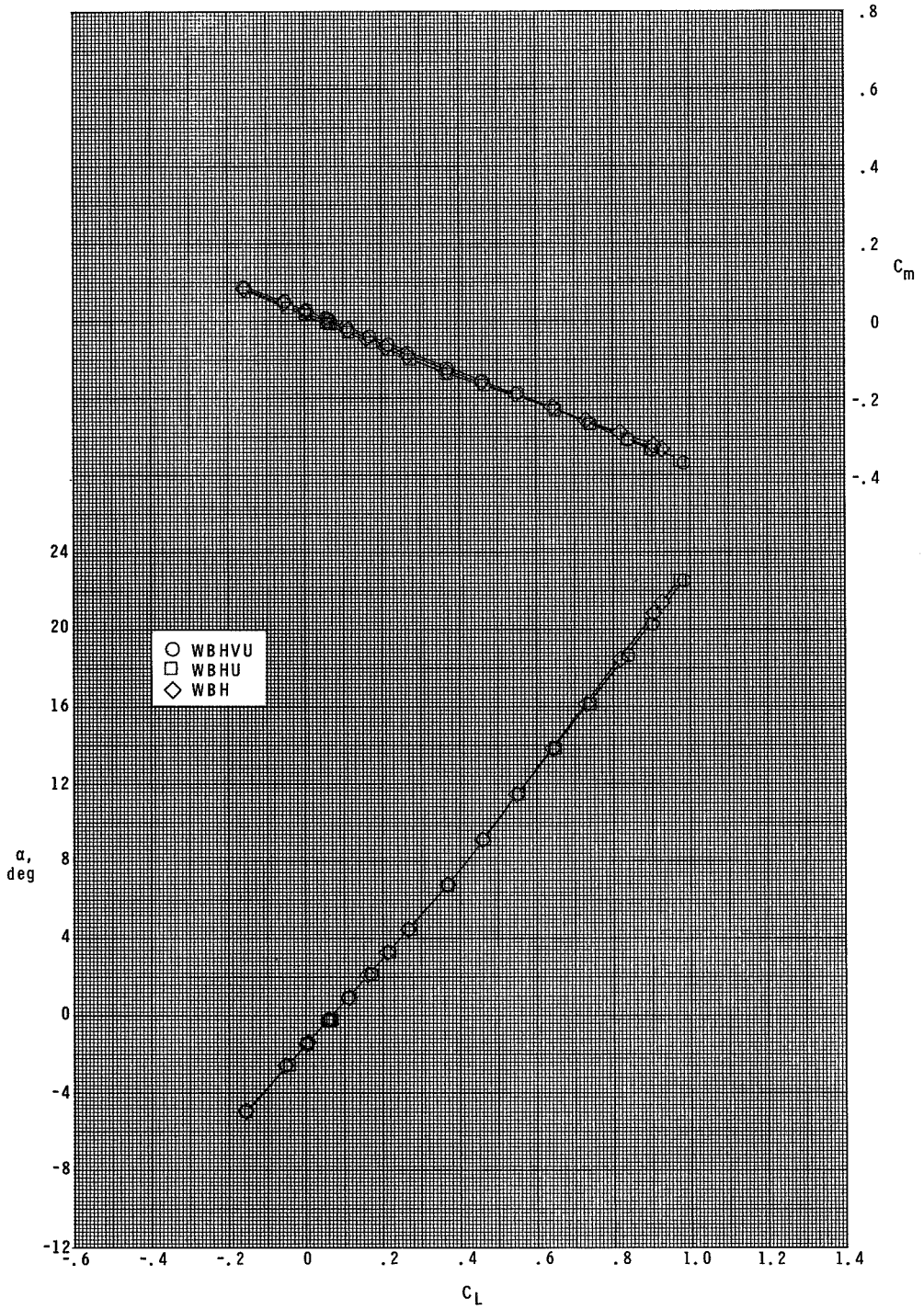

(c) M = 2.50.

Figure 11.- Continued.

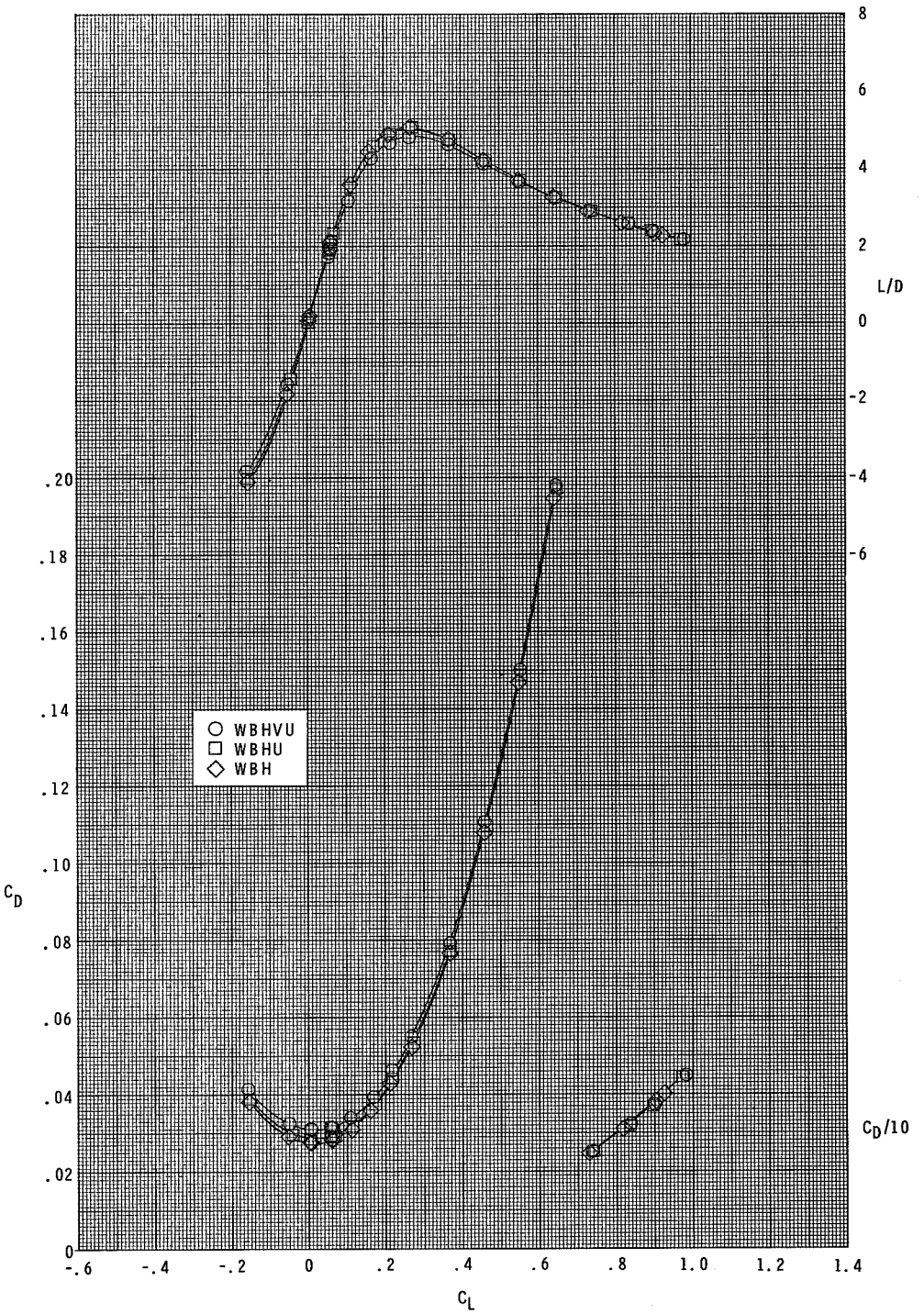

(c) Concluded.

Figure 11.- Continued.

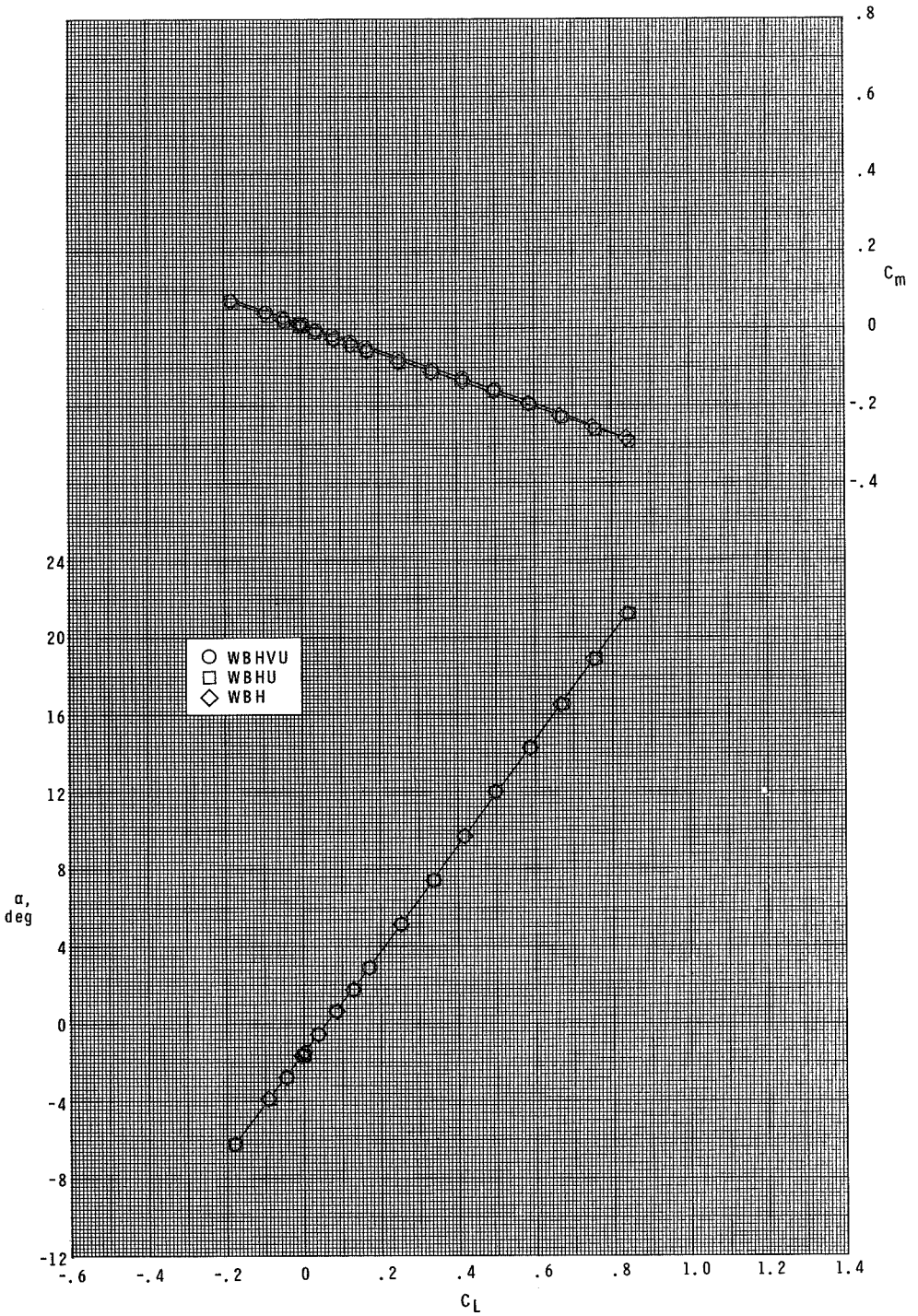

(d) M = 2.86.

Figure 11.- Continued.

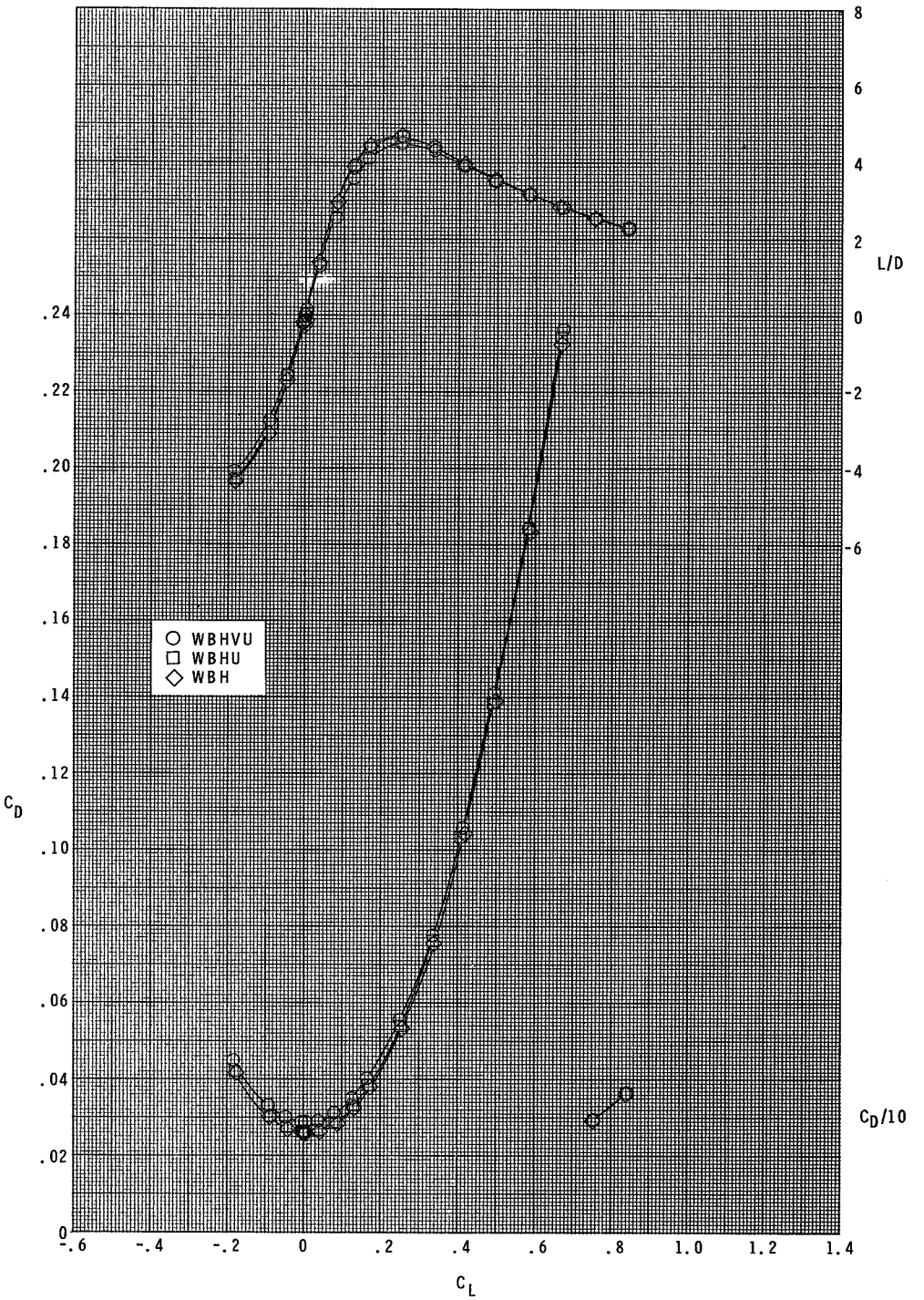

(d) Concluded.

Figure 11.- Concluded.

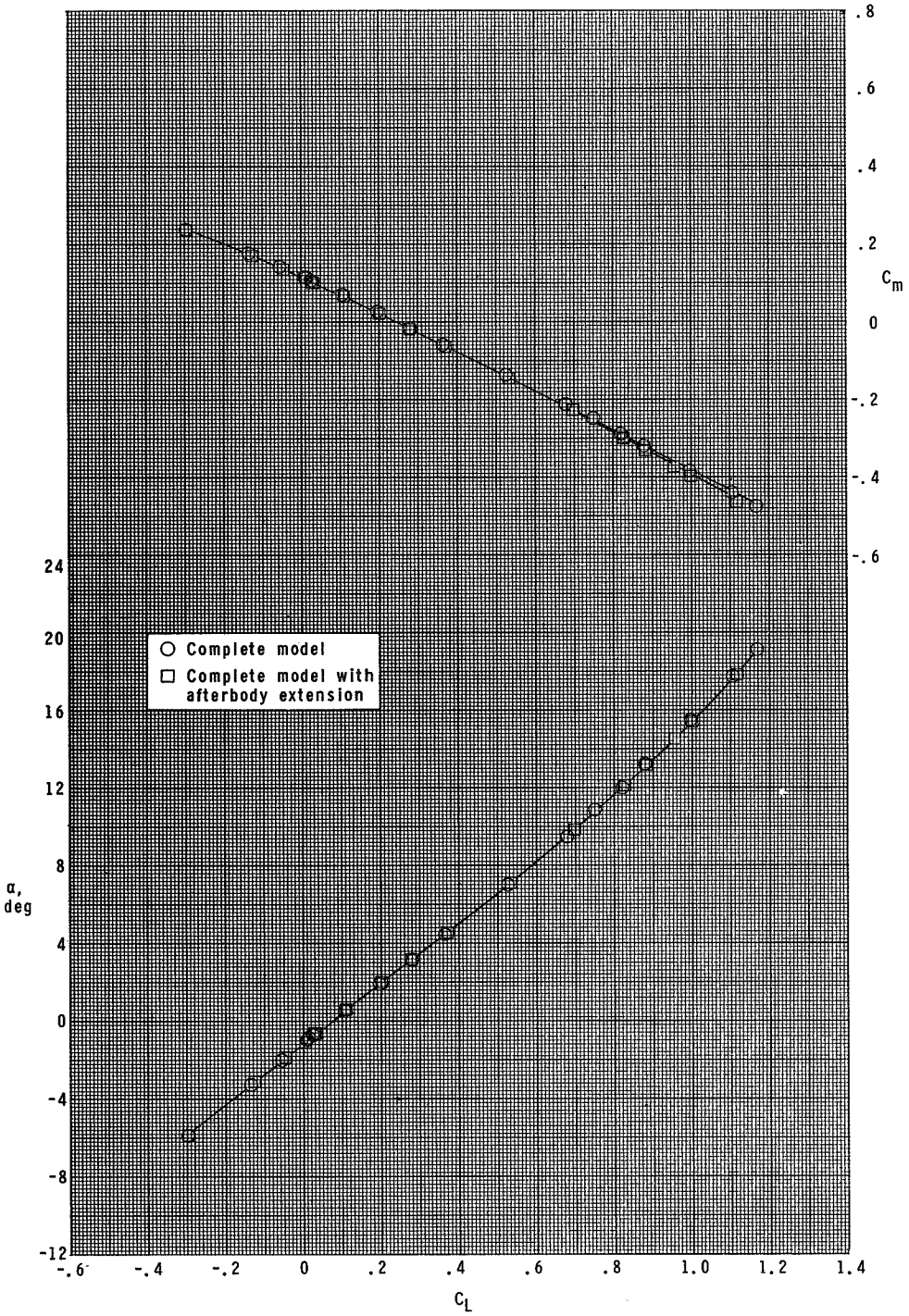

(a) M = 1.60.

Figure 12.- Effects of afterbody extension on longitudinal characteristics.

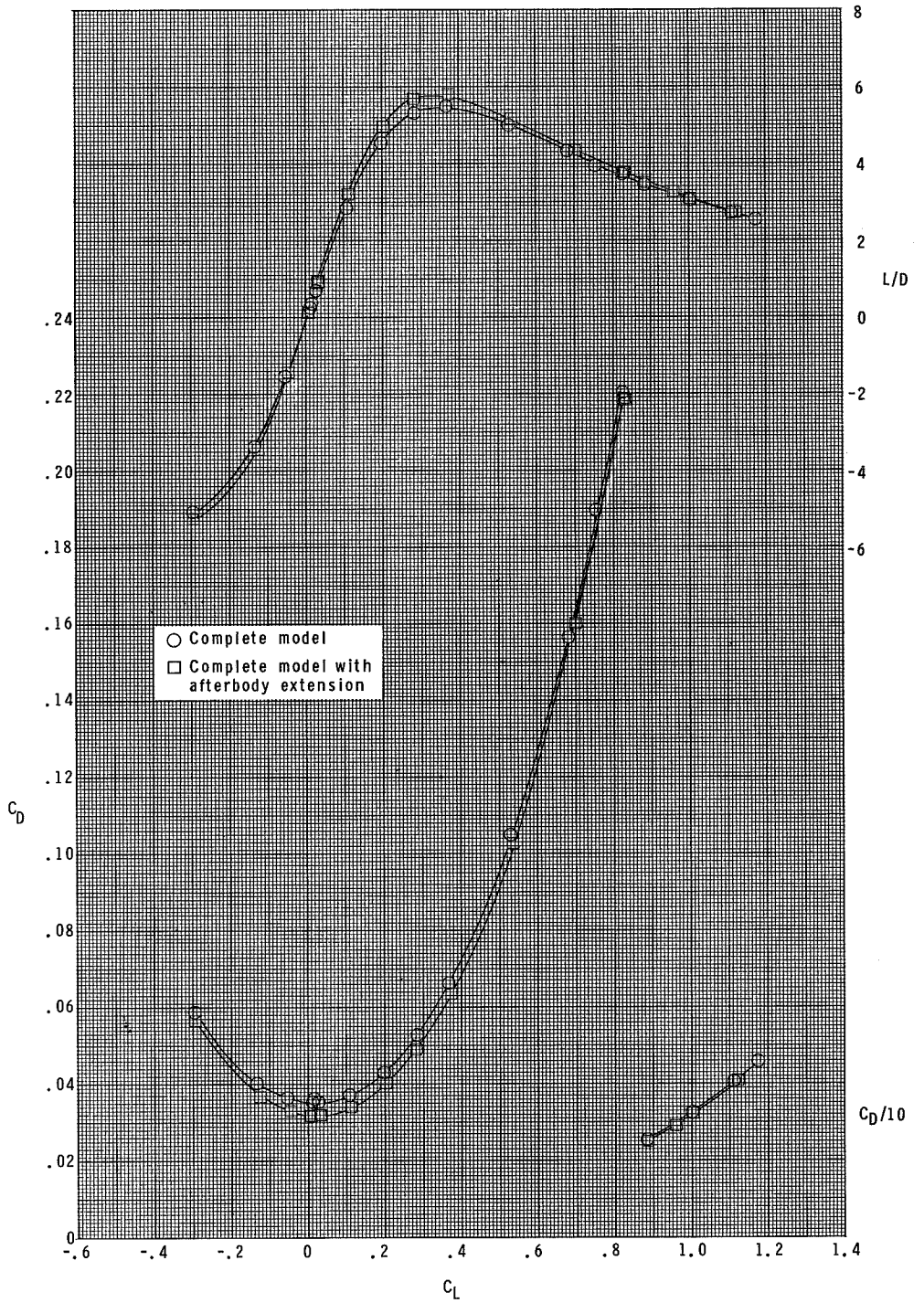

(a) Concluded.

Figure 12.- Continued.

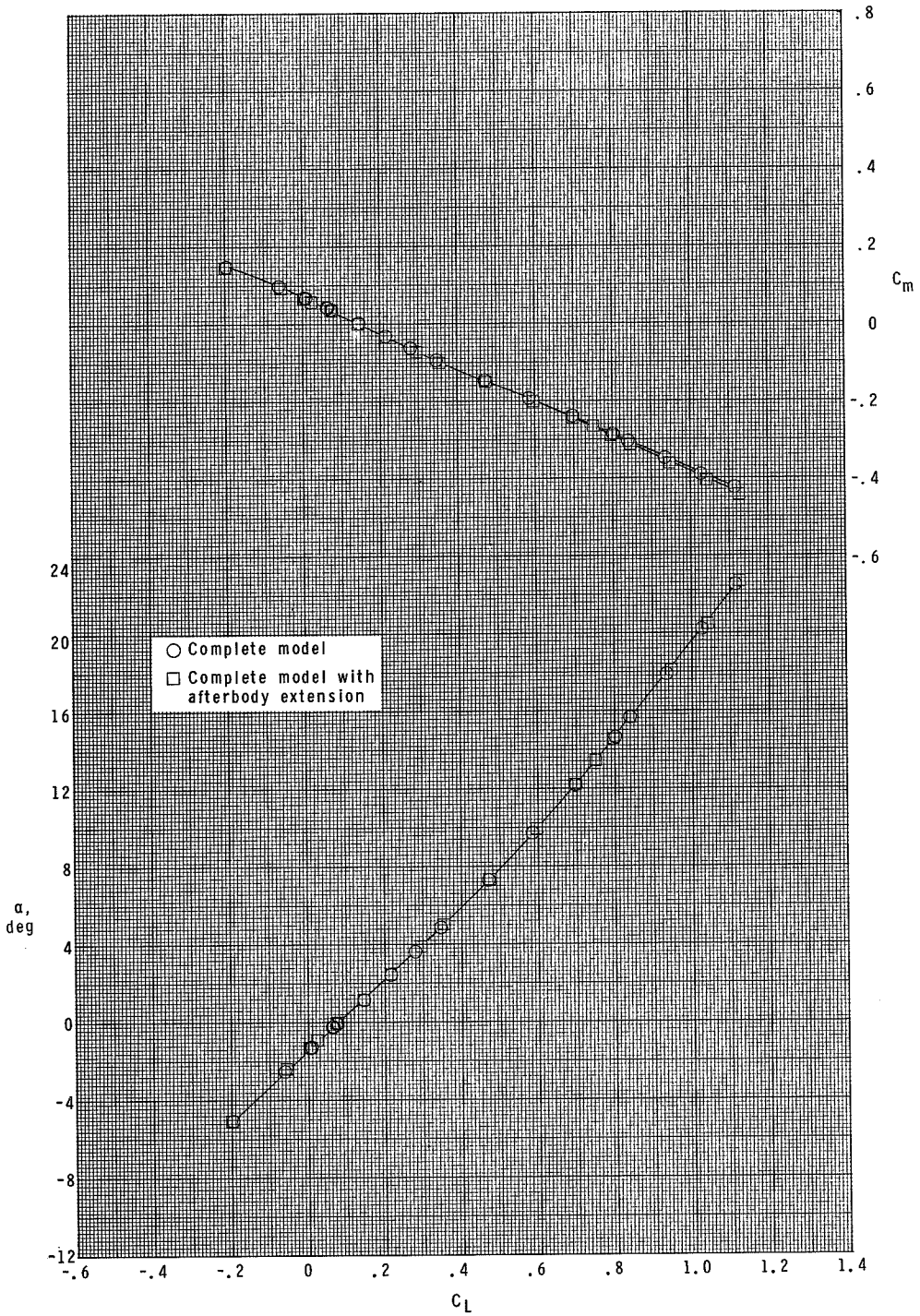

(b) M = 2.00.

Figure 12.- Continued.

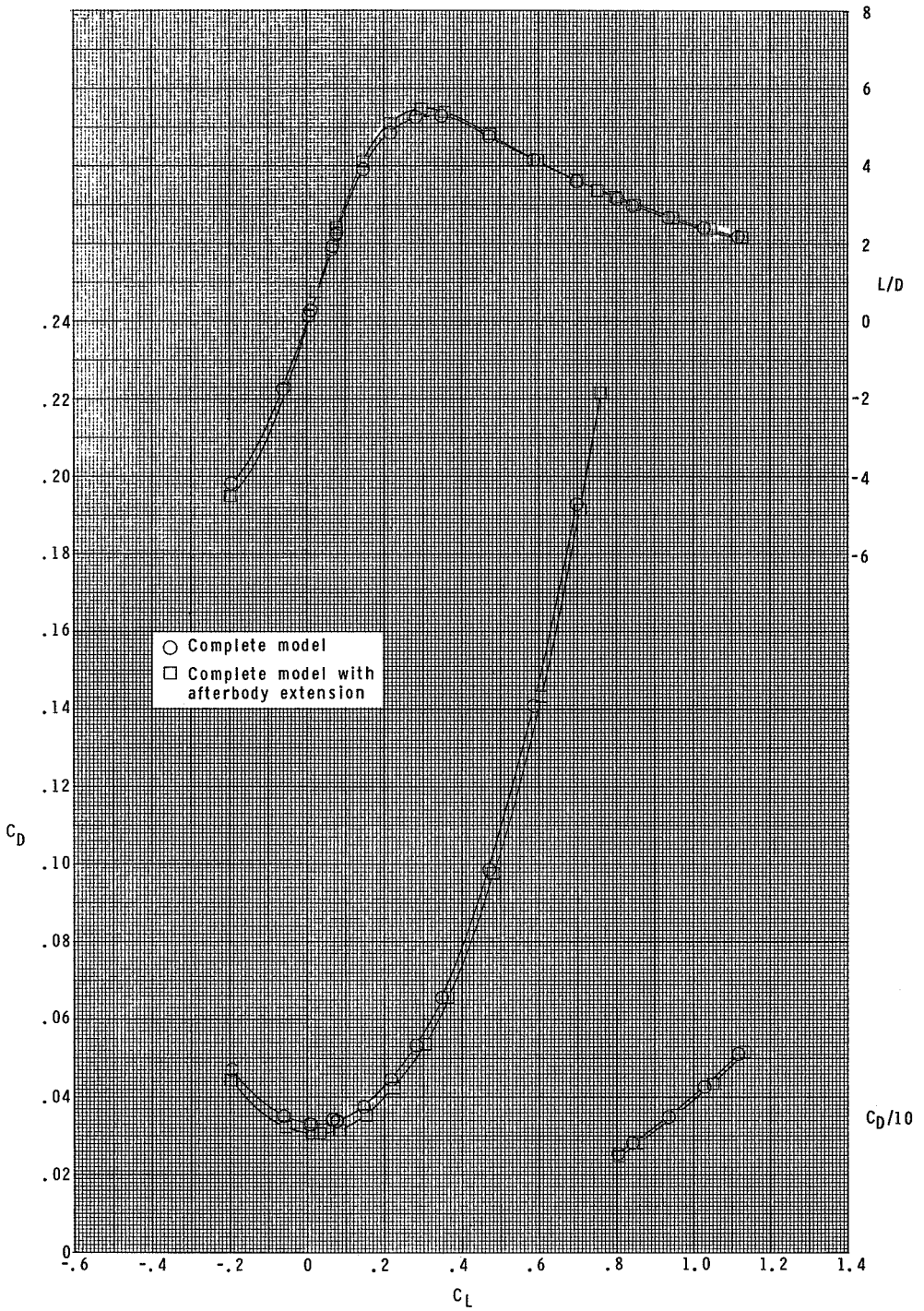

(b) Concluded.

Figure 12.- Continued.

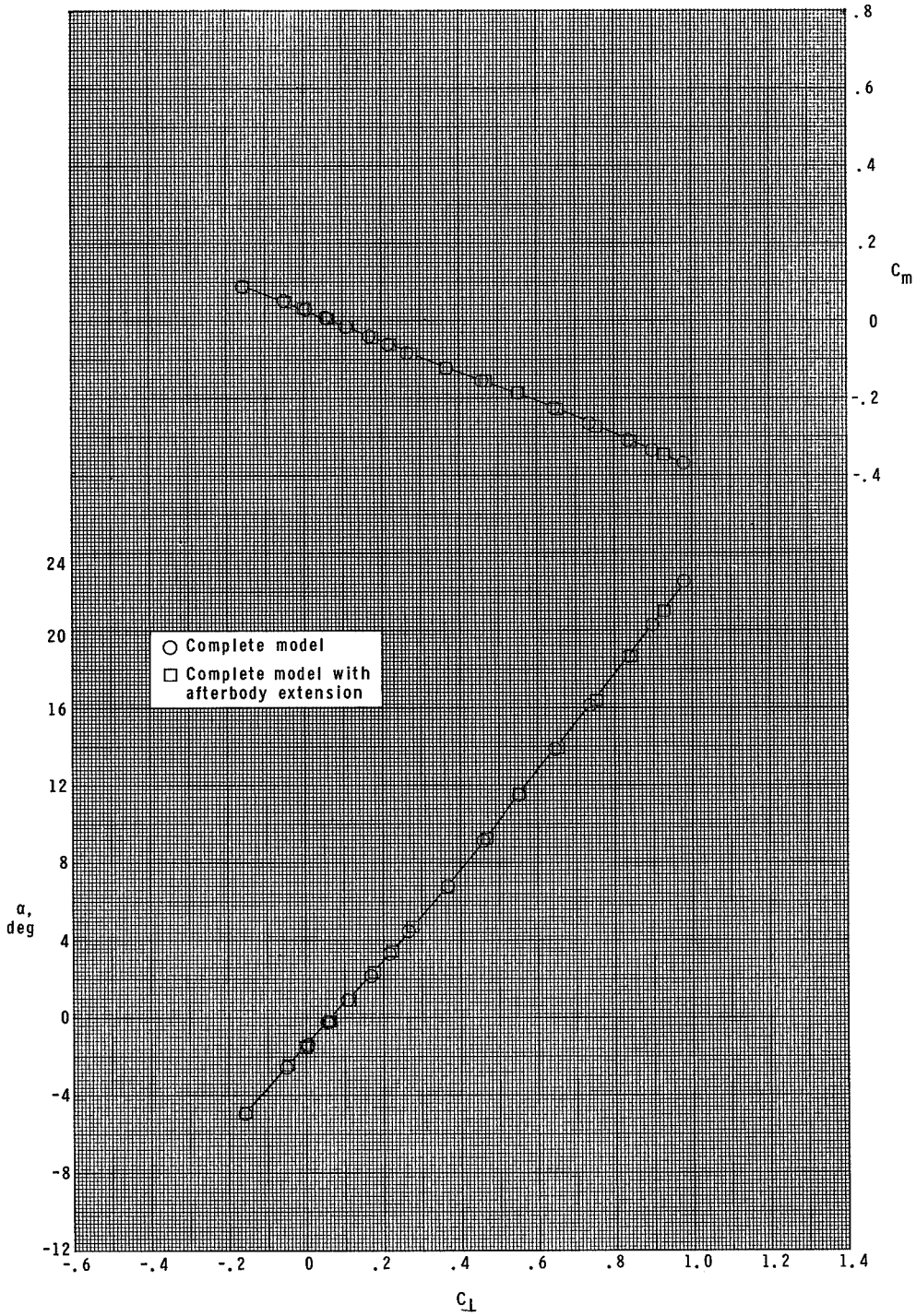

(c) M = 2.50.

Figure 12.- Continued.

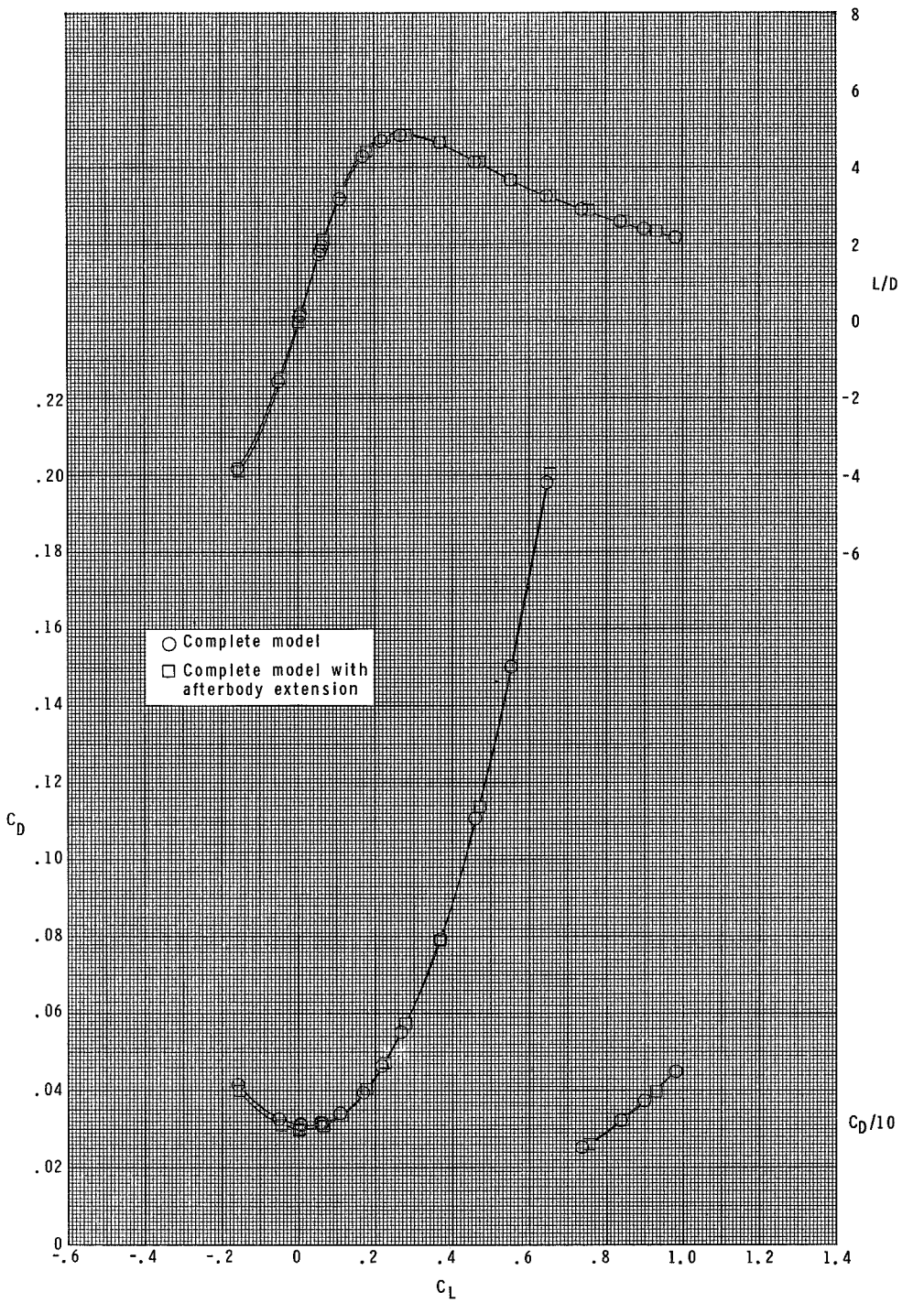

(c) Concluded.

Figure 12.- Continued.

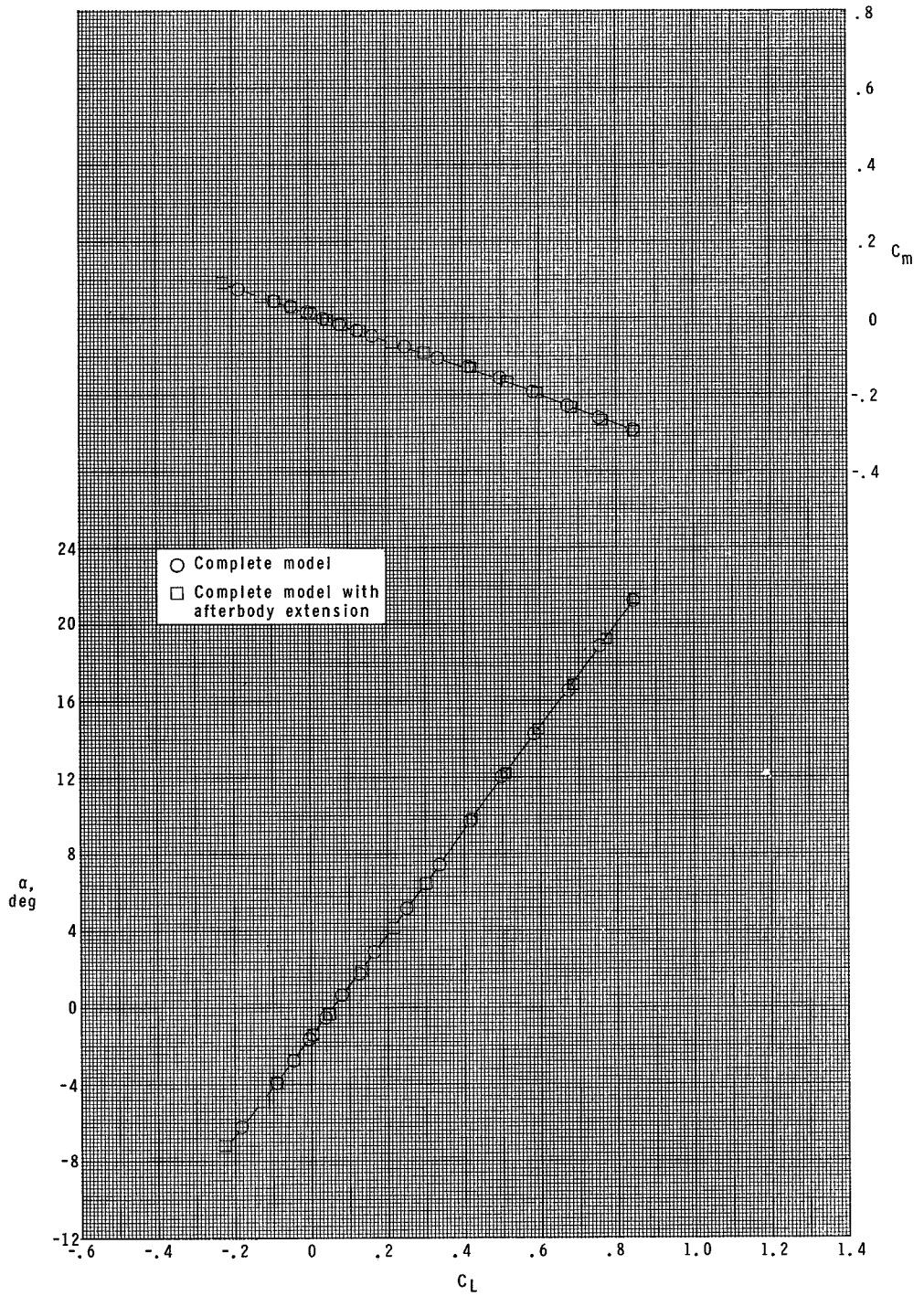

(d) M = 2.86.

Figure 12.- Continued.

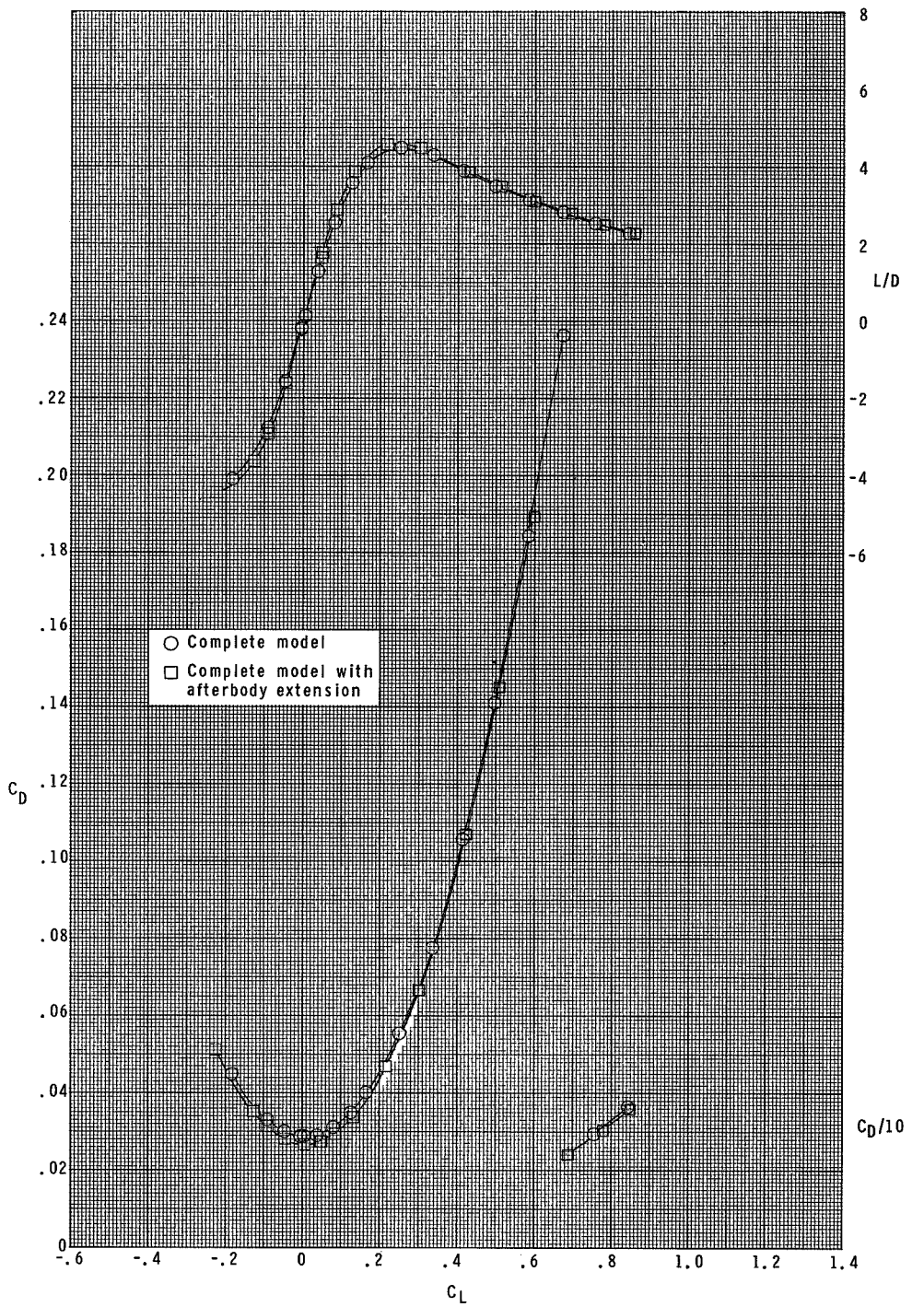

(d) Concluded.

Figure 12.- Concluded.

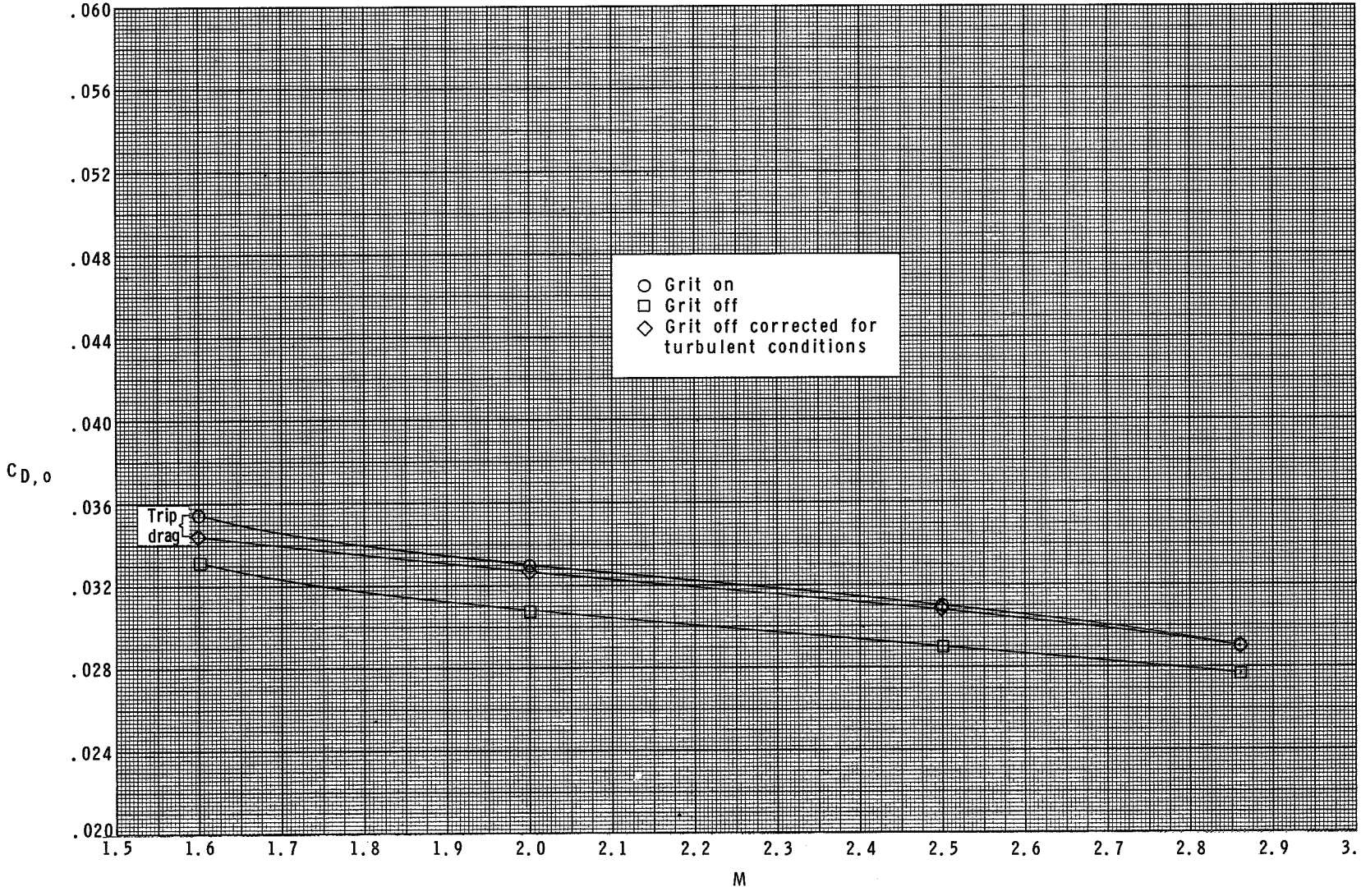

Figure 13.- Trip drag.

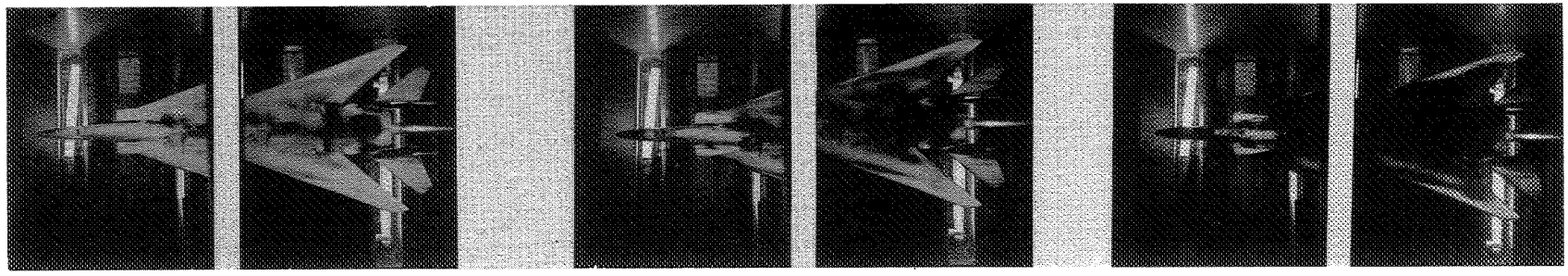

Top of model

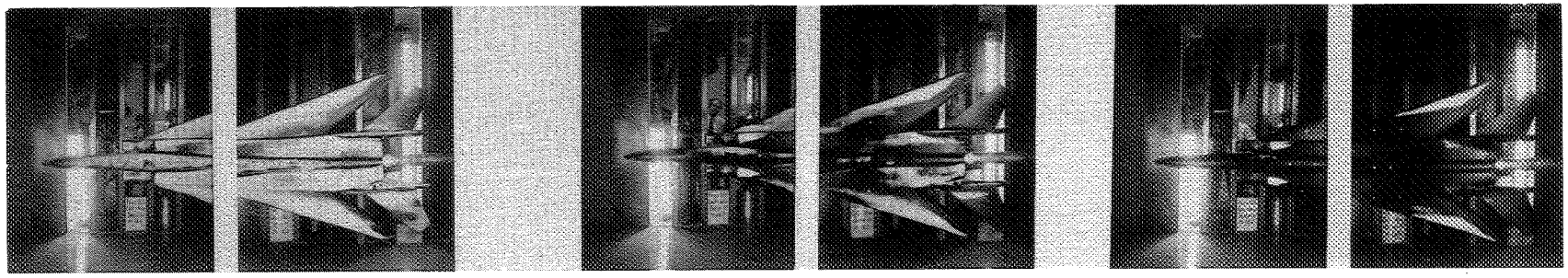

Bottom of model

L-71-560

(a) M = 1.60.

Figure 14.- Sublimation sequence.

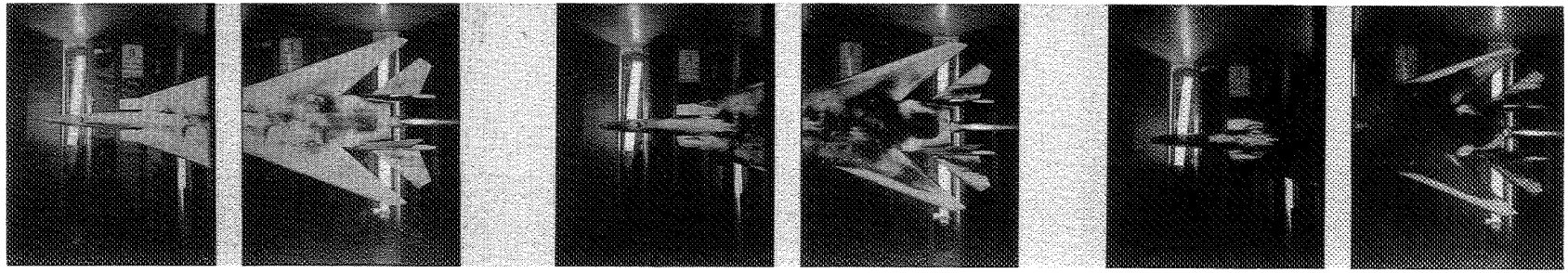

Top of model

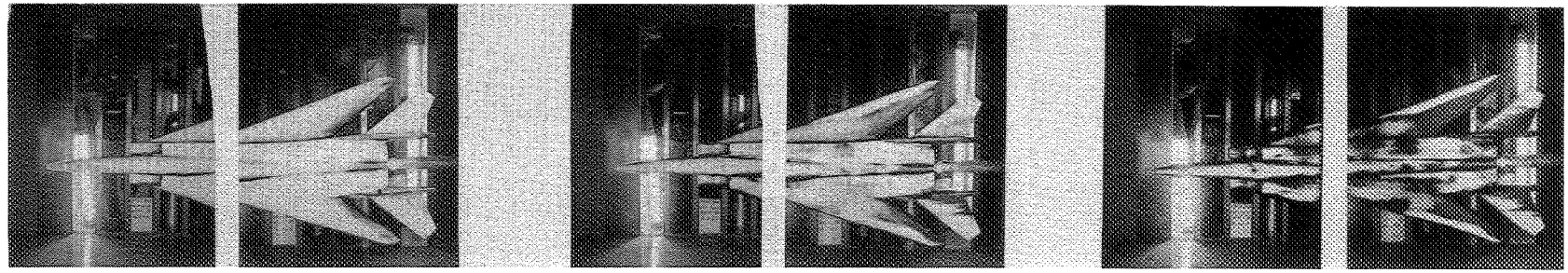

Bottom of model

L-71-561

(b) M = 2.00.

Figure 14.- Continued.

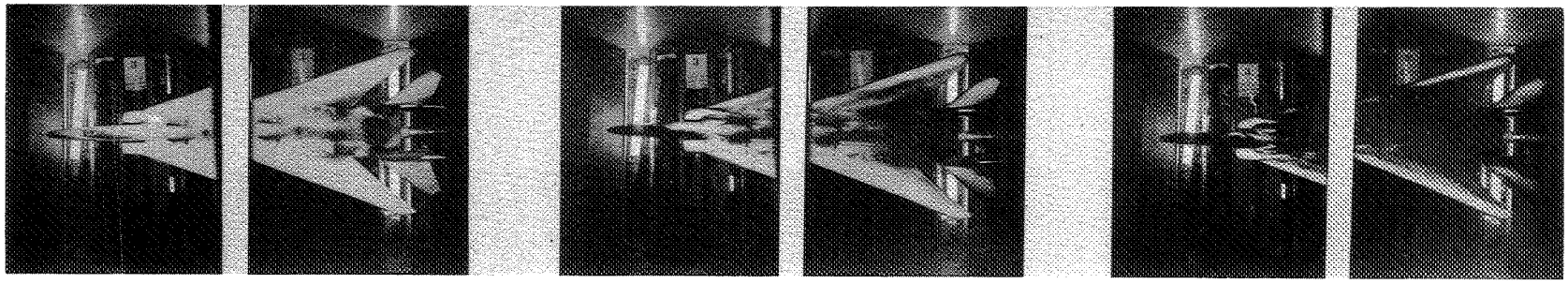

Top of model

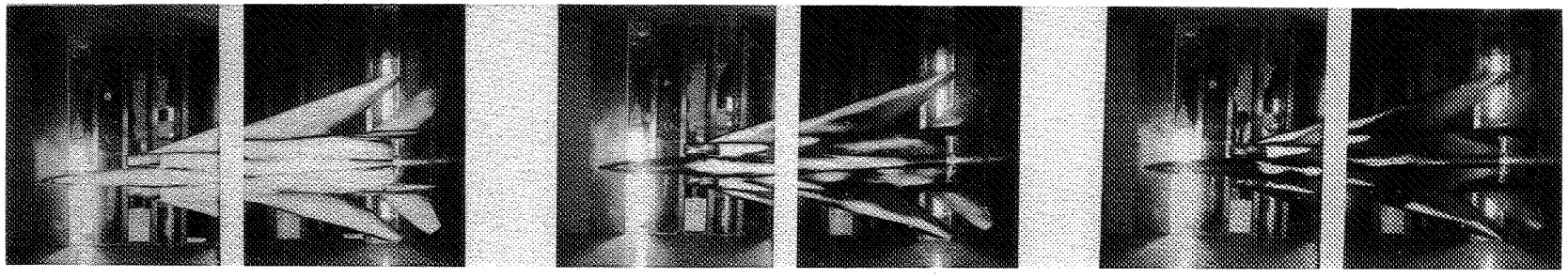

Bottom of model

L-71-562

(c) M = 2.50.

Figure 14.- Continued.

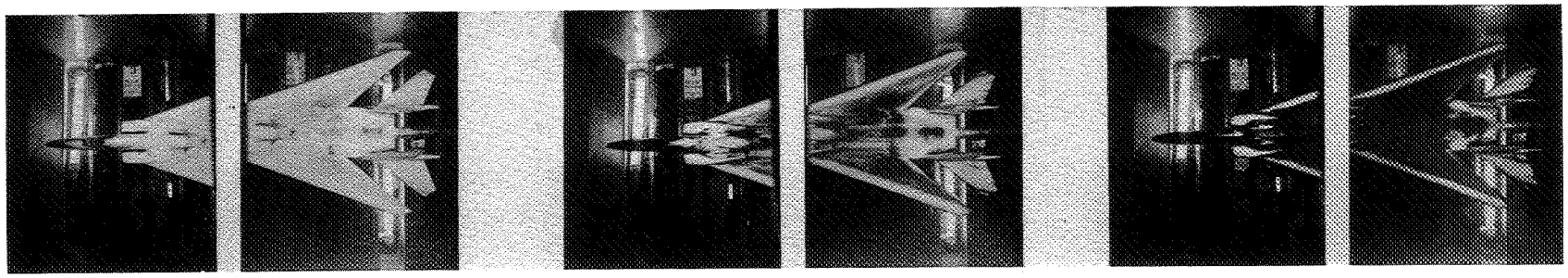

Top of model

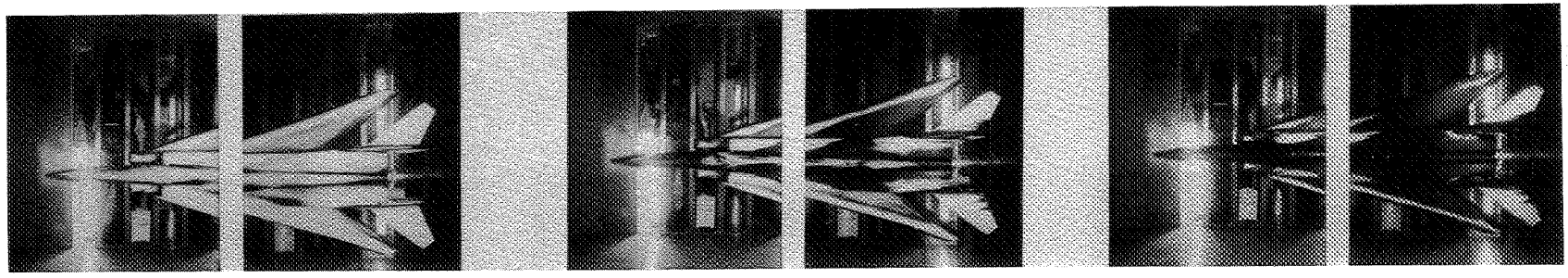

Bottom of model

L-71-563

(d) M = 2.86.

Figure 14.- Concluded.

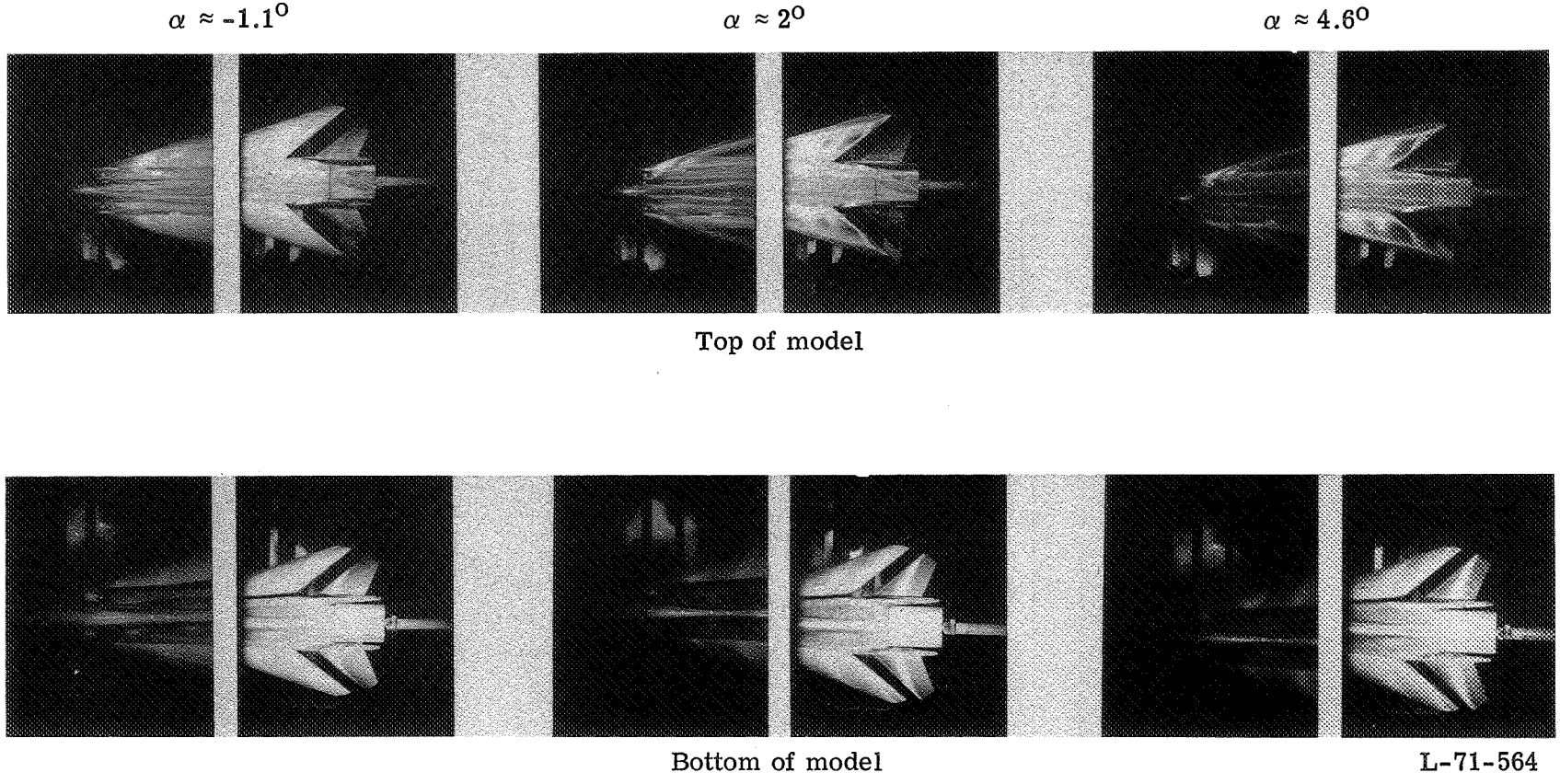

(a) M = 1.60.

Figure 15.- Oil flow.

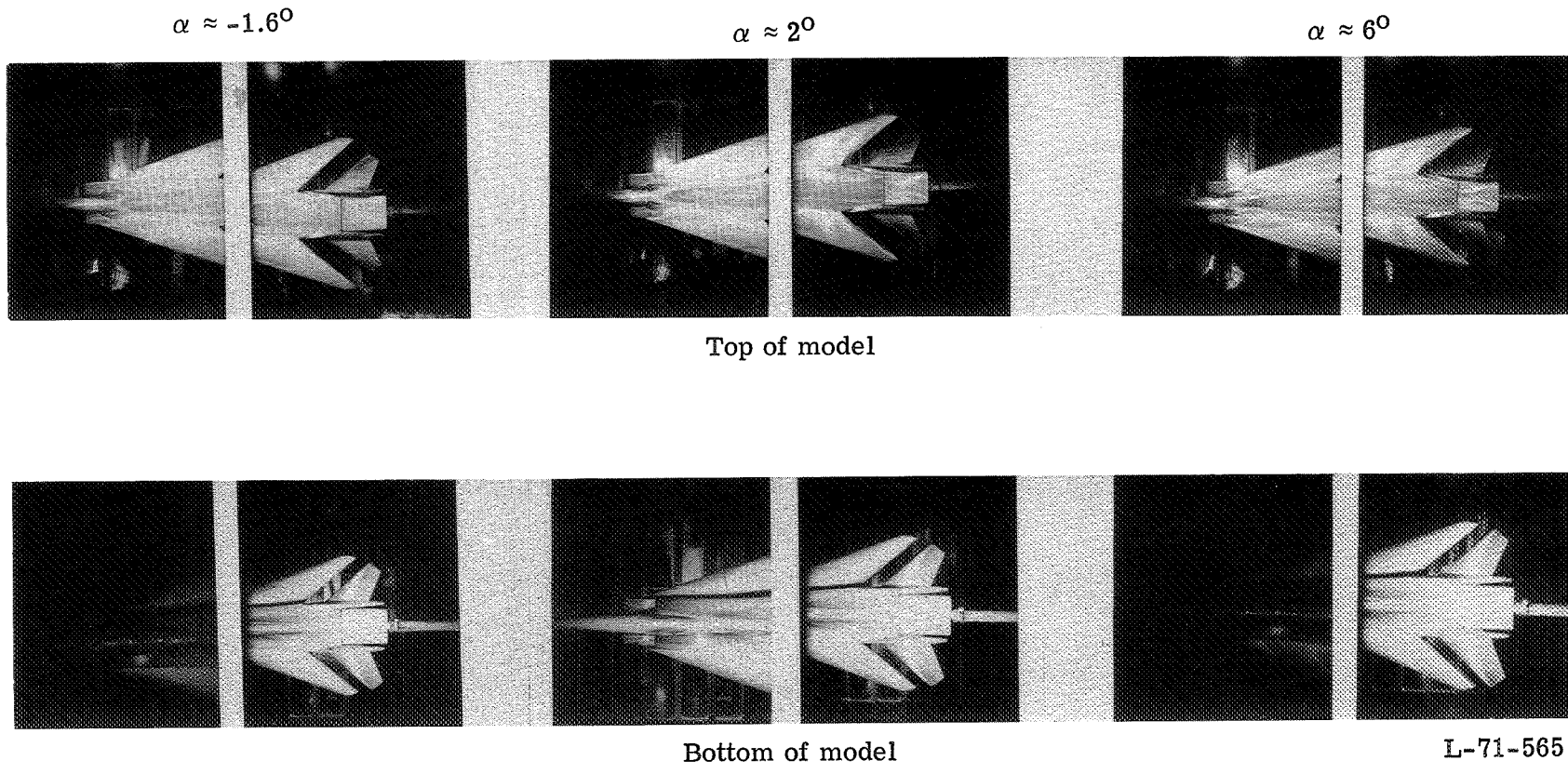

(b) M = 2.86.

Figure 15.- Concluded.

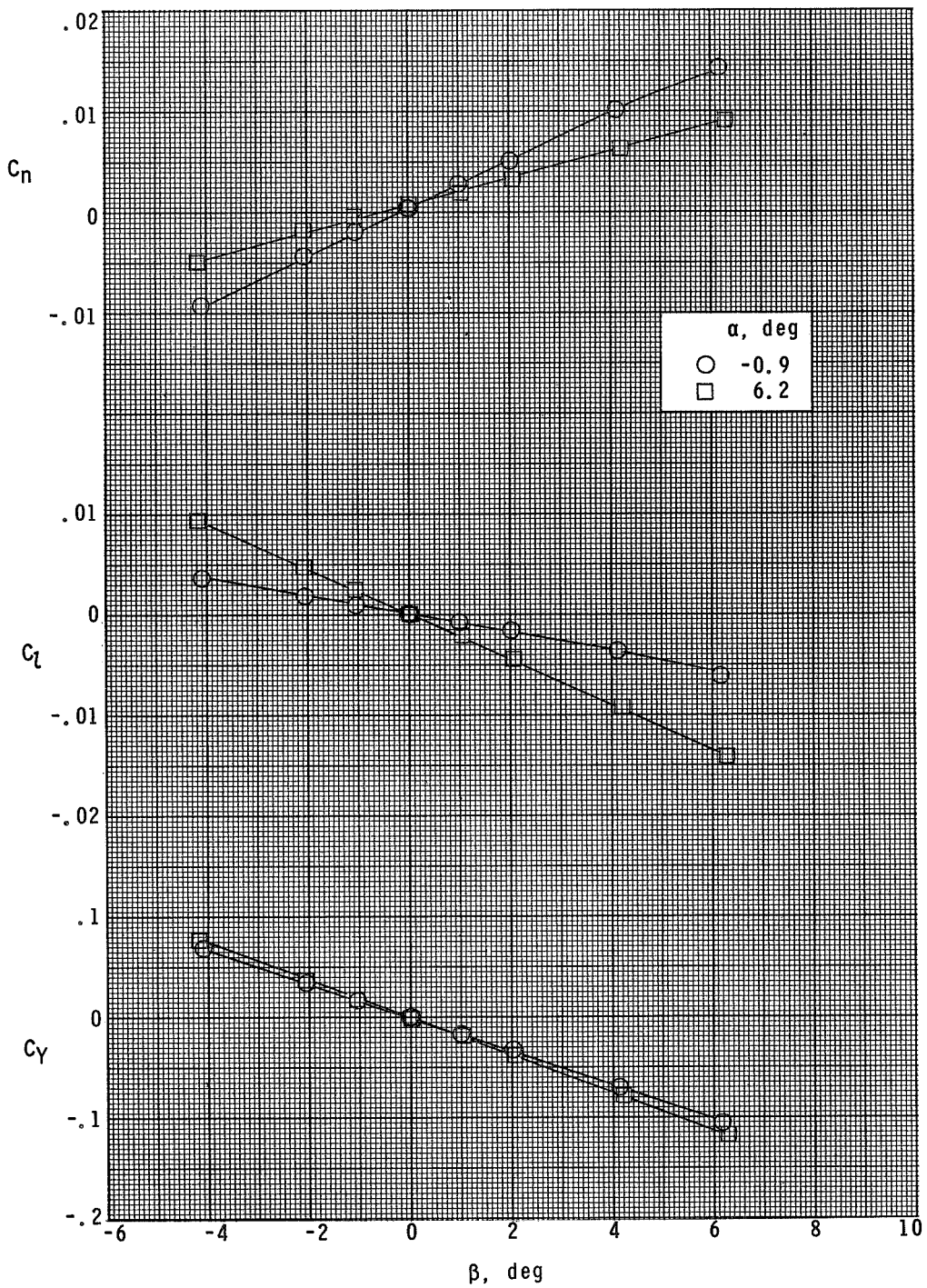

(a) M = 1.60.

Figure 16.- Lateral characteristics.

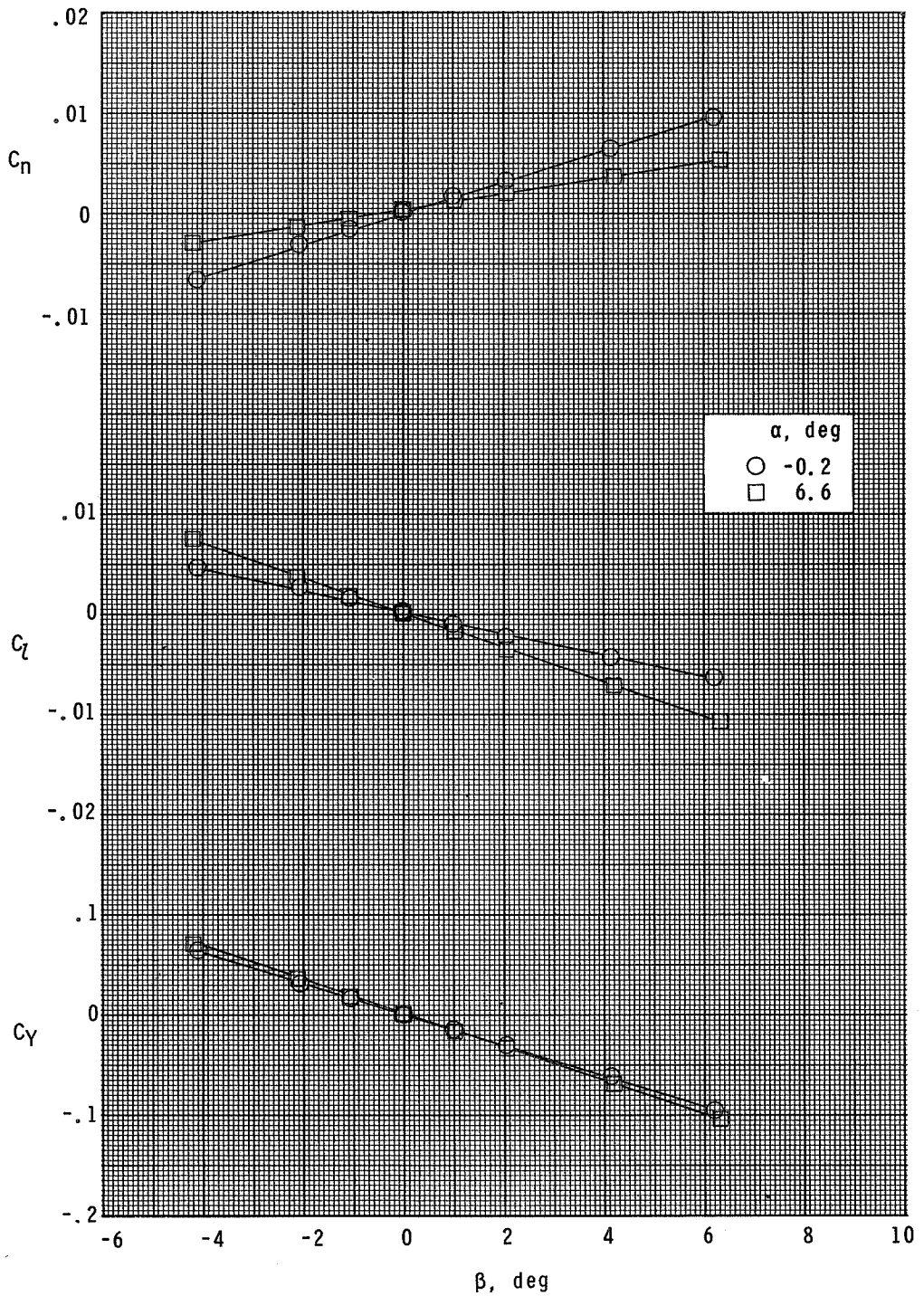

(b) M = 2.00.

Figure 16.- Continued.

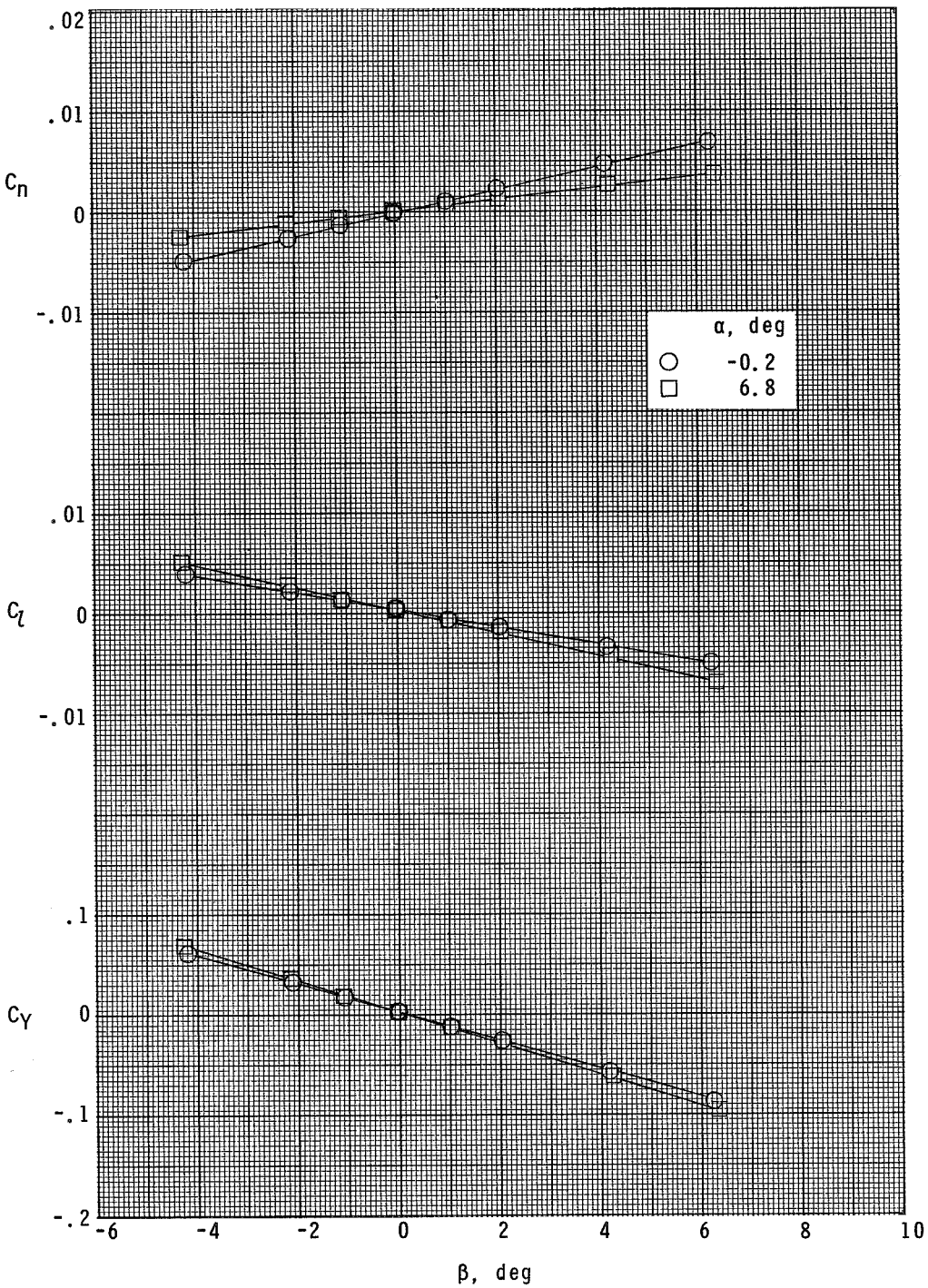

(c) M = 2.50.

Figure 16.- Continued.

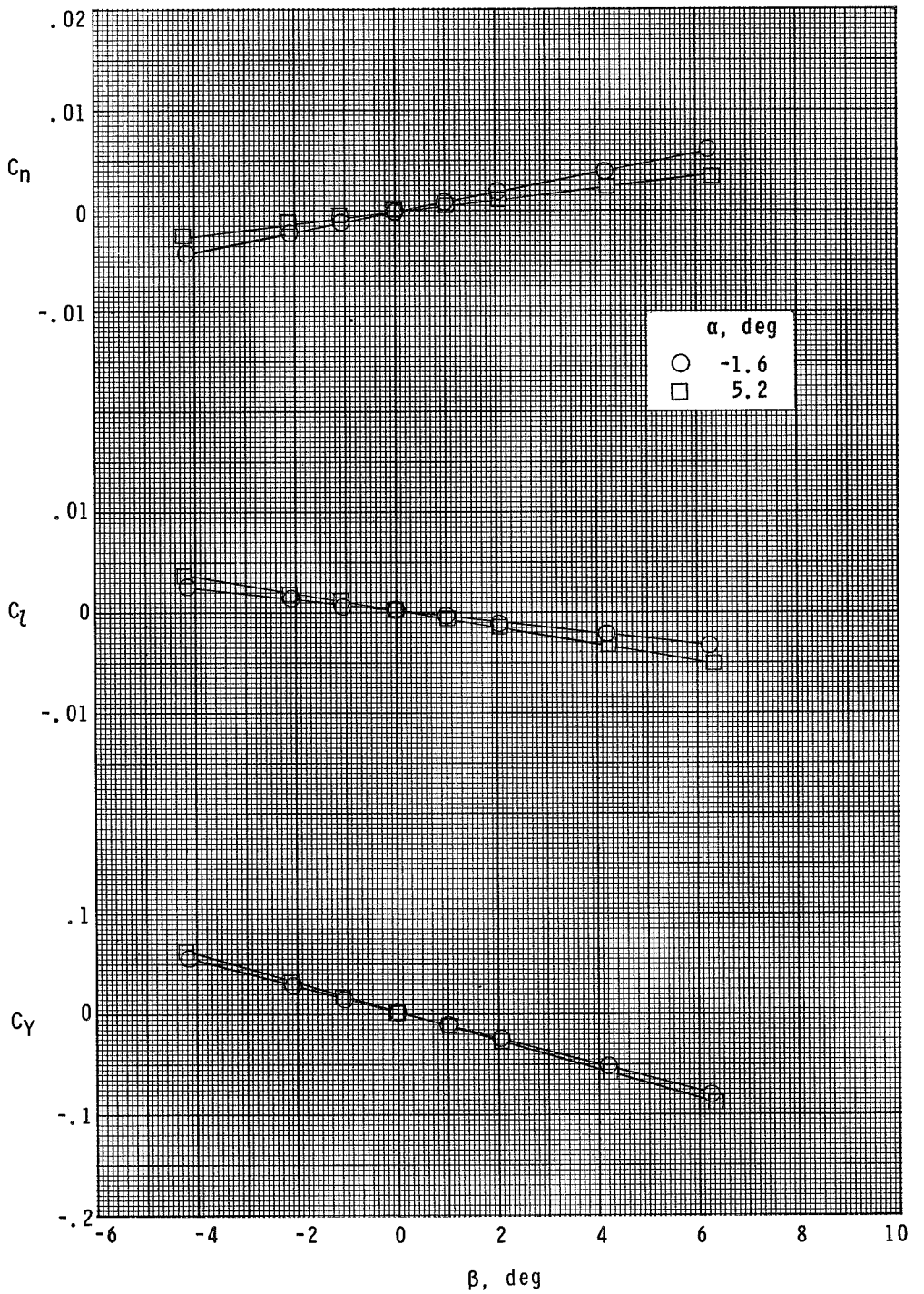

(d) M = 2.86.

Figure 16.- Concluded.

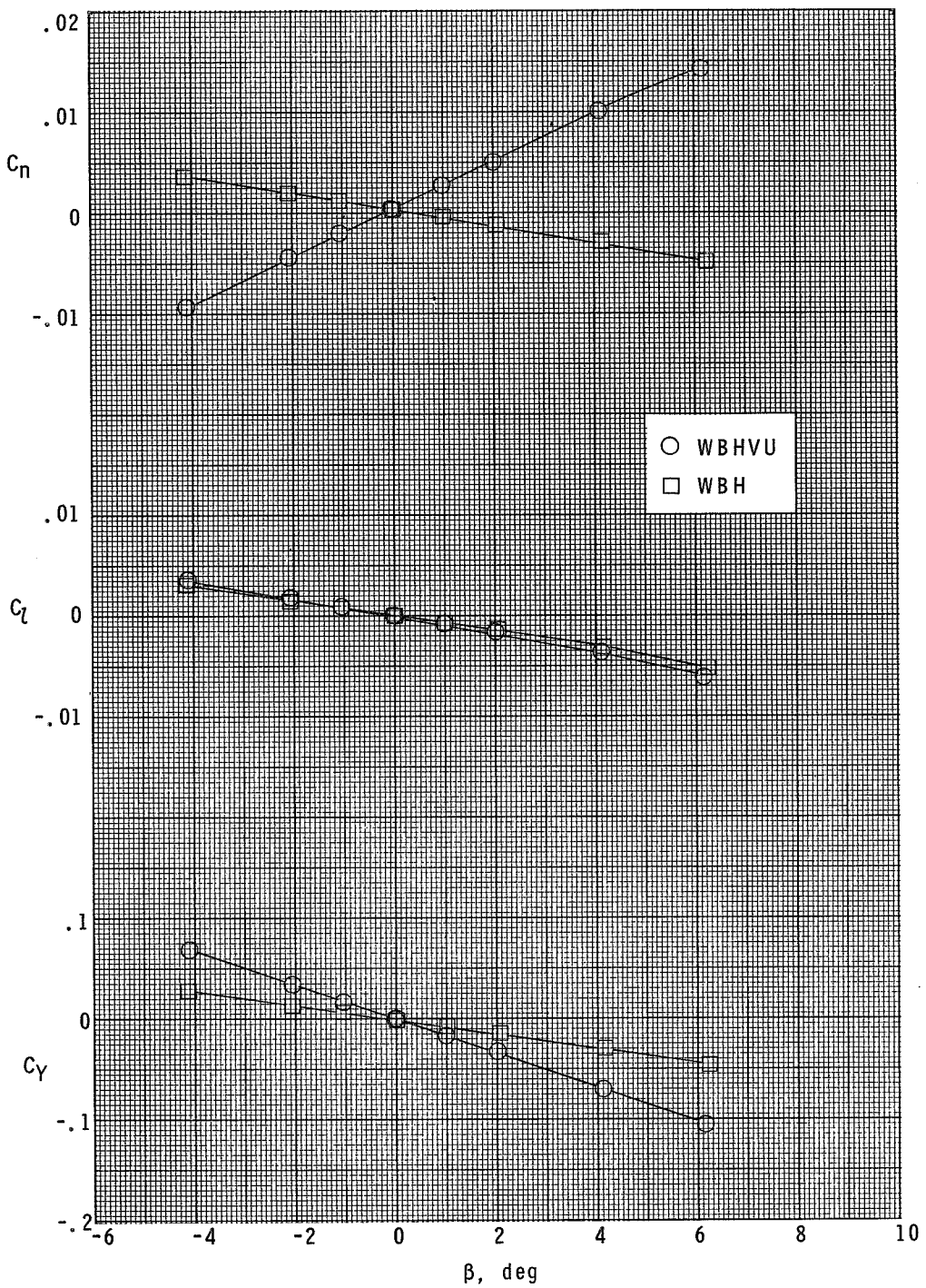

(a) M = 1.60.

Figure 17.- Effects of vertical components on lateral characteristics at $\alpha \approx -1^{o}$.

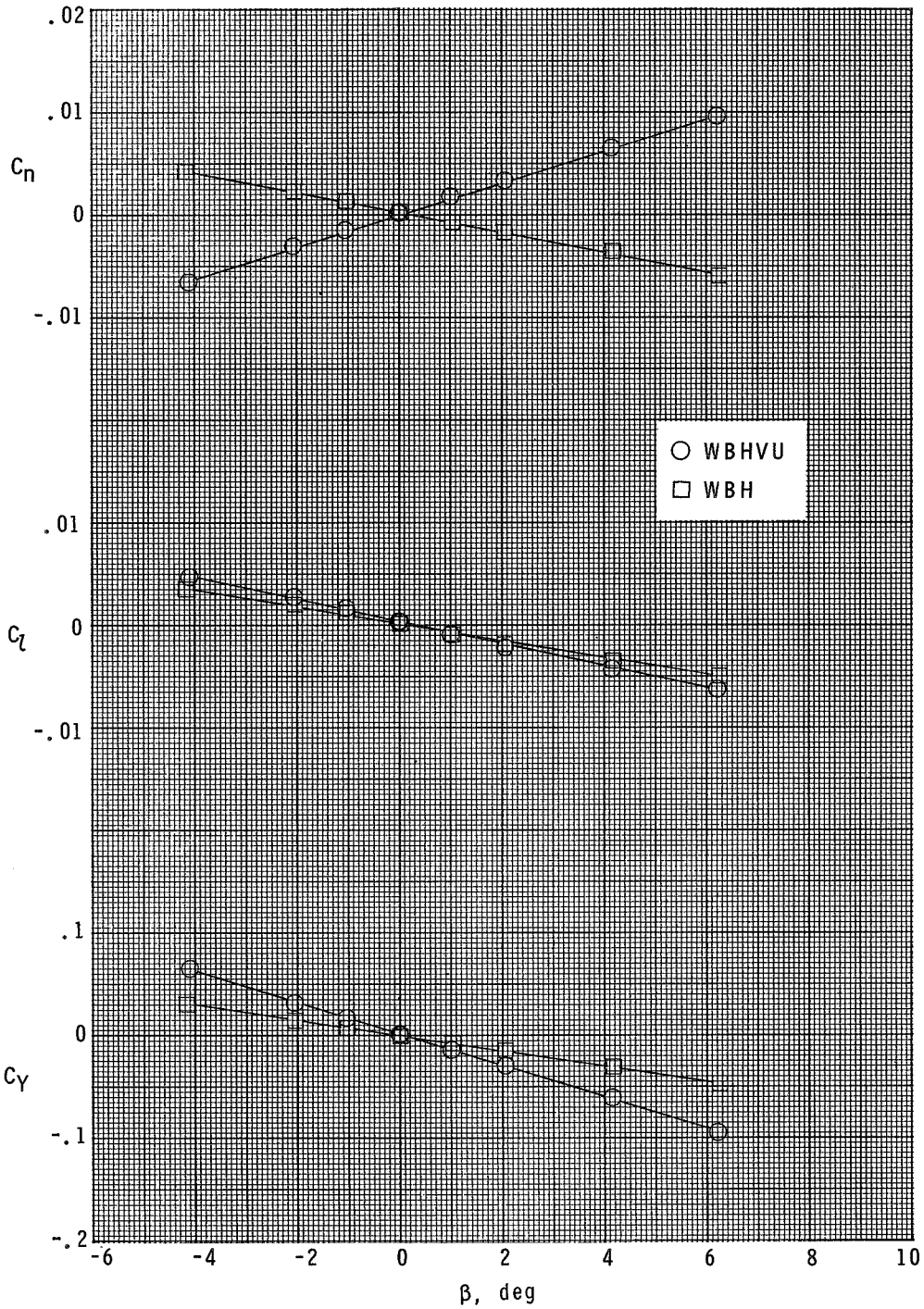

(b) M = 2.00.

Figure 17.- Continued.

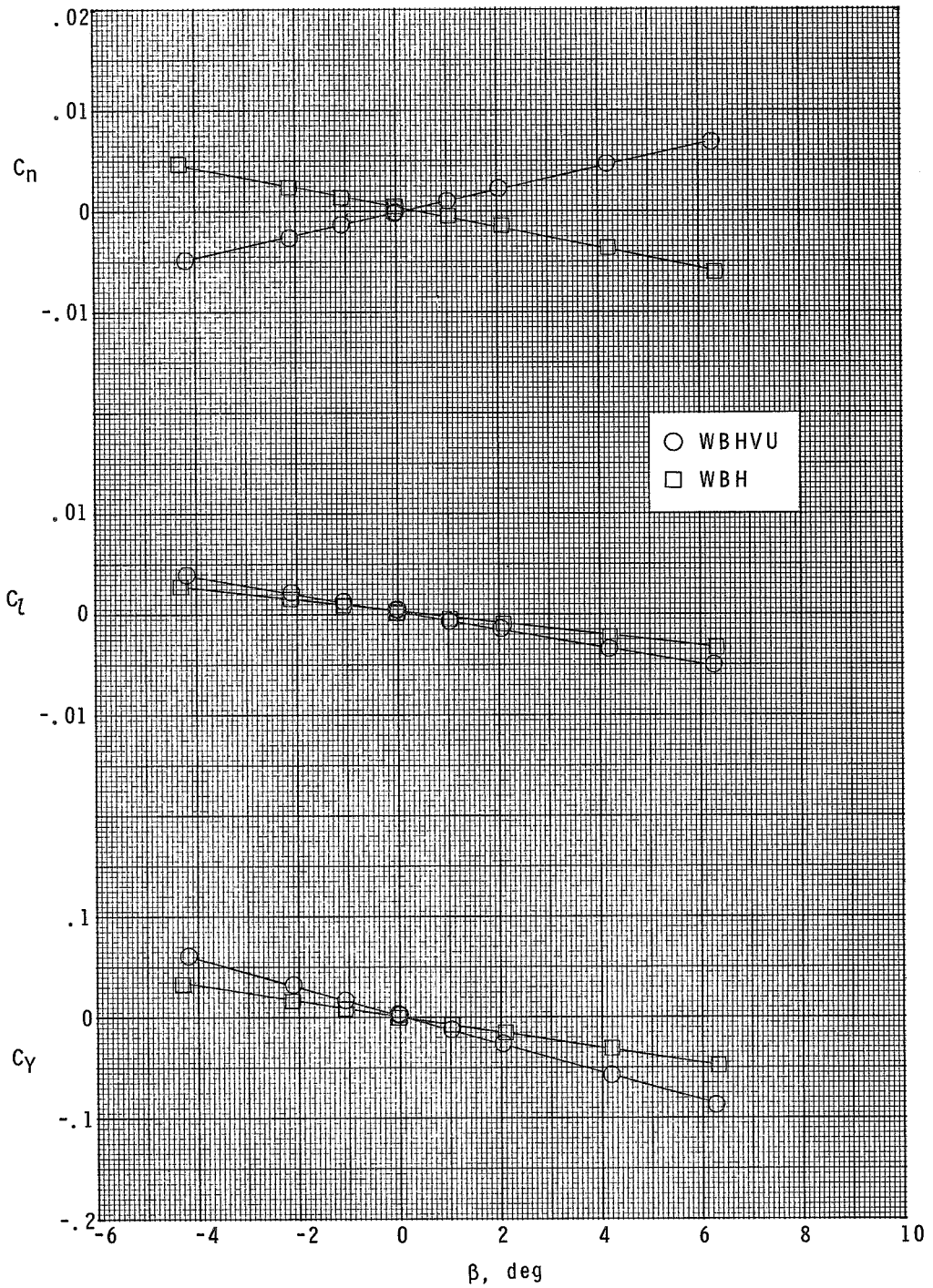

(c) M = 2.50.

Figure 17.- Continued.

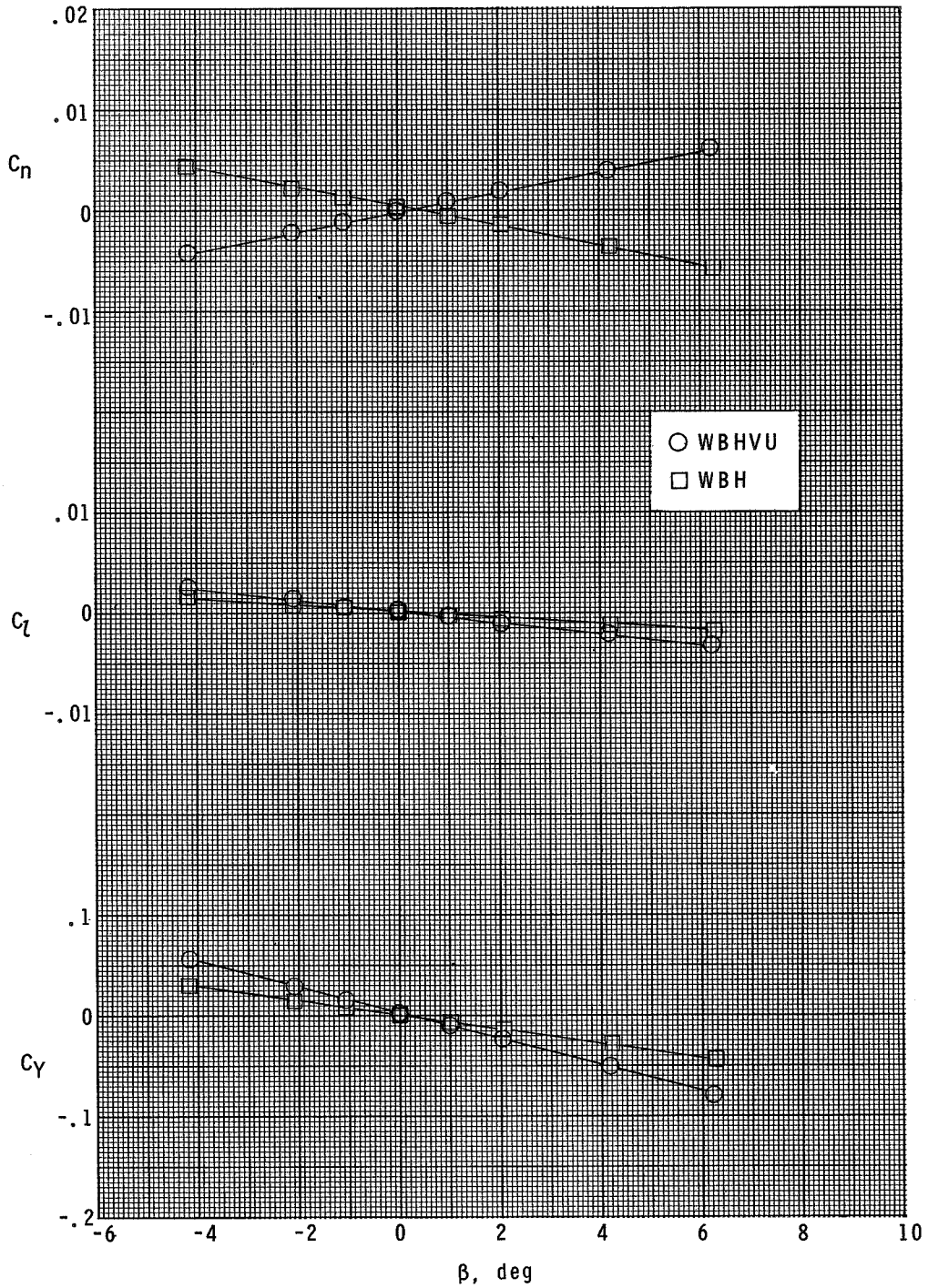

(d) M = 2.86.

Figure 17.- Concluded.

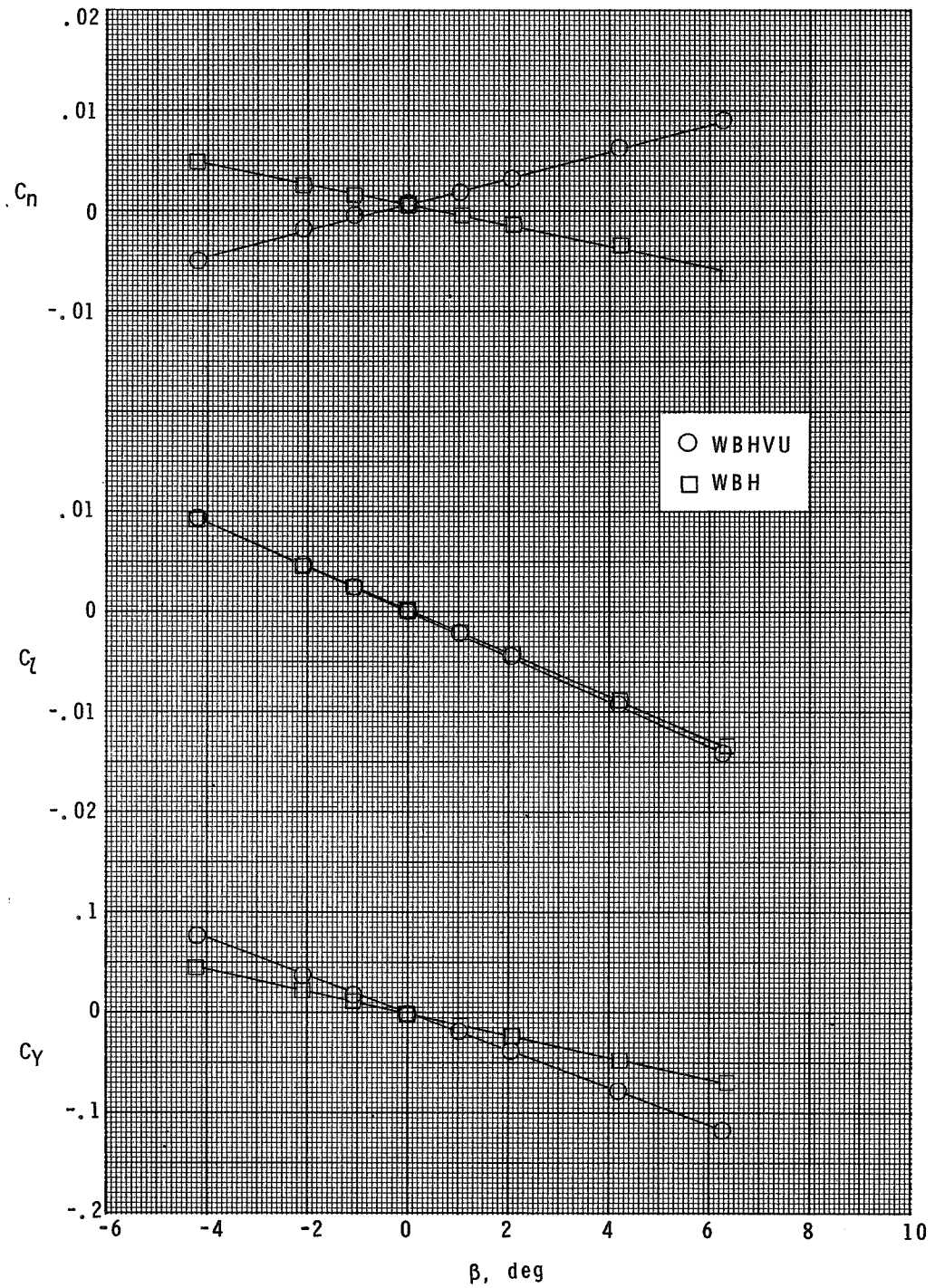

(a) M = 1.60.

Figure 18.- Effects of vertical components on lateral characteristics at $\alpha \approx 6^{o}$.

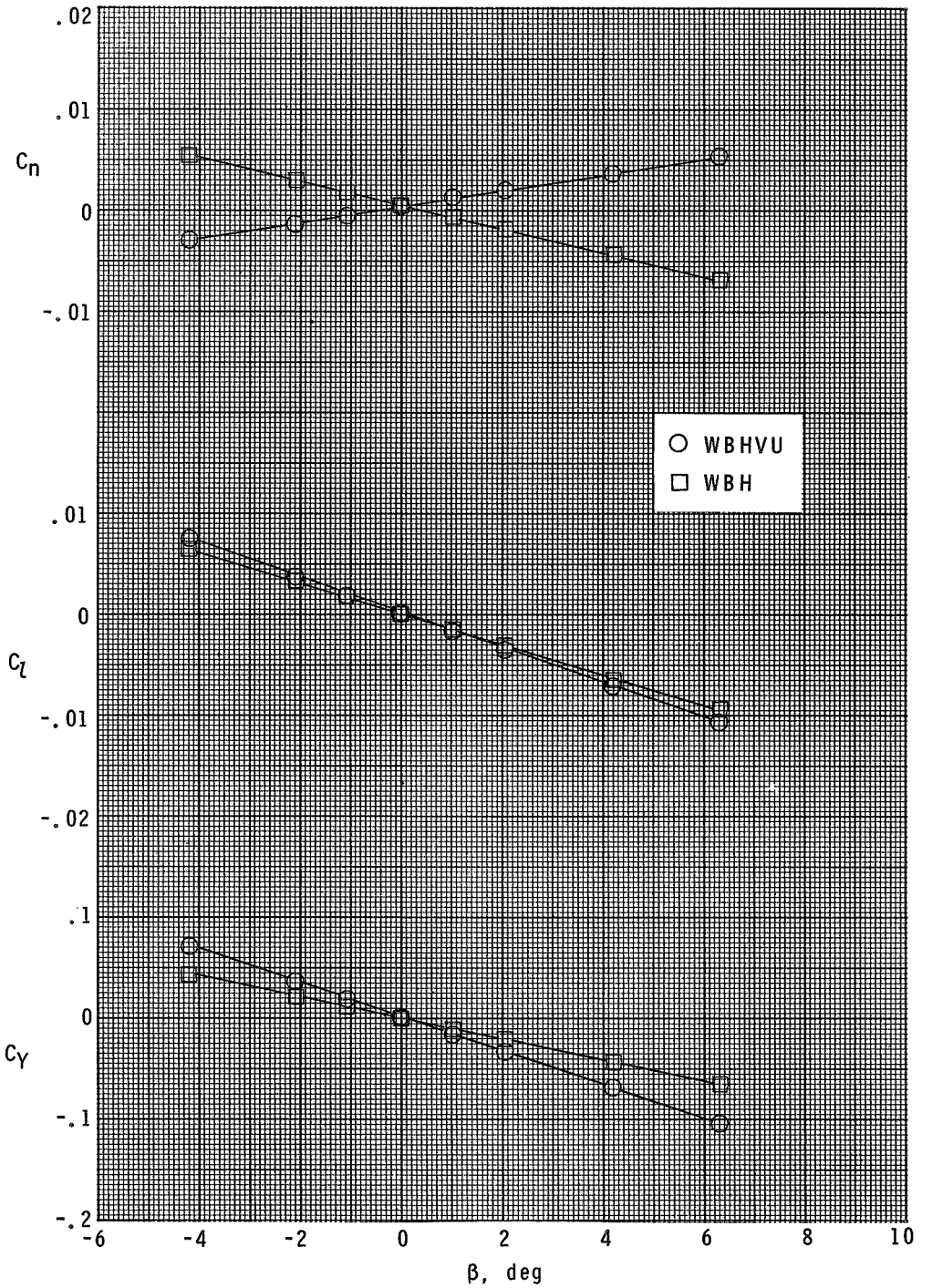

(b) M = 2.00.

Figure 18.- Continued.

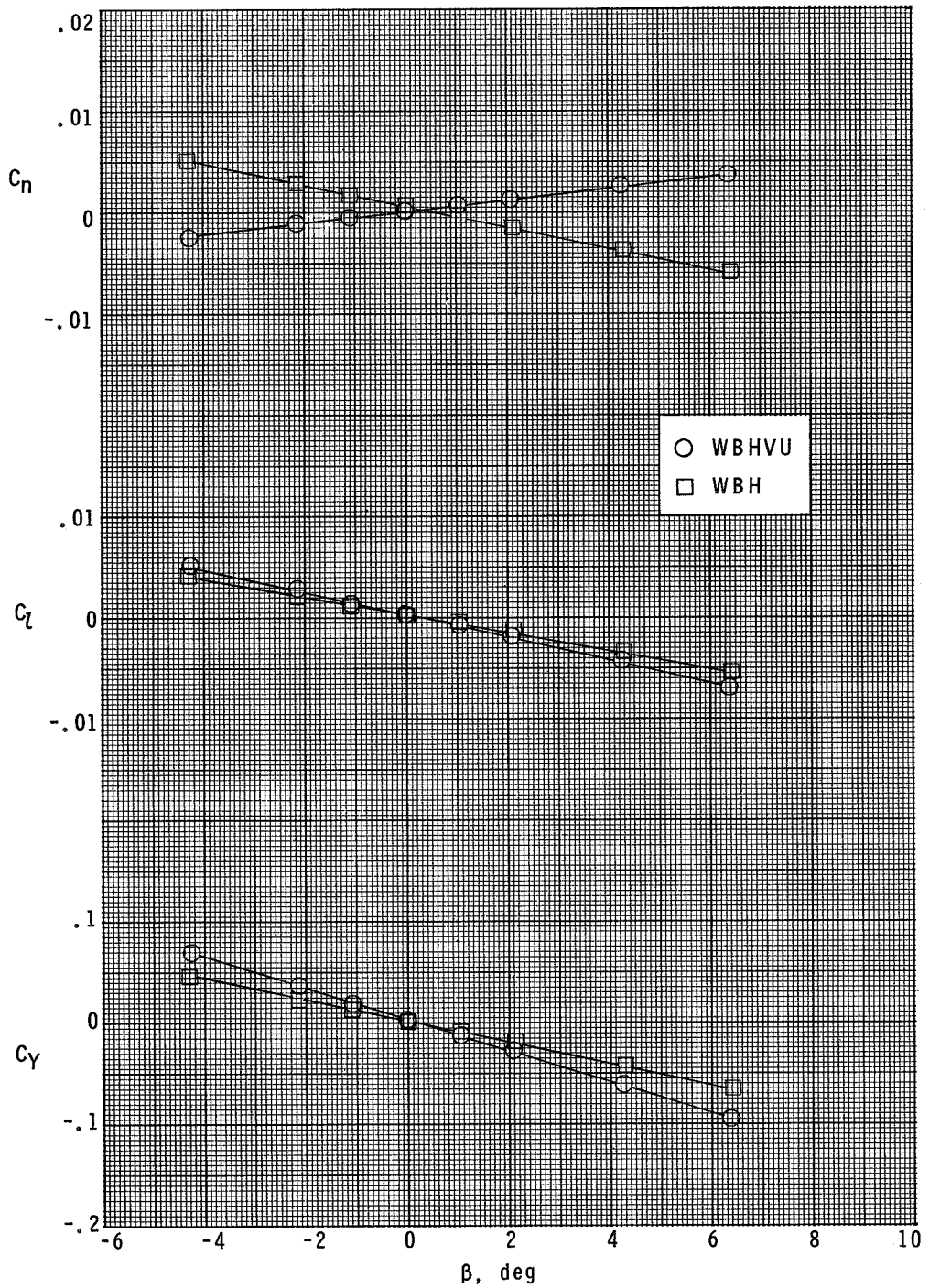

(c) M = 2.50.

Figure 18.- Continued.

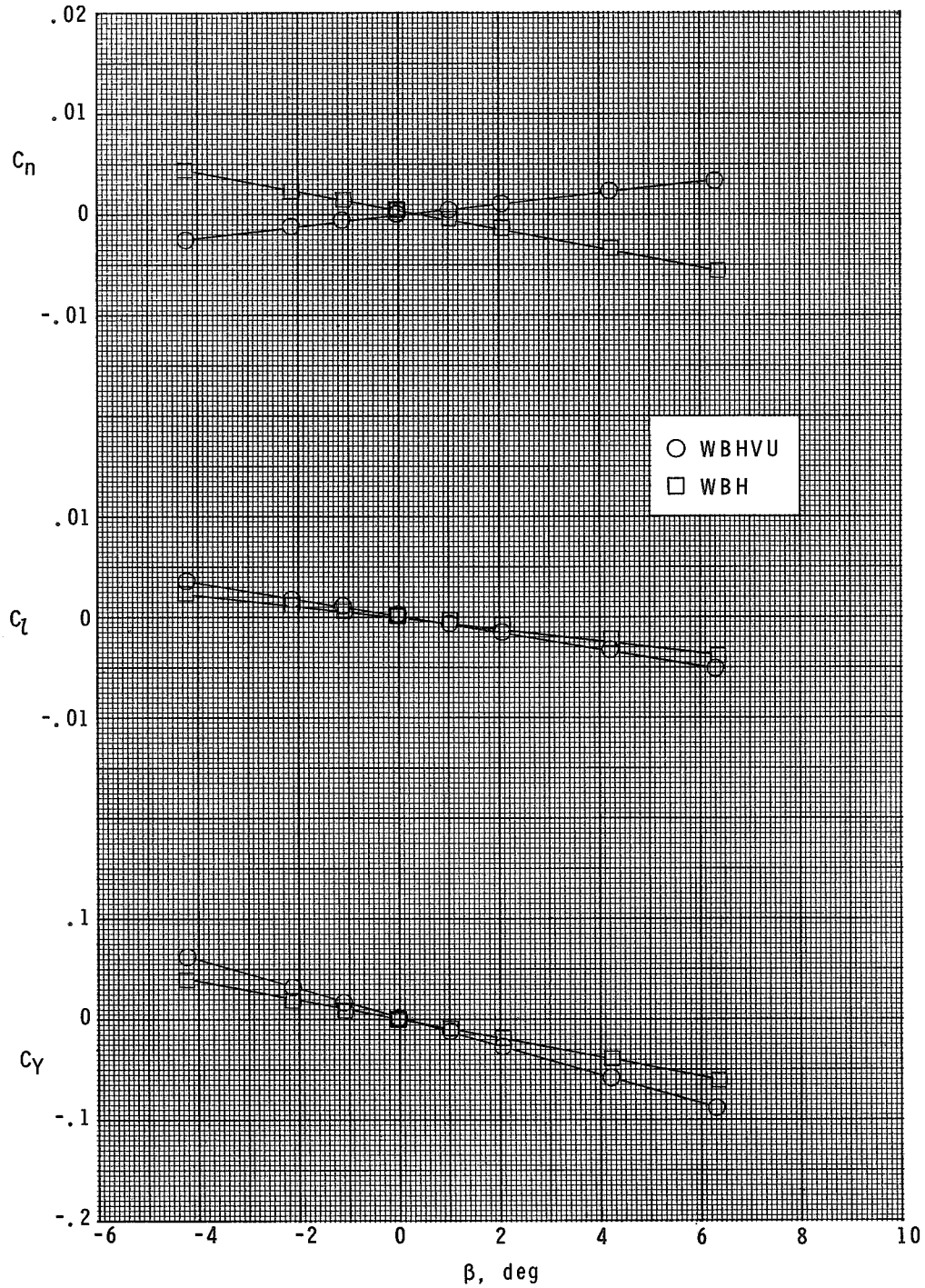

(d) M = 2.86.

Figure 18.- Concluded.

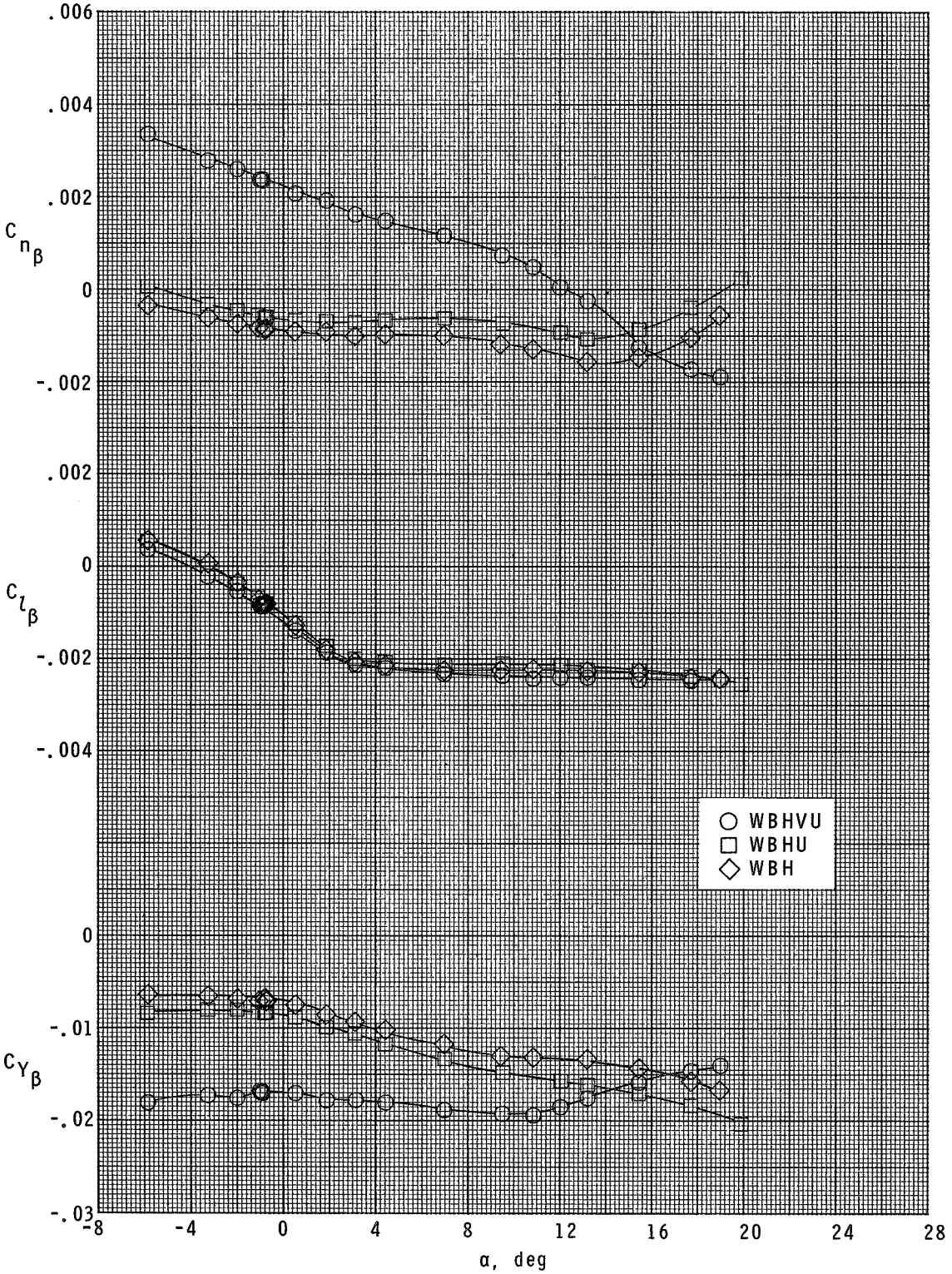

(a) M = 1.60.

Figure 19.- Effects of vertical components on sideslip derivatives.

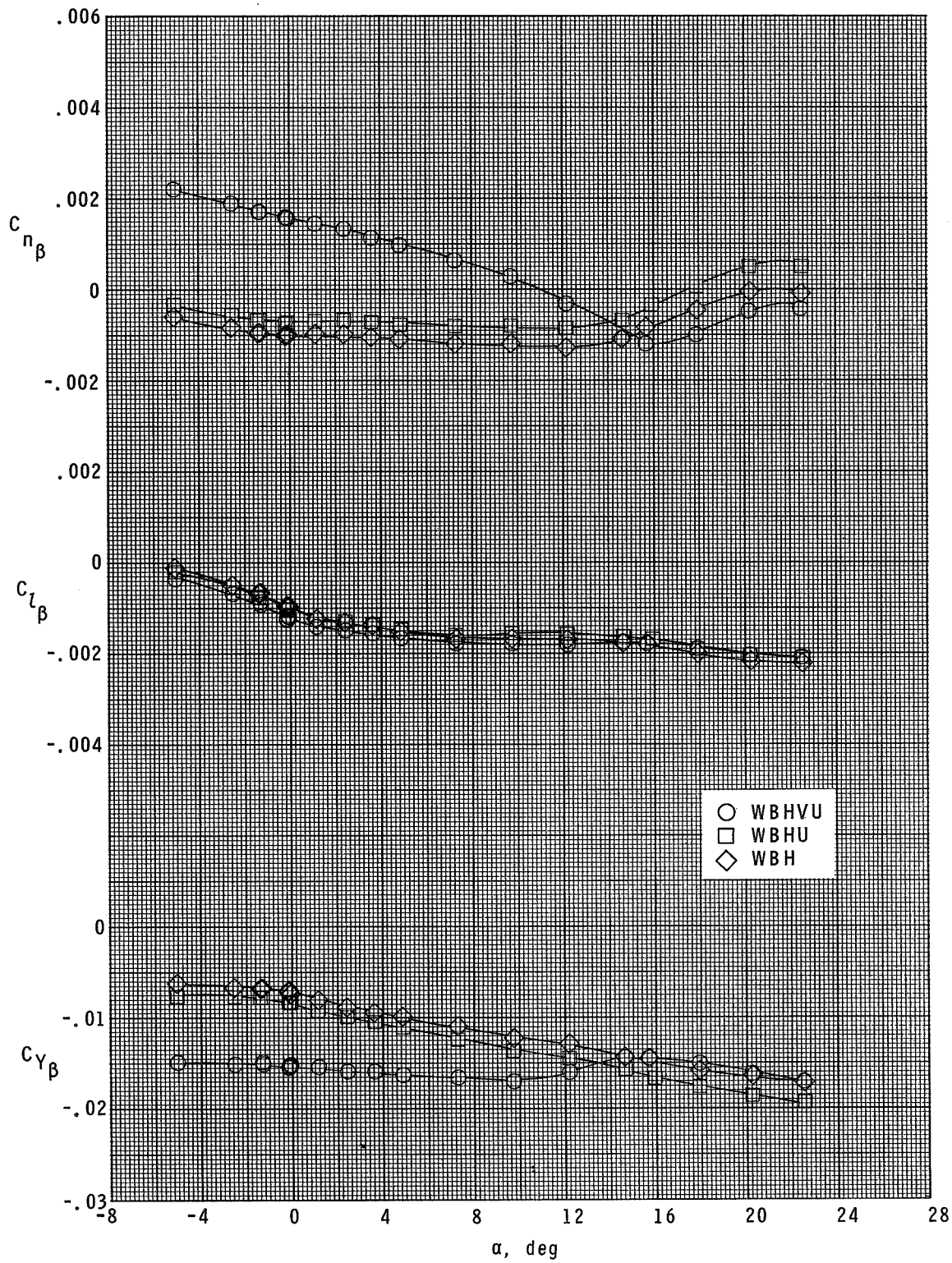

(b) M = 2.00.

Figure 19.- Continued.

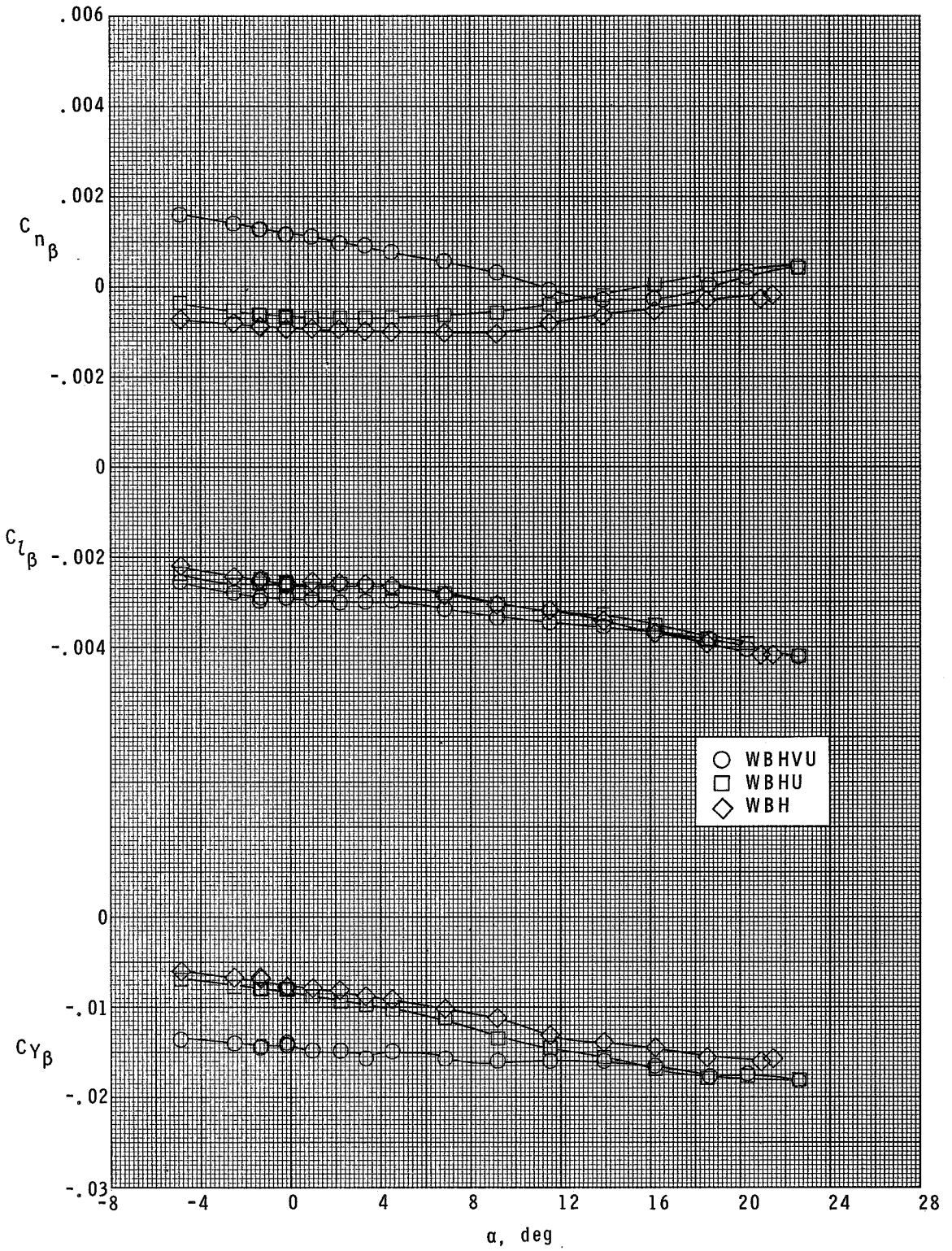

(c) M = 2.50.

Figure 19.- Continued.

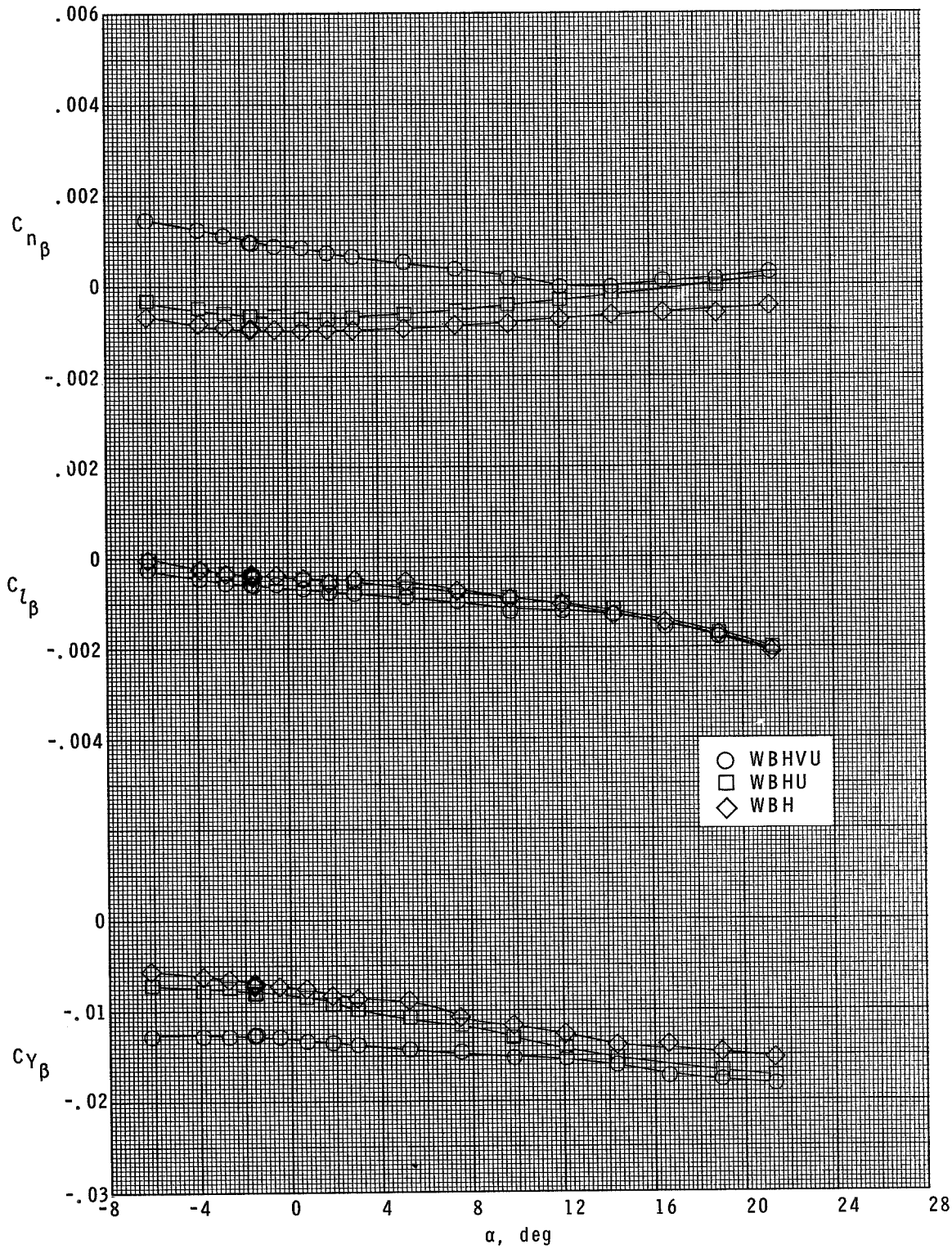

(d) M = 2.86.

Figure 19.- Concluded.

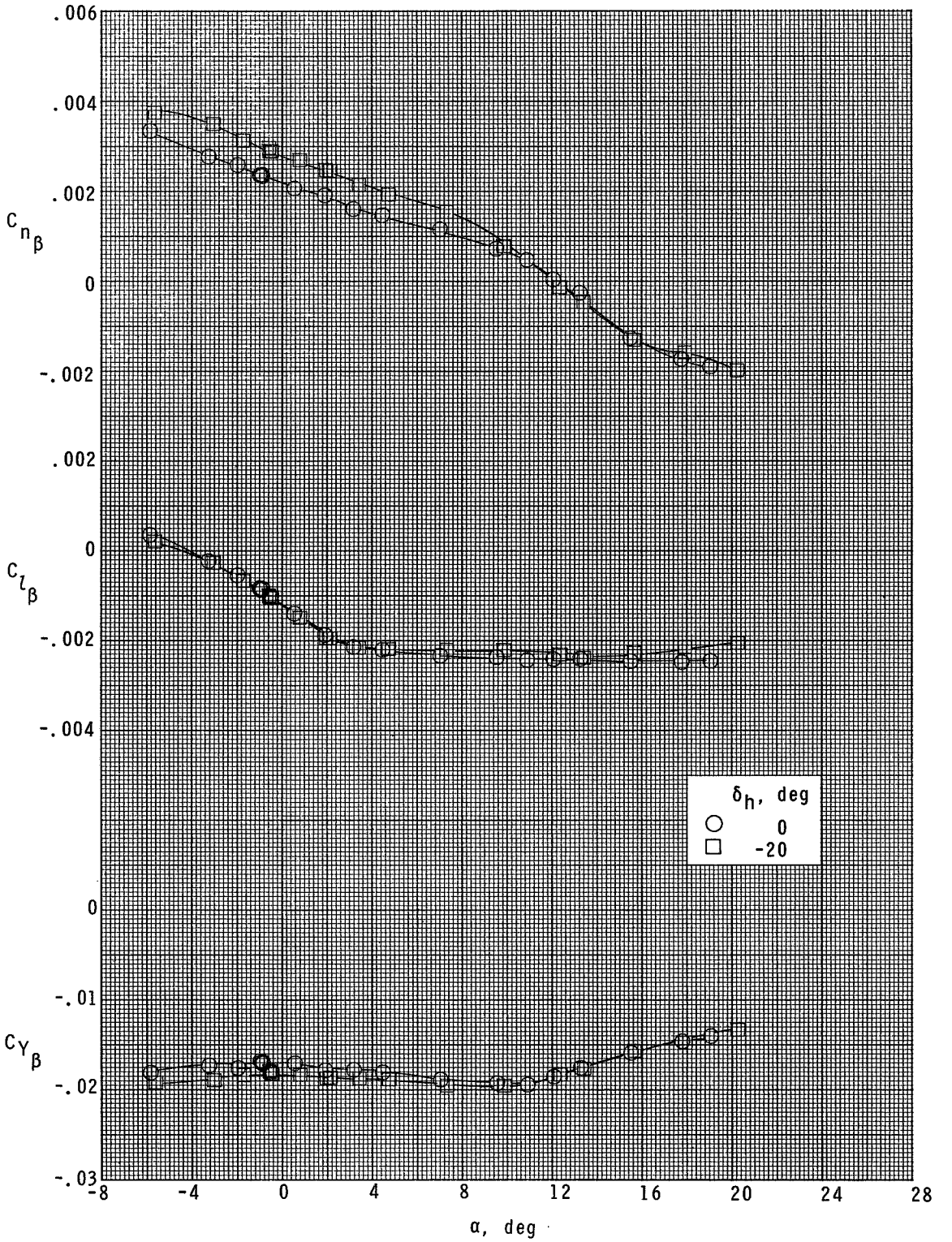

(a) M = 1.60.

Figure 20.- Effects of tail deflection on sideslip derivatives.

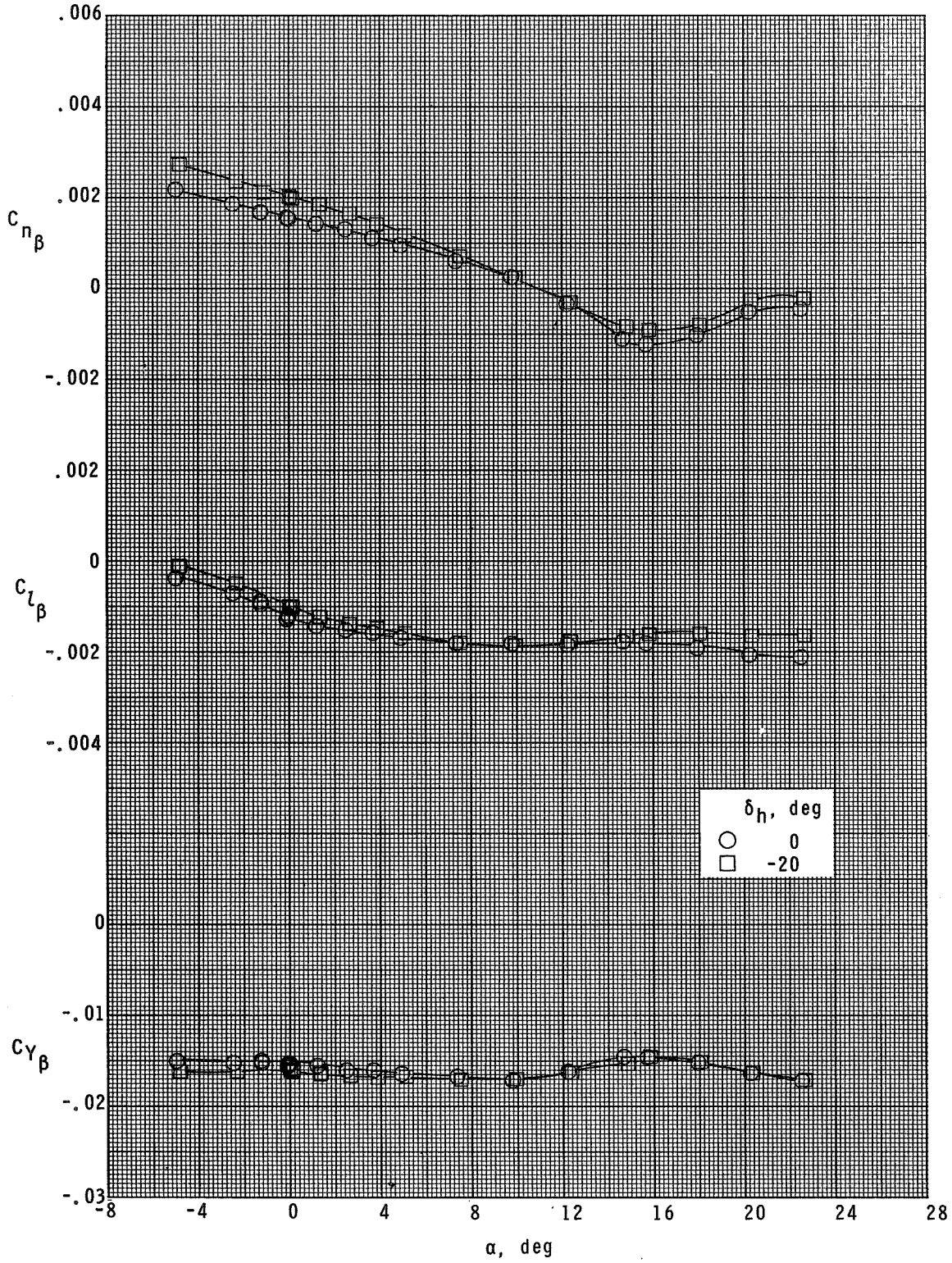

(b) M = 2.00.

Figure 20.- Continued.

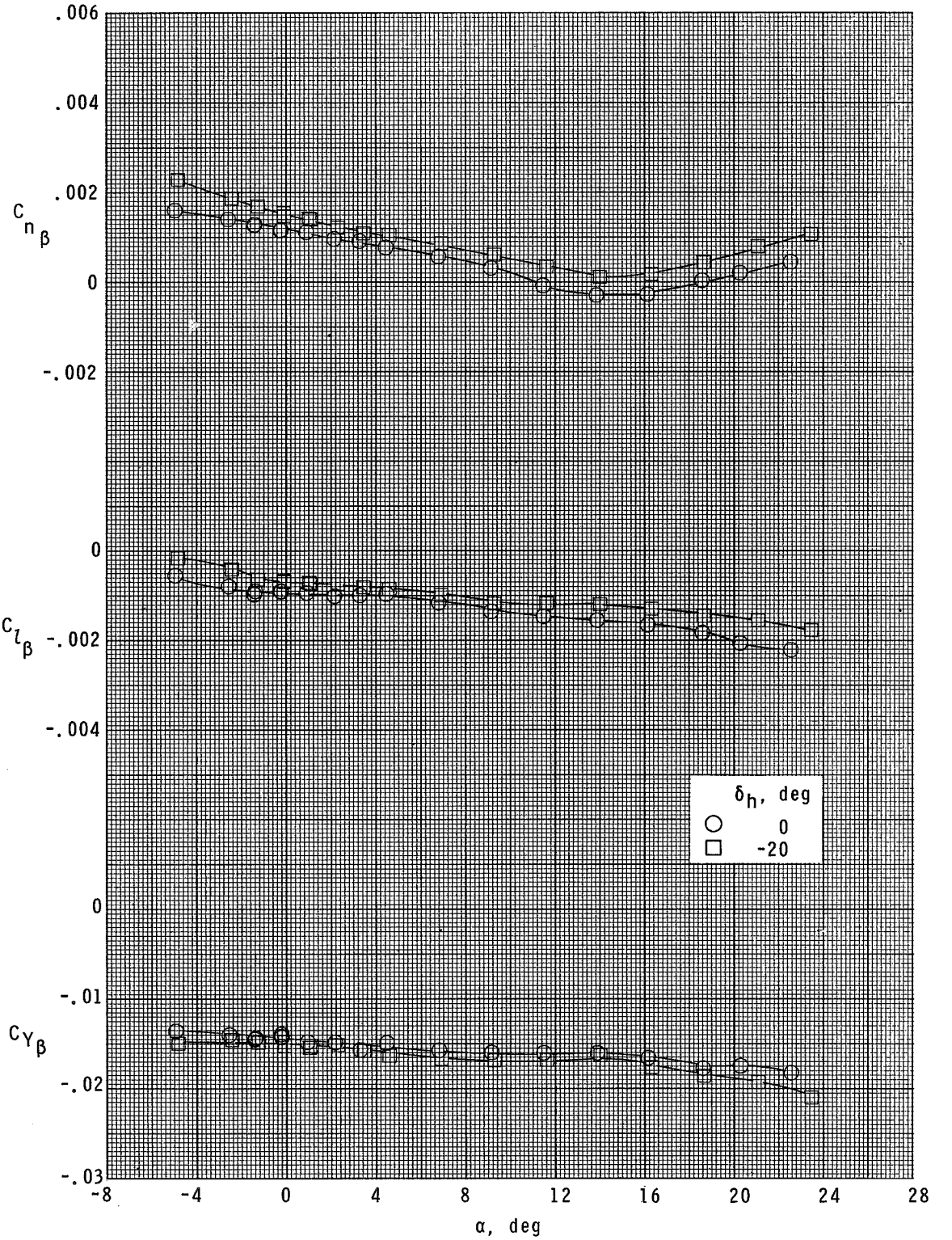

(c) M = 2.50.

Figure 20.- Continued.

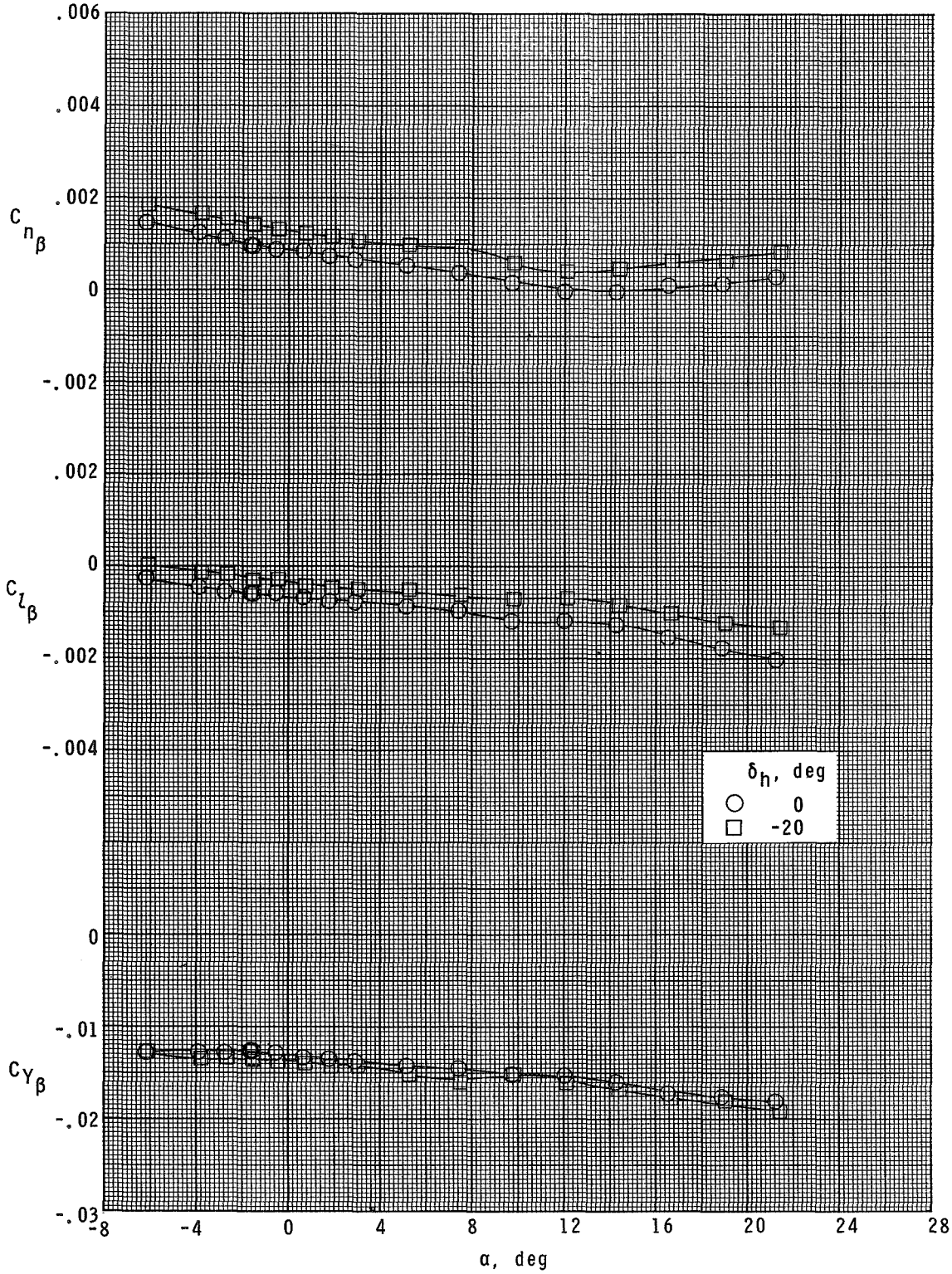

(d) M = 2.86.

Figure 20.- Concluded.